Stony Brook University

ADAM10 Regulates NSC Properties Via a JAM-C/Rap1 Axis

A Dissertation Presented

by

Nadia McMillan

to

The Graduate School

in Partial Fulfillment of the

Requirements

for the Degree of

Doctor of Philosophy

in

Neurobiology and Behavior

Stony Brook University

May 2017

Stony Brook University

The Graduate School

Nadia McMillan

We, the dissertation committee for the above candidate for the

Doctor of Philosophy degree, hereby recommend

acceptance of this dissertation.

Dr. Adan Aguirre, Ph.D.- Dissertation Advisor
Assistant Professor, Department of Pharmacological Sciences

Dr. Joel M. Levine, Ph.D.- Chairperson of Defense
Professor, Department of Neurobiology and Behavior

Dr. Styliani-Anna E. Tsirka, Ph.D.- Committee Member
Professor, Department of Pharmacological Sciences

Dr. James E. Goldman, M.D., Ph.D.- Outside Committee Member
Professor, Pathology and Cell Biology, Columbia University, College of Physicians and Surgeons
.

This dissertation is accepted by the Graduate School

Charles Taber
Dean of the Graduate School

Abstract of the Dissertation

ADAM10 Regulates NSC Properties Via JAM-C/Rap1 Axis

by

Nadia McMillan

Doctor of Philosophy

in

Neurobiology and Behavior

Stony Brook University

2017

In the adult brain, the microenvironment that supports neural stem cell (NSC) properties is known as the subventricular zone (SVZ). The SVZ is organized into an apical compartment adjacent to the ventricular wall and a basal compartment containing a rich vascular network. In this context, quiescent NSCs are arranged at the ventricular wall, while mitotically activated NSCs are found near the basal, vascular region of the SVZ. Expression of extracellular and secreted niche elements are dynamic and tightly controlled to maintain NSC properties, and appear to correlate with NSC positioning within the niche to direct cell intrinsic programs. Despite identification of factors that govern NSC-niche interactions, the signaling mechanisms that regulate NSC positioning to maintain their properties within these niches are still not well defined. In this study, we found a novel role for the protease 'A disintegrin and metalloproteinase 10' (ADAM10) in the regulation of NSC anchorage to the ventricular wall and NSC lineage progression. Inhibition of ADAM10 maintains the undifferentiated state of NSCs in the adult SVZ by increasing NSC anchorage to the apical domain. We identified the junctional adhesion

molecule C (JAM-C), an apical stem cell marker, as a substrate for ADAM10 in NSCs. Processing of JAM-C by ADAM10 regulates Rap1 activity and this molecular machinery promotes NSC translocation from the apical to the basal compartment and subsequent lineage progression of NSCs. Taken together, our data suggests that ADAM10 activity mediates a pathway essential to the regulation of NSC anchorage to the SVZ ventricular wall and maintains their properties in the adult brain upstream of a signaling paradigm involving JAM-C and Rap1.

Dedication Page

Dedicated to my parents, Katherine Tsiakkirou and Peter McMillan, whose unconditional support and love made this possible. And to my twin sister, Alexandra McMillan, who never let me give up and served as a sounding board for years. Finally, I would like to thank Benjamin Newcomb for his abundant patience, support, and valuable advice.

Table of Contents

List of Illustrations

List of Figures

List of Abbreviations

NSC(s): Neural Stem Cell(s)
NPC(s): Neural Progenitor Cell(s)
SVZ: Subventricular zone
RMS: Rostral migratory stream
DG: Dentate Gyrus
SGZ: Subgranule zone
OB: Olfactory bulb
GL: Glomerular Layer of Olfactory Bulb
GC: Granule Cell
GCL: Granule Cell Layer of Olfactory Bulb
BrdU: Bromo-deoxyuridine
CldU: chloro-deoxyuridine
IdU: Iodo-deoxyuridine
GFAP: Glial Fibrillary Acid Protein
DCX: Doublecortin
Nestin-YFP: GFP expression under the nestin promoter
GFAP-GFP: GFP expression under the GFAP promotor
JAM-C: Junctional Adhesion Molecule C
IF: immunofluorescence
IH: immunohistochemistry
LRC-BrdU: BrdU label-retaining cells
LTR-BrdU: long term retaining BrdU+ cells
TAM: tamoxifen
4-OHT: Hydroxy-tamoxifen
Acitretin: AC
GI: GI 254023X (ADAM10 inhibitor)
8-CPT: 8-CPT-2-O-Me-cAMP (Rap1 Activator)
P: Post-natal day
DIV: Days in Vitro
CNS: Central Nervous System
CTF: C-terminal fragment

Acknowledgments

I would like to thank my family for their support. My parents provided encouragement, and were always ready to provide help in whatever capacity they were able. They taught me the importance of hard work by example. My sister, Alexandra (also an MSTP student) served as a resource and a friend. They made this possible by believing in me and providing unconditional love and support. My boyfriend Benjamin Newcomb has sat through several practice talks and provided comfort and advice over the years.

I would like to thank my advisor, Dr. Adan Aguirre. Dr. Aguirre has been a great advisor. He taught me a number of techniques and served a very hands- on role these past couple years. I could always come and ask him questions regarding a result or experiment. His high standards forced me to grow as a student and a scientist.

.

I would like to thank the members of my committee, Dr. Joel Levine, Dr. Stella Tsirka, and Dr. James Goldman. The questions and comments during and after my committee meetings helped me think critically about my project and helped focus my experiments.

I would like to thank past and present members of the lab who taught me techniques and provided advice over the years, including Michael Klingener and Manideep Chavali.

I would also like to thank and acknowledge the contributions the MSTP has provided over the years, particularly Dr. Michael Frohman and Dr. Markus Seeliger.

Nadia McMillan
75 Mud Road, East Setauket, New York
(646) 203-1882
Nadia.mcmillan@stonybrookmedicine.edu

Education

Current MSTP (MD/PhD) Candidate
Stonybrook University, 2011- 2019
Department of Neurobiology and Behavior
Step1 Score: 255

B.A. Degree in Neuroscience
Johns Hopkins University, Baltimore, MD
Neuroscience Departmental/General Honors
G.P.A. 3.7

Publications

Abernathy's Surgical Secrets 6e. Crisostomo PR, **McMillan N,** Meldum DR. Lung Transplantation (Chapter 17), pp 444-453. In "Surgical Secrets", Sixth Edition, Eds. Harken and Moore, Mosby, 2008.

Michael Klingener, Manideep Chavali, Jagdeep Singh, **Nadia McMillan**, Alexandra Coomes, Peter J. Dempsey, Emily I. Chen, and Adan Aguirre (2010) N-Cadherin Promotes Recruitment and Migration of Neural Progenitor Cells from the SVZ Neural Stem Cell Niche into Demyelinated Lesions. J Neurosci. 34(29): 9590-9606

Abstracts

Michael A. Muniak, Vikas N. Kodali, Makoto Tanigawa, Catherine J. Connelly, Kristyna Hnizda, **Nadia F. McMillan**, Tan Pongstaporn, David K. Ryugo (2011). Garvan Institute of Medical Research. Reciprocal Connectivity Between the Central Nucleus of the Inferior Colliculus and the Dorsal Cochlear Nucleus of the CBA/CaJ Mouse, Johns Hopkins University, Association for Research in Otolaryngology.

Research Experience

Full-time Research Technician- Johns Hopkins University SOM, lab of Dr. David Ryugo, Department of Otolaryngology, 2009-2011, Garvan Institute of Medical Research, Sydney Australia, April 2011

Undergraduate Research, Johns Hopkins Medical Institutions, lab of Dr. Raja Srinivasa, Department of Anesthesiology and Critical Care, 2007-2009

High School/Undergraduate Research, Indiana University, lab of Dr. Keith March, Indiana Center for Vascular Biology and Medicine, 2006-2008

Employment

Neuroscience Lab Head Teaching Assistant, Johns Hopkins University, 3 semesters, 2008-2010

Center for Educational Resources (CER) Technology Fellow in Psychological and Brain Sciences, Johns Hopkins University, *Neuroscience Undergraduate Teaching Lab Videos*, 2008

Conferences: Yearly MD/PhD Research Day (20013-2017), APSA/ASCI (Chicago, 2014), CSCTR (Trainee Travel Award; Chicago, 2015), MD/PhD National Conference (Denver, 2016), Association for Research in Otolaryngology (ARO; Baltimore, 2010)

Extracurriculars:
10 Seasons of Varsity Athletics: Cross Country, Indoor Track, Outdoor Track (2005-2009)
All -Academic, All-Region, and All-District Cross Country honors.

Chapter 1: Introduction

1.1 Adult Neural Stem Cells and Neurogenesis

Until the late 1960's, it was believed that ongoing neurogenesis, the process by which neural stem cells (NSCs) give rise to neurons, ended in the period just after birth. It was thought that neurogenesis did not persist in the adult mammalian central nervous system (CNS) [1]. The belief that neurons were static cell populations incapable of expanding or replenishing themselves was deeply entrenched [2]. Following reports providing evidence of adult neurogenesis compounded with the advent of new methods to study the adult CNS slowly changed this perception. For example, studies by Altman in the 1960s described adult neurogenesis following tritiated thymidine incorporation in the rat brain and suggested that adult born neurons were added in discrete locations [3-6]. These studies were largely ignored until many years later when the introduction of the thymidine analog, bromo-deoxyuridine (BrdU), and retroviral lineage tracing allowed for the identification of dividing cells in the CNS [7-9]. In particular, the discovery of adult neurogenesis and radial-glia like cells in songbirds by Nottebohm and colleagues laid the groundwork for future studies in adult neurogenesis [10, 11]. Later, the identification of cells from the mouse "striatum," tissue adjacent to the lateral ventricle, that could proliferate in vitro with the addition of growth factors renewed interest in the field of adult neural stem cells (NSCs) [12].

The NSCs isolated by Reynolds and Weiss formed free floating aggregates of cells called “neurospheres,” that expressed nestin, the intermediate filament protein found in neuroepithelial stem cells [12]. Furthermore, the neurospheres were able to produce both neurons and glial cells in vitro, highlighting the ability of NSCs to give rise to the principle cells of the CNS [13]. The discovery of neurospheres provided researchers an *in vitro* system to produce new neurons from adult mammalian brains in large quantities, allowing further investigation into NSC regulation and neurogenesis.

Adult NSCs are defined by their ability to self-renew and differentiate into all types of neural cells, including neurons, astrocytes and oligodendrocytes [14]. In vivo, the process of neurogenesis primarily occurs in two regions of the adult mammalian brain: the subventricular zone (SVZ) of the lateral ventricles [12] [15] and the subgranular zone (SGZ) of the dentate gyrus in the hippocampus [16]**.** These two niches are illustrated in **Figure 1** adapted from [15].

In a multi-step process, adult-born neural progenitors in the SVZ commit to a neural fate and become neuroblasts. Neuroblasts migrate from the SVZ through the rostral migratory stream (RMS) to the olfactory bulb (OB) where they differentiate into inhibitory interneurons [17, 18] [19]. In a similar process, newly generated neurons of the SGZ integrate into the immediately adjacent granule cell layer as dentate granule cells [19-22]. The SVZ serves as the richest source of stem cells constantly generating neurons destined for the olfactory bulb. In the adult SVZ-OB neurogenic cascade, it has been hypothesized that NSCs (also known as type B cells) give rise to rapidly dividing

progenitors (type C cells), and these neural progenitors (NPCs) give rise to proliferating neuroblasts (type A cells), which eventually incorporate into the existing functional circuitry of the OB [23, 24]**.** Moreover, it has been suggested that differentiation of type B NSCs into type A neuroblasts is a necessary amplification step and even small changes in cell cycle length or number of divisions can have significant effects on the number of neurons produced [25]. Therefore, every step of the neurogenic cascade is a tightly controlled process. Several studies have taken advantage of the cell cycle differences between SVZ cells. Infusion of the antimitotic drug, Ara-C, eliminates dividing type A and type C cells while the slowly cycling or quiescent NSCs are left intact. This method allows for studies of the regenerative properties of NSCs. The type B neural stem cells are not affected and are capable of replenishing the entire stem cell population as well as the lineage [26]. After Ara-C removal, type B cells begin dividing and within 2 days type C cells appear, followed by type A cells after another 2 days. Within 4.5 days PSA-NCAM+ migratory neuroblasts appear and are soon connected by chains [26]. An image of the SVZ stem cell niche containing the major cell types cells can be found in **Figure1.**

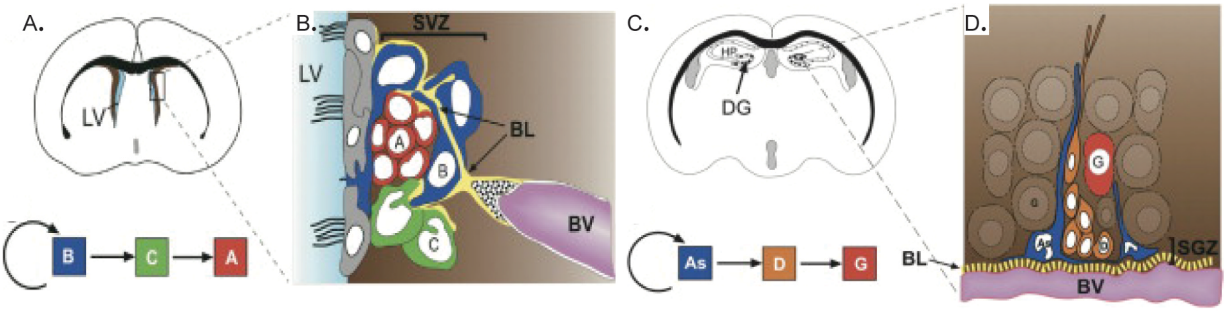

Reprinted from For the Long Run Maintaining Germinal Niches in the Adult Brain, Vol /edition number, Arturo Alvarez-Buylla,Daniel A Lim, 2004, with permission from Elsevier

Figure 1. The subventricular zone (SVZ) and dentate gyrus (DG) niche. A) Schematic Illustration of a coronal view of the SVZ located adjacent to the lateral ventricles B.) Zoomed in representative diagram depicting the architecture of the SVZ. B cells (dark blue) are the NSCs seen contacting the ventricle via a single cilium. C cells (green) are the rapidly dividing transit amplifying cells derived from B cells. The C cells give rise to neuroblasts or type A cells (red). Neuroblasts migrate to the olfactory bulb where they differentiate into interneurons. The basal lamina (BL) is shown extending from the blood vessels (BV) where it interfaces with cells in the niche C.) Coronal view of the dentate gyrus of the hippocampus. D.) Zoomed in view of the subgranular zone (SGZ). The stem cells (dark blue) give rise to progenitors or type D cells, which mature into granule cell neurons (type G cells) that integrate into the dentate gyrus layer. Blood vessels (BV) are located closer to the subranular zone layer.

More than 30,000 progenitors migrate from the SVZ into the olfactory bulb daily [27]. A diagram of neurogenesis from the SVZ to the olfactory bulb is shown in **Figure 2** [28]. In general, an RMS neuroblast can travel up to 720 μm per day [18]. The olfactory bulb is a multilayered structure consisting of the glomerular, external plexiform, mitral cell, internal plexiform, and granule cell layers (from closest to the brain surface to deeper layers) [29]. Once in the OB, progenitors that arose from the SVZ differentiate into granule and periglomerular neurons to replace older granule cells and maintain the OB network [30-32]. Early rat studies that traced the percentage of tritiated-thymidine positive cell in the granule cell layer of the adult olfactory bulb indicate that from the time of labeling in the SVZ to arrival in the GCL peaks at about 12 days [6]. More recently, studies using BrdU to label proliferating SVZ cells demonstrated newly formed Nestin-derived (Nestin::CFP) neuroblasts appearing in the core of the OB after 7 days. By day 14, more mature neurons appeared in the granule cell layer of the olfactory bulb and by day 31 the CFP+ cells had characteristics of mature neurons, such as synaptic spine formation and GAD67 and calretinin expression [33]. These newly integrated granule cells are able to form dendrodendritic synapses with the existing cells [34] and respond to odor stimulations [35, 36]. Moreover, lineage tracing (Nestin::YFP) showed a plateau of Nestin-derived cells in the OB after 12 months. Based on this and recombination

efficiency, the authors estimated that the majority of pre-existing granule cells in the OB are replaced by new neurons after 12 months [33]. This estimation is in line with previous observations that the size of the olfactory bulb does not vary considerably despite continued neurogenesis [37].

Interestingly, GCL recruitment of newly born interneurons differs from that found in the neonate. During the first postnatal week, newly formed cells are targeted to the superficial GCL, whereas adult-born cells are directed toward the deeper layers [38]. The superficial GCL cells have a much higher survival rate than the adult generated deeper cells, suggesting adult neurogenesis is important for processing newly encountered stimuli within the environment [39]. Moreover, superficial and deep granule cells display different electrophysiological properties [40]. In both the adult and the neonate, emerging cells in the OB are distributed evenly in the rostro-caudal axis, however, differences in the laminar organization suggests both common and distinct signaling molecules regulate early postnatal (or embryonic) and adult stem cell niches [38]. It is possible that the deep GCs and superficial GCs direct different components of olfactory information. Deep granule cells form dendrodendritic synapses with mitral cells while superficial granule cells direct tufted cell properties [41, 42]. Based on these differential contacts, Lemasson et al. suggested that the early born superficial granule cells might regulate odorant detection while adult born deep granule cells participate in mitral cell spike response to specific odors [38]. Moreover, the shorter-lived adult generated granule cells could contribute to fine tuning olfactory processes [38].

Within the SVZ, migratory neuroblasts form tangentially oriented chains wrapped by tunnel-like glial tubes formed by astrocytes that extend into the RMS [43]. Differences also exist between the neonate and the adult neuroblast chains. While migration along the SVZ-RMS-OB pathway begins at birth, the glial tube is not fully mature until 3 weeks after birth (post natal) [43-45]. Differences in tube formation could account for the finding (above) that adult newborn cells migrate to the OB faster than neonate cells [38]. Indeed, astrocytic release of molecules that promote neuroblast migration has been identified and may explain the altered migration speeds [46].

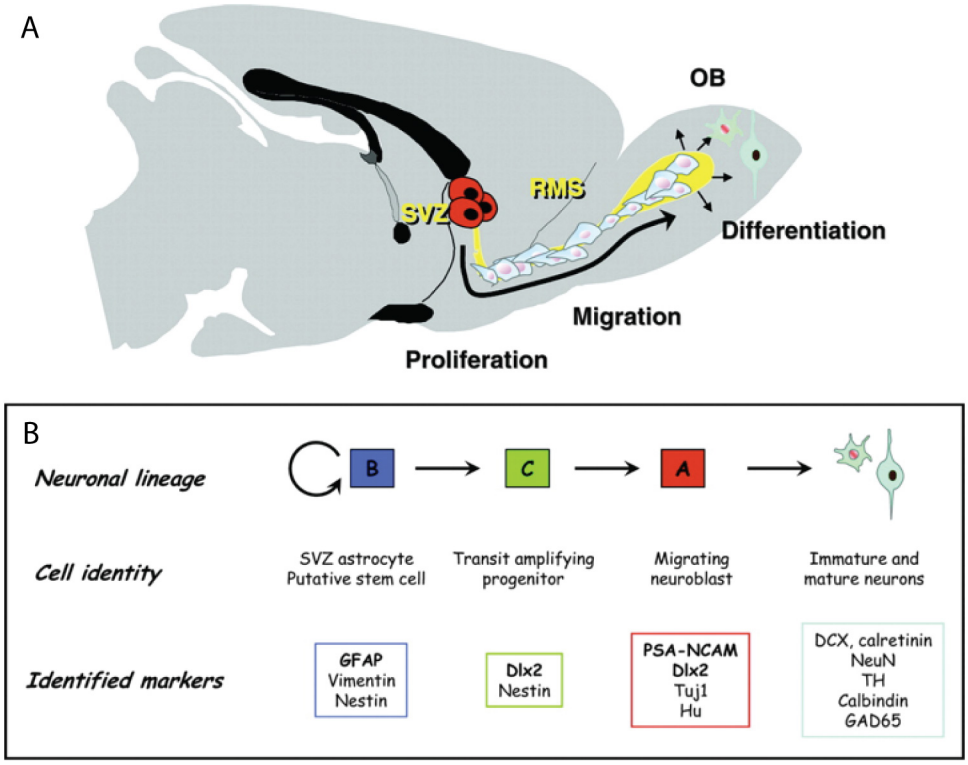

Figure 2. Neurogenesis in the subventricular zone (SVZ)/olfactory bulb (OB) system. A) Illustration of a sagittal view of the rodent brain showing the SVZ-RMS-OB axis. Proliferating cells in the SVZ migrate along the rostral migratory stream (RMS) to the OB where they migrate radially and terminally differentiate. B) Cells of the neuronal lineage with specific markers for identification are indicated. Permission not necessary. (Abrous, 2005).

The subventricular zone of the postnatal rat forebrain produces both glia and neurons, however, most gliogenesis occurs in the perinatal period [47]. During

gliogenesis, progenitors migrate from the SVZ into the white matter and cortex where they differentiate into astrocytes and oligodendrocytes. Progenitors can migrate in at least two directions, i) radially, where they subsequently generate glial cells or ii.) in a rostro-caudal direction to generate OB neurons [48]. Regional specification of the phenotype and destination of cells based on their origination in the SVZ has been identified. Initial retroviral lineage tracing demonstrated that the anterior SVZ generates the cells that ultimately differentiate into inter-neurons in the granule cell and periglomerular layer of the olfactory bulb [9]. However, additional studies showed that cells originating from positions within the full rostro-caudal extent of the SVZ migrate rostrally to reach the olfactory bulb at both adult and post-natal timepoints [47, 49]. Moreover, the dorsal SVZ was once thought to only provide astrocytes and oligodendrocytes to the overlying white matter and cortex while the ventral SVZ provided interneurons [50]. This was logical considering that during embryogenesis, the ventrally located ganglionic eminences generate the bulk of interneurons [50, 51]. However, GFAP+ fate mapping using a combination of retrogradely transported adenovirus and lentivirus, to control for diffusion, demonstrated the dorsal SVZ, in addition to the ventral portion, is capable of generating olfactory bulb inter-neurons [52].

Chemically distinct subpopulations of neurons exist in the layers of the OB. For example, within the glomerular layer three distinct populations of neurons exist, which can further be divided into subpopulations (calretinin, calbindin, and tyrosin-hydroxylase (dopamine) expressiong cells. Similarly, granule cells can be divided into deep, superficial, and calretinin positive cells [53-55]. Although OB interneurons can be

produced from the entire SVZ, each region gives rise to a specific subtype of interneuron [54]. For example, the majority of dopamine+ and calbindin+ periglomerular cells arise from stem cells located in the dorsal and ventral regions, respectively. Granule cell precursors demonstrate a similar regionalization. Interestingly, every region throughout the SVZ produces granule cells, however, dorsal regions are more likely to produce superficial granule cells, while ventral regions produce mainly deep granule cells. Therefore, the site of origin within the adult SVZ determines the specific markers and final position of postnatally generated interneurons [53, 56, 57].

To assess the functional significance of adult neurogenesis in the OB circuitry and the effect on different odor-mediated tasks, Breton Provencher et. al. designed a series of experiments. An in-depth analysis of the morphology, electrophysiology, and behavioral changes in the OB of mice following AraC treatment to abolish adult neurogenesis was performed. Osmotic minipump infusion of the antimitotic drug, AraC, for 28 days into the lateral ventricle inhibited neural progenitor cell (NPC) proliferation and ultimately prevented the generation and appearance of new neurons in the OB. Reduced olfactory neurogenesis had no effect on the pre-existing OB cells as evidenced by the unaffected granule cell density, dendritic arborization, and spine density. Interestingly, the main output of the OB, the mitral cell, displayed reduced inhibition and altered synchronization. As a functional consequence, mice with interrupted neurogenesis displayed reduced short-term olfactory memory despite normal odor detection, discrimination, and long-term associative odor memory. This

study provided a functional role for newly generated neurons in the OB circuitry and in some olfactory behaviors [58].

The working hypothesis for signaling in the OB is that inter-neurons sculpt mitral cell firing by lateral inhibition. This inhibitory input provides contrast enhancement between OB circuits and drive synchronous activity among groups of mitral cells. At the cellular level, suppression of neurogensis results in fewer inhibitory synapses on mitral cells. Therefore, feedback inhibition onto mitral cells is driven by adult neurogenesis to drive short-term olfactory memory formation. Results by Breton Provencher and colleagues, demonstrate that ongoing neurogenesis supplies the inter-neurons necessary to maintain proper inhibitory strength within the OB network [59]. A schematic depicting the OB circuitry is show in **Figure 3** [59].

Based on an OB cell's origin in the SVZ and relatively long path to its final destination in the OB, it is obvious that a number of factors in this process can affect neurogenesis. For example, NSC proliferation and lineage progression as well as progenitor differentiation and migration can all affect adult neurogenesis. Moreover, different external stimuli, such as learning, environmental enrichment, and exercise affect the rate of proliferation, differentiation, and survival of newborn neurons [60-62]. On the other hand, aging, disease, and occlusion of the nose can result in a reduction of newborn neurons [63, 64]. Remarkably, systemic perturbations can augment the decline in neurogenesis seen with age as evidenced in studies by Villeda et. al. They showed that exposing a young mouse to soluble factors present in the plasma of old mice

decreases hippocampal neurogenesis and impairs spatial learning and memory [65]. While the details are still being elucidated, it is clear that intrinsic and extrinsic factors cooperate to regulate many aspects of neurogenesis in the SVZ.

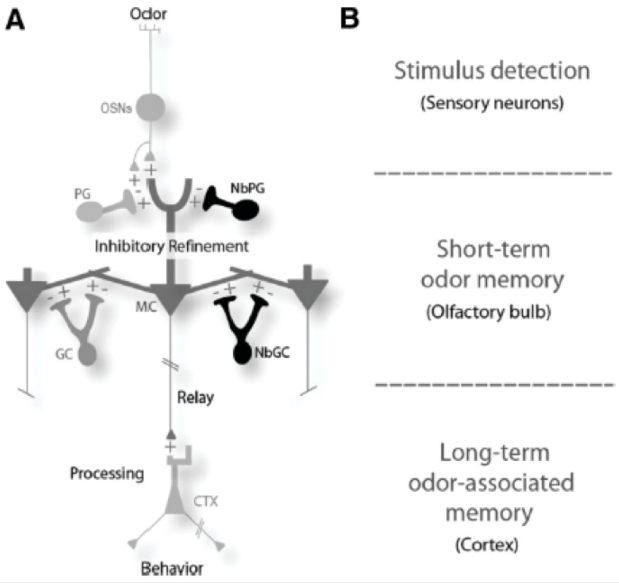

Figure 3. Adult neurogenesis modulates behavior by sculpting OB output. A) Adult neurogenesis provides the interneurons to maintain inhibitory feedback information onto mitral cells to drive short term olfactory memory. B.) Sites of information relay within the input-OB-output axis. (B.R. Arenkiel, 2010). Permission not necessary.

1.2 NSCs as a Promising Therapeutic Tool

The discovery of neural stem cells brought with it the concept of cell replacement for the purposes of functional recovery following CNS injury. The idea behind utilizing endogenous mobilization for repair is that NSCs generate neurons that must incorporate into the existing circuitry. Similarly, during the process of adult neurogenesis, newly born neurons are incorporated into existing circuits of the mature brain. By controlling this process, one can ultimately replace cells lost following injury or disease. Therefore, it is logical that by understanding NSC regulation during homeostatic conditions and the process of adult neurogenesis one can direct endogenous NSC recruitment or neuronal transplantation. Therefore, the study of adult neurogensis can guide therapeutic

strategy for endogenous mobilization or cell transplantation to replace cells lost due to neurologic disease. However, lessons learned in the rodent may not translate to the human. While new born neurons do appear to migrate from the SVZ to the olfactory bulb and cortex in humans, this process in is still debated in adults [66]. In adults, the "SVZ" consists of a ribbon of proliferating astrocytes that is slightly displaced from the ependymal layer by a hypocellular gap. Cells isolated from the wall of the adult lateral ventricle are capable of forming neurospheress in the presence of EGF and FGF, as well as generating astrocytes, neurons, and oligodendrocytes [67]. In vivo, these GFAP+ cells co-express with proliferation markers such as Ki67 and BrdU indicating they actively divide similar to rodent NSCs [67]. While these studies demonstrated that human astrocytes could function as neural stem cells, migrating neuroblast chains have not been identified, although neuronal precursor cells were found located between the ventricles and the OB [67, 68].

1.3 Defining Neural Stem Cells

Mechanisms directing NSC biology and the generation of lineage cells are only uncovered with proper identification of stem cells and their progeny. Hence, initial research into neural stem cell biology focused on the histology and identification of NSCs. The functional properties of stem cells, namely, their ability to self renew and differentiate can also serve to distinguish neural stem cells, retrospectively. NSCs share several properties with astrocytes such as expression of glial fibrillary acidic protein (GFAP), however, they contain stem cell properties of self-renewal and differentiation both in vivo and in vitro [24]. By cycling slowly and decreasing metabolic activity,

quiescent neural stem cells maintain the ability for prolonged self-renewal. Label retention assays using BrdU take advantage of this slow cycling to demarcate the quiescent cell populations within the SVZ [25]. This is contrast to the rapidly dividing progenitors which quickly dilute the BrdU label by dividing rapidly or leaving the niche within the chase period [69].

Since initial characterization began, Nestin expression has been considered a feature of NSCs during both development and in the adult [70, 71]. Nestin gene expression was first identified in the developing neuroepithelium of the neural tube where it “distinguished the stem cells from the more differentiated cells” [70]. Since its identification in rat neuroepithelial stem cells, Nestin has also been identified in the human and mouse [30, 72]**.** Based on its core domain structure and response to drug treatments, Nestin is classified as a type VI intermediate filament [70]. Of note, Nestin has been suggested to help coordinate changes in the intermediate filament network [72]. Expression of intermediate filaments themselves is not unique to neural stem cells. Rather, at transition steps during differentiation intermediate filament expression converts from one to another. For example, neurons express neurofilament, or peripherin and astrocytes express GFAP [70, 73, 74]. Functionally, loss of Nestin expression has no overt effect on the cytoskeletal network but does decrease self-renewal in conjunction with elevated apoptosis [75].

Nestin is expressed in proliferating neuronal stem cells and only after terminal differentiation is expression down regulated [74]. Additionally, expression has been

identified during regenerative processes and in progenitor cells in several tissue types including muscle, testis, and teeth [76-78]. Within the CNS, Nestin can be found in endothelial cells during developmental periods and in proliferating endothelial cells in the adult during angiogenesis [79, 80]. In the CNS, Nestin expression has also been identified in terminally differentiated ependymal cells [23]. Interestingly, expression can be re-induced in reactive astrocytes following injury [81]. However, Nestin immunoreactivity in glial cells after injury is distinct from stem and progenitor cell expression. Reactive astrocytes express Nestin in addition to the post-mitotic marker, S100β allowing for distinction [82]. These findings suggest that Nestin induction correlates with dynamic cellular changes to allow for structural remodeling.

Nestin Cre^{ER}/R26R-yellow fluorescent protein (YFP) mice have been successfully used to label Nestin-expressing stem cells and their progeny in the SVZ following administration of the estrogen ligand, tamoxifen (TAM). Tracking YFP+ cells after tamoxifen induced recombination in stem cells and their progeny revealed that the majority of Nestin+ cells become OB neurons with a greater percentage contributing to the granule cell layer (GCL) rather than the glomerular layer [30]. Interestingly, YFP+ cells in the OB increases up to 100 days after TAM administration before reaching a plateau. Within the SVZ, recombined NSCs are still present after 100 days. Twelve days following TAM administration, 97% of NSCs expressing GFAP and Sox2 with a radial glial morphology are recombined, demonstrating the usefulness of Nestin in identifying NSCs [30].

Since the identification of Nestin, various molecular markers have been used to identify stem cells and their progeny in vivo and aid in their purification. Compounding the identification of neural stem cells is the fact that many of these markers are also expressed on other cell types. For example, CD133 (Prominin), a transmembrane glycoprotein, is expressed on primary cilia of neural progenitors as well as ependymal cells while GFAP is found in NSCs as well as parenchymal astrocytes [83-86]. Co-expression of markers can be used to more specifically identify neural stem cells in both embryonic and adult brain tissue. For example, Nestin and the pluripotency transcription factor, Sox2, are widely used to identify neural stem and progenitor populations [87]. Also, co-expression of GFAP and CD133 has been used to distinguish stem cells from niche astrocytes. It has been observed that the relatively quiescent neural stem cells express GFAP. Once GFAP+ NSCs give rise to their progeny, the transit amplifying progenitor cells, GFAP expression is down regulated and the cells express Dlx2, a homeobox protein, Mash1, and epidermal growth factor receptor (EGFR) [88-90]. These progenitors generate neuroblasts expressing doublecortin (DCX) or PSA-NCAM, markers of neurogenesis, before their terminal differentiation into NeuN postive mature neurons [91-93].

In recent years, discovery of quiescent and activated stem cell pools and their potential to swap between these two pools was made possible with the identification of a GFAP+CD133+EGFR- quiescent (qNSC) population and a GFAP+CD133+EGFR+ activated stem cell (aNSC) population [94]. Of note, microarray analysis demonstrated that qNSCs actually express very low levels of Nestin mRNA. Codega and others

showed that only after activation do NSCs up-regulate both Nestin and EGFR expression [94]. These pools of qNSCs and aNSCs exhibit different functional characteristics both in vivo and in vitro. qNSCs divide slowly, leaving them resistant to anti-mitotic treatment. As a consequence, the qNSCs population is responsible for regeneration of the lineage after AraC treatment to eliminate the more actively dividing aNSCs and progenitors. Additionally, neuron generation is much slower in the qNSC population vs. the aNSC population as revealed by transplantation experiments. In vitro, qNSCs rarely form spheres, however, spheres that do form are large and able to generate neurons, oligodendrocytes, and astrocytes [94]. In the same study, gene analysis of qNSCs showed increased expression of transcripts associated with cell-cell adhesion, extracellular-matrix-response, and anchorage-dependent niche signals. For example, *VCAM1* expression was highest in qNSCs vs. both aNSCs and total SVZ tissue. In contrast, the aNSCs showed enrichment in genes associated with the cell cycle and DNA repair. Moreover, the transcriptome of qNSCs and aNSCs revealed differences in their energy requirements. Glycolysis and fatty acid genes were increased in qNSCs while aNSCs were enriched in oxidative phosphorylation and protein synthesis [94]. This study identified key elements in the maintenance of quiescence such as adhesion molecules and cell cycle regulation.

1.4 The Neurosphere Assay

The neurosphere assay, as first described by Reynolds ad Weiss, is often used to isolate, expand, and retrospectively identify NSCs [12, 95]. This assay is based on the analysis of a population of growth factor responsive cells. In the presence of

epidermal growth factor (EGF) and fibroblast growth factor (FGF), NSCs form free floating clonally derived spheres, whereas the more differentiated cell types die in culture. The neurosphere itself consists of cells embedded in a rich ECM. After passaging, reformation of the sphere is taken as a measure of the self-renewal capacity of the NSC population [96]. However, one must take into account the absence of the stem cell niche, which has a major impact on the identity of a stem cell [97, 98]. More recently, the sphere formation assays has been considered a means of evaluating the potential of a cell to behave as a stem cell outside its niche [96]. Altogether, the neurosphere culture allows for the study of NSC properties as well as the role of cell-cell and cell-extracellular matrix (ECM) interactions in directing those properties [99].

1.5 The Stem Cell Niche

Within the SVZ, two distinct domains have been identified i.) the apical domain, consisting of ependymal cells and quiescent neural stem cells and ii.) the basal domain, which consists of an elaborate vascular plexus and rich ECM [100]. The vasculature of the basal domain is tightly associated with mitotically active stem cells and transit amplifying progenitors whereas the dormant NSCs associate with the ependymal side [100]. Similar to their precursor, the radial glial cells, adult NSCs maintain apical-basal polarity. Via specialized apical processes containing a single primary cilium, B1 cells contact the ventricle while long basal extending processes contact blood vessels [101-103]. Therefore, NSCs are uniquely situated to receive cues from the CSF on one side and vasculature on the other.

At the apical SVZ, an *en face* view of the ventricular wall reveals a unique pattern. A characteristic pinwheel architecture is formed by ependymal cells situated around central clusters of NSCs [101]. It is thought that these contacts and the spatial organization are important for maintaining NSC properties such as self-renewal. Interestingly, when SVZ proliferation is stimulated the number of SVZ B1 cells making contact with the ventricle via an apical membrane increases [26]. On the other hand, lack of apical cell constituents seems to be associated with neuronal differentiation [104]. The apical membrane is enriched in prominin-1 (CD133), par-3, and junctional complexes [26] and may determine the symmetry of radial glial cell division [105].

The functional properties of stem cells, namely, their ability to self renew and differentiate, are not only important in maintaining homeostasis, but in providing cells for tissue repair. Crucial to the maintenance of NSC properties is niche control. The SVZ and dentate gyrus niche provide extracellular cues to regulate NSC behaviors such as self-renewal and differentiation [14, 24, 86]. NSCs interact with their microenvironment either through direct cell-cell contact, via an intermediate, or the release of a soluble mediator. In turn, external cues provided by the niche are integrated with cell intrinsic factors to direct NSC properties. The SVZ niche is a highly specialized microenvironment consisting of ependymal cells, type B1 NSCs, and their progeny (the transit amplifying progenitors and neuroblasts) [23]. In addition to the cellular constituents, the SVZ houses a rich vascular network and elaborate mixture of extracellular matrix (ECM) and adhesion molecules [100, 106, 107]. Together, these elements maintain the balance between quiescence (qNSC), self-renewal, and

activation (aNSCs) to ultimately direct lineage progression [97, 98, 108, 109]. Additionally, it is thought that specific cues provided by the environment influence the total number of NSCs and timing of lineage progression [110].

The importance of the ECM in directing stem cell properties was previously demonstrated in experiments where organs were de-cellularized, leaving only the ECM intact. When stem cells are seeded on the ECM-only scaffolds, they are guided by the tissue type to differentiate into cells specific for the tissue of origin [111]. Additional evidence for the significance of the ECM comes from studying the aging brain. ECM aging can occur via excessive protease activity or the release of free radicals that degrade the matrix [112]. For example, fibroblast expression of the matrix metalloproteinase-1 (MMP-1) within the dermis significantly increases with age and leads to fragmentation and disorganization of collagen fibrils. As the major structural protein in connective tissue this has adverse effects on the organism [113]. Moreover, the senescent cells themselves alter cell-ECM communication by either altering their own secretion of ECM containing altered protein composition or modifying their protease activity. Overtime, degradation of the ECM can weaken cell-ECM interactions. [113]. These changes can modify proliferation or differentiation. For example, when mesenchymal stem cells (MSCs) acquired from senescent adherent cultures are seeded on the ECM from young MSC spheres, pluripotency markers increase and differentiation potential is improved [112].

Within the SVZ, the ECM consists of laminin, collagen IV, fibronectin, syndecan, agrin, etc. These ECM components are highly expressed and their receptors can be found on NSCs, progenitors, and neuroblasts [98, 114]. Expression of both receptors and ECM is finely tuned to govern NSC properties to control neurogenesis [115]. For example, laminin is expressed throughout the SVZ [102]. Interestingly, laminin rich hubs have been identified in the ependymal layer. By P21, the laminin hubs localize to ependymal cell borders and near the center of pinwheels [116]. This unique distribution indicates an essential role in directing NSC properties. In particular, laminin expressed in the ECM surrounding blood vessels is necessary for NSC adhesion in the basal niche [102]. NSCs can also associate with basal lamina projections that extend from the vasculature to the ependymal surface referred to as fractones. These fractones are enriched in laminin [117] as well as proteoglycans [118]. Heparan and chondroitin sulfate proteoglycans, can present growth factors to NSCs to regulate proliferation and differentiation [119-121]. Heparan sulfate proteoglycans (HSPGs) are present on the cell surface (i.e. syndecans and glypicans) and as secreted ECM molecules (perlecan, agrin, and collagen type XVIII). By functioning as a co-receptor for growth factors, heparan sulfate (HS) facilitates ligand-receptor binding to lower the threshold for signal activation and modify the duration of growth factor response. The best-characterized example of HS dependent ligand-receptor interactions is in modulation of FGF2 binding and signaling. Additionally, HS chain dependent signaling has been described for BMP, Wnt, hedgehog, PDGF, and VEGF. HS signaling is finely tuned by the sulfation profile. For example, neuroepithelial HS sulfation pattern changes as the cells start to differentiate, resulting in a switch from FGF2 to FGF1 signal potentiation. Moreover, HS

chains facilitate cell-ECM contacts and migration. By serving as receptors for proteases and protease inhibitors HS can regulate sheddase activity and distribution (reviewed in [119]). The SVZ is additionally enriched for chondroitin sulfate proteoglycans (CSPGs). Inhibition of the enzyme chondroitinase ABC (ChABC) to degrade the CSPG glycosaminoglycans in vitro results in decreased proliferation and neuronal differentiation. In vivo, ventricular injections of ChABC during embryogenesis similarly results in decreased radial glia proliferation and inhibition of neurogenesis [122]. These results identify the ECM constituents as crucial factors in NSC maintenance as well as neurogenesis.

Recent studies have demonstrated that loss of NSC interactions with niche elements can alter NSC self-renewal and proliferation [102, 123]. For example, N-cadherin and vascular adhesion molecule 1 (VCAM-1) have been implicated in maintenance of qNSC positioning at the ventricular wall while EGFR and CXCR4 promote activation and translocation towards the vasculature [123, 124]. More specifically, VCAM-1 expression has been localized to the apical endfeet of NSCs at the center of pinwheels [123]. Interestingly, the in vivo polarization of VCAM-1 is maintained in vitro, where it localizes in culture to adult GFAP+ cells. Delivery of VCAM-1 blocking antibody via osmotic minipump infusion into the lateral ventricle results in disordered pinwheel architecture within the apical niche and an increase in GFAP+ cell proliferation. Blocking antibody infusion also results in disrupted neuroblast chains with bare areas and uncharacteristic DCX-positive clumps. Overlap between Nox2 and VCAM-1 expression prompted Kokovay and colleagues to suggest that cells rich in VCAM-1 are also rich in oxidative phosphorylation, which has been identified as

important for NSC maintenance [123]. Interestingly, infusion of cytokines such IL-1β increase VCAM-1 expression [123]. Based on the robust effect of VCAM-1 on niche structure and NSC maintenance, it would be interesting to identify additional factors that regulate VCAM-1 expression and subsequently NSC maintenance in the SVZ.

Based on the close proximity of the SVZ to the CSF, it is logical that the contents would influence cells in the apical domain via direct interactions. B1 NSCs found adjacent to the ependymal cells extend a long primary cilium that is able to contact the CSF [101]. B1 cells also contact one another and ependymal cells via gap and adherens junctions physically linking adjacent cells [101]. While activated (B2) NSCs are located closer to the striatal side of the niche and do not make direct contact with the CSF, it is plausible that factors are able to diffuse through the niche to influence B2 cells [125]. The composition of the CSF is largely determined by the choroid plexus secretome which provides proteins and small molecules that can reach the SVZ either directly, by diffusion, or by signaling to the ependymal cells which are in contact with other cell types [125, 126]. The choroid plexus is a monolayer of epithelial cells found within the walls of the ventricles that receives an astonishing 10 times higher blood flow than the adjacent brain parenchyma [127]. In addition, CSF itself is able to promote primary and secondary neurosphere proliferation and maintenance in vitro [128]. An example of CSF regulation of SVZ cells, is the apically localized Igf1R on NSCs, which responds to Igf2 in the CSF to promote progenitor proliferation in an age-dependent manner. Peak Igf2 activity occurs in the embryonic CSF and decreases into adulthood [129]. This and other studies identified the CSF as an important regulator of NSC

maintenance. Moreover, the CSF contains a number of additional factors produced by the choroid plexus including FGF, EGF, TGF-alpha, and PDGF to name a few [125].

NSCs must also integrate cues from either the perivascular ECM or soluble factors released by the vasculature [101, 102]. For example, endothelial cell derived SDF1, promotes vascular homing in a CXCR4 dependent manner by up-regulating expression of EGFR and alpha6integrin (α6β1) in activated NSCs and type C cells. By promoting the activated state and expression of adhesion molecules, SDF1 is able to support progenitor occupancy in the basal niche [124]. On the other hand, neuroblasts respond to SDF1 by increasing niche exit and migration to the OB. Hence, differential response to SDF1 promotes residency within the niche and neurogenesis [124].

In addition to the ECM and CSF components, adhesion molecules within the SVZ regulate NSCs. The standard view of adhesion molecules and their role in SVZ architecture is that they retain stem cells in the niche, and in this manner serve a support function. Recent literature, however, point towards a more dynamic role for these interactions in all features of NSC-niche contacts. Adhesion molecules appear to direct retention, division, and SVZ exit [130]. Interestingly, differential activity of two adhesion molecules, cadherins and integrins, can regulate whether a division will be asymmetric or symmetric based on partitioning of apical membrane components, thus governing whether a division is neurogenic or proliferative [131]. In neuroepithelial cells, a cadherin-negative prominin-1 positive segment referred to as the “cadherin hole” is used to identify the apical membrane of a single cell [132]. A switch from proliferative to

neurogenic division is associated with symmetric vs. asymmetric distribution of the apical plasma membrane, respectively [132].

Cadherins are calcium -dependent homophilic adhesion receptors that are traditionally thought to mediate cell-cell contact and polarity [133, 134]. Several types of cadherins are expressed in the CNS. N-Cadherin has been implicated in a number of processes and has since become of interest in directing both NSC and neuronal properties. For example, a role for N-Cadherin has been identified in maintaining NSCs at the ventricular wall and in neuronal migration [135, 136]. Over-expression of N-cadherin in NSCs increases anchorage to ependymal cells therefore promoting their quiescence, whereas, loss of N-cadherin is though to promote NSC activation. Once NSCs lose contacts to the ventricular wall, they are able to respond to additional cues from the blood vessels resulting in translocation to the basal niche [135, 137]. Meanwhile, trafficking of N-cadherin to the cell surface directs neuronal migration during development [136]. However, blockade of endocytic trafficking of N-cadherin by inhibition of Rab5 and Rab11 results in increased cell surface N-cadherin. The defective neuronal migration caused by loss of Rab –GTPase activity is rescued by partial knockdown of N-cadherin indicating a proper balance of N-cadherin is necessary for neuronal migration [138]. Similarly, E-cadherin in the Drosophila gonadal stem cell niche is important for retention of gonadal stem cells (GSCs). Loss of E-cadherin in GSCs leads to detachment from support cells and “drifting away” [139]. On the other hand, GSCs over-expressing E-cadherin displace stem cells expressing lower levels of E-cadherin suggesting that cadherin expression levels direct niche occupancy.

Therefore, adhesion molecule expression provides a mechanism for niche anchoring as well as displacement of differentiated or dysfunctional stem cells [140].

Additionally, the integrin, α6β1, and its binding partner, laminin, appear to have multiple roles in the ultimate emergence of neurons in the olfactory bulb. As neuroblasts travel from the anterior SVZ to the olfactory bulb, α6β1 expressed by the neuroblasts maintains the direction and cohesiveness of cells within the RMS. Injections of neutralizing antibodies against either the α6 or β1 integrin subunits above the RMS leads to disruption in the migratory stream while intact laminin injected as a tract acts as a chemoattractant to draw cells away from the normal RMS-OB axis [141]. These studies demonstrated a role for both the integrin and its ligand in controlling neuroblast migration. Integrin binding also plays a role in stem cell maintenance. In the SVZ, both neuroblasts and NSCs are in close contact with laminin expressing blood vessels and express α6β1 [102]. Shen and colleagues demonstrated that α6β1 is a major regulator of this association. To test this interaction in vitro, neurospheres were plated on top of a monolayer of endothelial cells in the presence of GoH3 antibody to block α6β1 binding to laminin. Almost half of the neurospheres plated in the presence of the blocking antibody did not attach compared to control antibody treated cells. Additionally, in vivo blockade of α6β1 resulted in S phase+ progenitor cells moving away from the vascular surface [102]. These studies demonstrated that α6β1 integrin-laminin interactions retain NSCs in the vascular niche and direct neuroblast migration to the OB. Moreover, these studies show that expression of cell surface proteins is tightly controlled and appear to correlate with NSC positioning within the niche [88, 97, 109, 123, 124, 135, 142].

1.6 Growth Factors Regulate NSC Properties

Despite progress in the field, the molecular mechanisms of NSC maintenance in the adult mouse brain are still largely undefined. Intriguingly, NSC maintenance declines with age resulting in fewer NSCs and subsequently, a decrease in OB neurogenesis. Based on this observance, the study of aging mice could serve as a useful tool to study NSC maintenance [143, 144]. Several studies have highlighted a role for mitogens such as epidermal growth factor (EGF) and fibroblast growth factor (FGF) in directing NSC proliferation. An FGF2 response is evident by E8.5 while EGF response does not appear until E14.5 due to lack of EGFR expression on NSCs until later in development. The majority of cells in the adult SVZ express both the FGF-R (receptor) and EGF-R. However, the two growth factors appear to regulate the cell cycle differently. EGF promotes symmetric division and expands the NSC pool compared to FGF2 [145]. Differences in growth factor response were identified in vivo, as well. For example, after two weeks of intracerebroventricular administration, both EGF and FGF increase the progenitor population. However, FGF-2 increases the number of newborn neurons in the olfactory bulb while EGF increases the production of astrocytes at the expense of newborn neurons reaching the olfactory bulb [146]. While these studies highlighted a role for mitogens in NSC regulation, others have emphasized signaling pathways in NSC maintenance [12, 13, 88, 145, 147]. For example the Notch, Wnt/B catenin, Sonic Hedgehog, and bone morphogenetic protein (BMP) signaling pathways direct self-renewal and maintenance of the stem cell pool and the composition of the SVZ niche [148-152].

Interestingly, NSCs, themselves, can regulate their own properties and their surrounding microenvironment via proteolytic processing of ECM and/or adhesion molecules. A number of ECM, adhesion molecules, and growth factors serve as substrates for proteases that include the matrix metalloproteins and proteins containing a distinegrin and metalloprotease domain (ADAMs family) [153]. As mentioned, NSCs and NPCs rely on molecules such as EGF, FGF, transforming growth factor receptor, and Notch-1 for proper self-renewal and proliferation [146, 154, 155]. Activation of several of these molecules requires extracellular cleavage by metalloproteases. By regulating cell surface protein expression, protease activity modifies their function to direct cell-cell adhesion as well as inter- and intra-cell signaling events [156]. A role for regulated proteolysis of ECM and cell surface receptors has increasingly been recognized as a means of directing stem cell properties such as adhesion, migration, and proliferation within the SVZ [142, 157-159].

1.7 Proteases Regulate Stem Cells

Porlan et. al. demonstrated that loss of the membrane-type metalloproteinase, MT5-MMP, maintains anchorage of NSCs to the apical niche by promoting N-Cadherin adhesion to ependymal cells. In vivo, lentiviral mediated over-expression of MT5-MMP activity increased cycling NSCs as evidenced by GFAP+Ki67+ staining as well as the number of LRC-BrdU+ cells in the olfactory bulb. The authors suggest that preventing MT5-MMP activity or over-expression of N-cadherin, promotes NSC anchorage to ependymal cells whereas the opposite signals promote NSC activation and subsequent translocation towards the blood vessels in the basal niche. Additionally, they show that

not only is MT5-MMP required for proper activation of NSCs under homeostatic conditions, it is necessary for niche reconstitution during regenerative conditions [135]. This study highlighted a role for proteases as well as adhesive interactions in regulating niche architecture and NSC properties. In addition, several other proteases have been identified to regulate NSCs and neurogenesis.

Matrix metalloproteins (MMPs) are members of the metazincin family, which includes ADAM proteins and ADAMs with thrombospondin motifs (ADAMTS). ADAMs, named for their disintegrin domain and protease domain, have been identified as crucial regulators of a number of biological processes. ADAMs are type I transmembrane proteins containing a zinc dependent protease domain, a disintegrin domain, a pro-domain and a short membrane-proximal domain (MPD) [160]. ADAMs are often first expressed as a zymogen, and only after removal of the prodomain do they become catalytically active. For example, the prodomain cleavage of ADAM10 is accomplished by the proprotein convertases (PC), PC7 and furin, within the trans-golgi network [161].

ADAMs exert their function via ectodomain shedding of a number of substrates known to promote neurogenesis in the SVZ [154, 156, 162, 163]**.** The functional consequence of substrate cleavage can lead to the release of soluble agonist/antagonists (i.e. TNF-alpha) or activate intracellular signaling by promoting the release of an intracellular fragment (i.e. Notch) [160]. ADAMs may also play a role in cleavage-dependent inactivation of proteins. For example, ADAM10 sheds ephrins therefore inactivating the ephrin/Eph complex [164, 165]. Alternatively, ADAMs can

serve a degradation function by shedding ECM. For example, ADAM13 regulates neural crest migration by cleaving fibronectin [166].

'A disintegrin and metalloproteinase 10,' ADAM10, is of interest due to its demonstrated function in a number of stem cell niches. In the intestinal stem cell niche, the protease ADAM10 was shown to act cell autonomously to direct progenitor cell lineage specification [156, 167]. Loss of ADAM10 on the basolateral side of epithelial cells in the developing and adult intestine results in perinatal lethality in a constitutive deletion model or death within 9 days of tamoxifen induced ADAM10 deletion. Histological analysis revealed altered intestinal morphology with blunted villi and a hypocellular epithelium after loss of ADAM10 activity. More importantly, there was a decrease in the number of proliferating cells resulting in the loss of cell density. This study highlighted Notch signaling as the principle pathway affected. While no changes were observed in *Notch1*, *Notch2*, *Dll-1* and *Dll-4* mRNA levels, downstream gene targets were altered [167]. Another study pointed to a role for ADAM10 in epithelial cell sorting [157]. The authors show that ADAM10 is required for EphB/ephrin-B-mediated cell compartmentalization. Moreover, they hypothesize that the EphB-E-cadherin-ADAM10 complex with ephrin-B ligands creates a recognition module for cleavage of E-cadherin to target cells for destruction [157].

A role for ADAM10 was additionally identified in porcine stem cell development. During porcine stem cell development, ADAM10 knockdown results in decreased adherens and tight junction expression, which deregulates the stability of cell-cell

junctions [168]. By interacting with CXADR, ADAM10 was demonstrated to regulate tight junction assembly during porcine embryo development. Interestingly, it was hypothesized that ADAM10 is actually a component of the tight junction complex in addition to its sheddase function [168]. Each of these studies identified a distinct substrate mediating a phenotype downstream of ADAM10.

1.8 ADAM10 in the CNS

ADAMs were initially characterized in the testis, however, recent evidence has highlighted a critical role for ADAMs in neural development. In particular, the embryonic lethality of ADAM10−/− mice at embryonic day (E) 9.5 due to major defects in development of the cardiovascular system and CNS highlighted ADAM10 as a critical mediator of neurodevelopment and neural progenitor proliferation [169]. Analysis of ADAM10 mRNA in human and mouse brains showed that two alternatively spliced mRNAs are present in humans. One is the “long” form that encodes a full-length precursor protein, and the second is a “short” form, encoding the precursor protein that ends after the disintegrin domain. Mouse brain tissue, however, only expresses the full-length form [170]. In another study, ADAM10 mRNA was widely expressed within structures of the telencephalon including the olfactory bulb and hippocampus, the diencephalon, the mesencephelon, and the cerebellum [171]. The wide expression in the CNS suggests a role for ADAM10 in a variety of processes including cell adhesion, signal activation of surface proteins, or ECM remodeling.

ADAM10, a transmembrane protease with alpha-secretase activity, has a number of identified substrates, of which Notch and amyloid precursor protein (APP) are well characterized [172, 173]. Notch signaling and the participation of ADAM10 in initiating this signaling was demonstrated to mediate neurogenesis via cell fate decisions [174]. First, Notch precursors are cleaved in the trans-golgi network by a furin-like protease at the S1 site. ADAM10s involvement in Notch activation involves release of the extracellular domain following cleavage at the S2 site. After S2 cleavage, a gamma-secretase is able to cleave the intracellular domain at the S3 site. Once freed, the Notch intracellular domain (NICD) translocates to the nuclease where it can regulate gene expression. The downstream effectors maintain neural stem and progenitor cells in an undifferentiated state [175, 176]. While some studies have named ADAM10 as the major Notch sheddase, others have pointed towards the closely related ADAM17. Mounting evidence suggests ADAM10 may be important for ligand-independent Notch activation whereas ADAM17 may be the primary protease in ligand-dependent signaling [177]. Interestingly, ADAM10 activity can also down-regulate Notch signaling via ligand shedding [178-180]. The antagonistic signaling could explain why mice studies did not identify a physiological role for ADAM10 in directing Notch activity in vivo [181, 182]. Moreover, the regulated intra-membrane proteolysis (RIP) of the ADAM10 substrates Notch, APP, and N-cadherin by the related proteases ADAM8, ADAM9, and ADAM17 (TACE) has been demonstrated [172] [158, 169, 183].

In another other study, mice deleted of the *Adam10* gene under the CAMKII-Cre promotor to target neurons in the cortex and hippocampus resulted in premature

neuronal differentiation and a reduction in the pool of proliferating NPCs in the dentate gyrus. Furthermore, the cKO mice displayed an age-dependent decrease in granule neurons due to early depletion of the NPC pool. These mice showed deficits in both learning and memory [173]. This study identified a reduction in the Notch target genes *Hes1, Hes5, Hey1, and Hey2*, and attributed the cellular changes to reduced Notch processing [184].

In further support of a role for ADAM10 in CNS function, conditional knockout (cKO) of ADAM10 using a Nestin-Cre driver to target NSCs and NPCs resulted in late embryonic lethality. Mice died perinatally with a disorganized neocortex and reduced ganglionic eminence due to precocious neuronal differentiation that, once again, depleted the progenitor pool. By E17.5, there was a decrease in the number of NeuN+ cells in the cortex and ganglionic eminence in ADAM10 cKO mice compared to controls. Based on results demonstrating scattered labeling and increased post-mitotic neurons in the intermediate zone, Jorissen et.al. suggested ADAM10 plays a role in cortical layering and neuronal migration. This study identified disrupted Notch-1 processing as responsible for the neurogenic phenotype while also highlighting a role for reduced APP processing [185].

More recently, a role for ADAM10 in embryonic neuronal radial migration has been described. While Jorissen et. al showed defective migration in neurons following deletion in progenitors, the effect of ADAM10 on migrating neurons required more specific Cre drivers. Yang et. al. suggested ADAM10 could provide a strategy for

newborn neurons to sense the external microenvironment and direct intracellular migratory machinery. Using a Dcx-Cre promotor to delete ADAM10 in neuroblasts, Yang et. al. explored whether RIP dependent or independent signaling mechanisms direct newborn neuron migration. They showed ADAM10 promotes the expression of microtubule associated protein (MAP) genes, such as Dcx, by cleaving Notch and initiating NICD signaling. In their mouse model, neuroblasts depleted of ADAM10 lead to deficient motility and altered microtubule structure (reflected by a decrease in Dcx expression) at developmental time points. Over-expression of Dcx rescued migration while replenished NICD levels also mitigated the defect placing the migration deficit downstream of Notch signaling [186]. However, a role for membrane receptors and cell-cell adhesion molecules such as ephrins and cadherins has been identified in the regulation of motility [187, 188].

For example, our group showed that ADAM10 regulates migration of adult NPCs from the SVZ into demyelinated lesions during CNS injury via N-cadherin cleavage [189]. Demyelinating injury to the subcortical white matter results in the secretion of EGF and TGF-alpha ligands that activate EGFR signaling. This signaling activation subsequently results in increased ADAM10 activity that promotes N-Cadherin shedding. Ecto-domain cleavage of N-cadherin by ADAM10 results in polarization and migration towards the site of injury. Taken together with evidence from studies during development, ADAM10 appears to play a critical role in directing NSC properties, however, the early embryonic lethality in cKO mice has masked investigation of processes regulated by ADAM10 in the adult.

1.9 Cell-Cell Interactions Direct NSC Properties

In vivo, NSCs and NPCs but not differentiating cells are arranged in cluster-like configurations around radial glial cells in the developing brain and around blood vessels in the adult SVZ (see **figure 4**) [190]). It has been hypothesized that the in vivo clustering can act to spatially limit local interactions between specific cell types or access to particular factors [190]. Likewise, dissociated subventricular tissue grown in the presence of growth factors form free-floating clusters of cells capable of expanding for upwards of 6 months in vitro. The sphere itself is comprised of stem and progenitor cells embedded in a rich ECM. Within the spheres, NSCs form the outer layer while the center consists of differentiating neural progenitor cells (NPCs). This unique clustering of cells is thought to maintain stemness, survival, and proliferative properties in vitro [99].

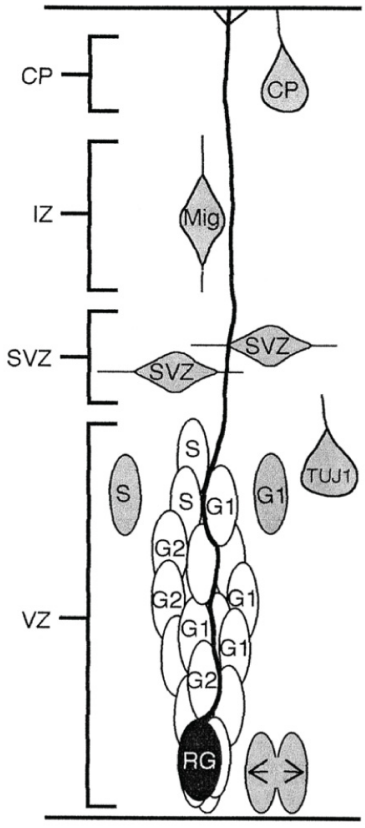

Figure 4. Diagram depicting the cellular clusters in the VZ. Clusters are organized around radial glial (RG) fibers and contain cells in G1, S, and G2. Shaded cells are not part of the clusters. Reproduced with permission (Bittman K., 1997).

Cell-cell interactions are regulated via direct interaction of adhesion receptors on opposing cells. NSCs express a number of well-characterized receptors such as integrins and cadherins that play a role in cell-cell as well as cell-ECM adhesion. For example, loss of E-cadherin in Nestin positive cells leads to defects in NSC self-renewal due to loss of cell-cell adhesion [191]. Additionally, by

binding its laminin counterpart, beta 1 integrin plays a role in neuroblast chain migration in the RMS [192]. Other proteins involved in neurogenesis include connexins (Cx), the proteins that form gap junction channels. Connexins have been demonstrated to connect proliferating NPCs aiding in their synchronization, and consequently, regulating neurogenesis. In particular, the gap junction Cx43 is expressed at high levels in progenitors in response to bFGF. Cx43 expression decreases as the cells differentiate into neurons or when bFGF is removed [190] [193]. These short-range factors can create locally restricted microenvironments to control the number and type of NSC division, thereby affecting the type of daughter cells produced [191]. Despite the vast majority of adhesion/junction molecules previously described, the full repertoire of molecules expressed in NSCs is still undefined [99, 194].

Another class of receptors, the tight junction proteins (TJPs) which consist of occludins, claudins, and junctional adhesion molecules (JAMs) not only connect adjoining cells, they also link to the actin cytoskeleton via the accessory/anchoring proteins ZO-1, -2, and -3. Considering that TJ complexes can respond to intracellular changes rapidly by changing their sub-cellular distribution, gene expression, or post-translational modification, they represent an interesting target for transducing extracellular cues into intracellular signaling programs [195-197]. Studies by Watters and colleagues showed down-regulation of the TJPs, ZO-1, occludin, claudin-1, -3, and -5 as differentiation of NSCs into neural lineage cells proceeds. ZO-1 knockdown leads to disruption of tight junction formation and subsequent loss of the stem cell marker

Nestin. These results suggest that TJPs play a role in neuronal differentiation and stemness programs [198].

Within the apical domain of the SVZ, ependymal cells form the characteristic pinwheels sourrounding B1 NSCs. Based on this unique configuration, it has been suggested that these cells must contain specialized intercellular junctions [101]. Electron microscopy analysis demonstrated tight junction expression between B1 cells (B1-B1), between ependymal cells (E-E), and between B1 NSCs and ependymal cells (B1-E) suggesting that tight junctions characterize cell-cell adhesion between cells in the apical SVZ niche [101]. Therefore, both cell-cell and cell-ECM interactions are able to direct NSC properties.

1.10 Junctional Adhesion Molecule C (JAM-C) Promotes Adhesion and Signaling

Another member of the TJPs are the junctional adhesion molecules (JAMs). JAMs are members of the immunoglobulin sub-family that include JAM-A as well as the related molecules JAM-B and JAM-C [199-204]. JAMs are characterized by two extracellular Ig domains capable of both homophilic and heterophilic interactions, a transmembrane region, and a short cytoplasmic domain [205, 206] (see **figure 5** [207]). These functional domain, allow JAMs to not only interact with extracellular binding partners, but also intracellularly with tight junction associated proteins. Extracellular ligands include the β1 integrin, α4β2, as well as LFA-1 and Mac-1, both β2 integrins. The intracellular proteins ZO-1, AF-6, MUPP1, and PAR-3 that bind tight junctions have also been implicated in cell polarity, allowing for a second mode of signaling [208].

Considering these potential pathways, it is tempting to consider that extracellular signals could be transduced intracellularly to govern cell properties such as polarity via tight junction initiated pathways.

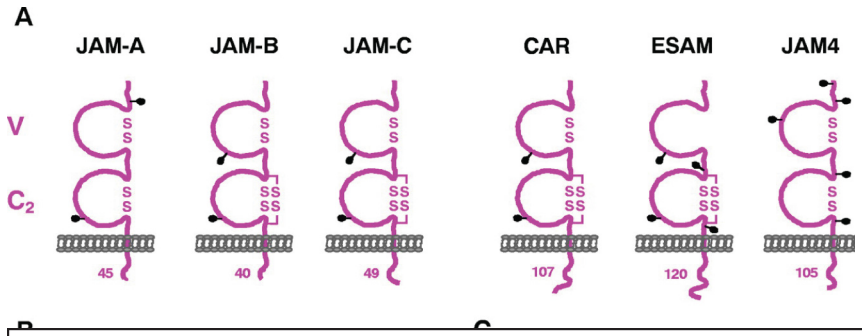

Figure 5. The Immunoglobulin-superfamily is present at tight junctions. Members contain a membrane-distal V-type Ig-domain and a membrane-proximal C2-type Ig-domain. Putative N-linked glycosylation sites are illustrated by dots. Disulfide bridges and putative additional intramolecular disulfide bridges formed by conserved cysteine residues in the C2-type Ig-domain are indicated. The sizes of the cytoplasmic domains are indicated at the bottom of each molecule. Reproduced with permission. (Ebnet, K., 2004).

A role for the junctional adhesion molecule JAM2 has been discovered in the CNS where it was demonstrated to mediate neuronal to oligodendrocyte signaling. An important question in the field of oligodendrocyte myelination is how axonal targets are discriminated [209]. By comparing the transcriptome of dorsal root ganglion neurons (DRG), which lack true dendrites, with spinal cord neurons (SCN) via next generation sequencing, Redmond et. al. identified increased *JAM2* expression in SCN somatodendritic compartments compared to DRG cell bodies [210]. This study identified SCN JAM2 as necessary and sufficient to inhibit oligodendrocyte myelination. In vitro addition of JAM2-Fc in oligodendrocyte/SCN co-cultures reduced myelin formation while WT oligodendrocytes co-cultured with SCNs from JAM2-KO mice resulted in increased myelination. Similar changes were observed in vivo using the JAM2-KO mice [210]. This study highlighted a role for junctional adhesion molecules in CNS function.

Junctional adhesion molecule C (JAM-C) directs multiple biologic processes in stem cell niches such as in the hematopoietic stem cell (HSC) niche. HSCs reside in the bone marrow niche where adhesive interactions with the surrounding stromal cells maintain their quiescent properties. Arcangeli and colleagues showed that JAM-C expressed by HSCs interacts with JAM-B on the surrounding stromal cells, but this interaction is lost as HSCs differentiate. They also show *jam-b* deficient mice present with an enhanced response to mobilizing agents, consistent with JAM-B/JAM-C interactions serving to reduce HSC niche egress during mobilization [211]. Furthermore, addition of a blocking antibody directed against JAM-C promoted HSC mobilization and blocked progenitor cell homing to the bone marrow niche [212]. These results correspond with a model in which adhesion molecules, specifically JAMs, are involved in stem cell retention in their niches by anchoring stem cells to the niche.

Additionally, a role for JAM-C has been identified in the polarization and differentiation of round spermatids by acting upstream of a cell polarity complex. While the majority of *Jam-C*$^{-/-}$ pups die at early postnatal developmental timepoints, roughly 40% survive. However, the viable males are infertile presenting with a 50 % reduction in testes size and inhibited differentiation of round spermatids into elongated spermatids. The authors of this study conclude that engagement of JAM-C at the spermatid-sertoli cell junction promotes spermatid polarization by recruiting the cell polarity complex proteins Par6, Cdc42, PKCλ and PATJ [213]. This study highlighted a role for JAM-C in regulating adhesion and polarity in stem cell niches.

Initially, JAM-C expression was described on vascular and lymphatic endothelial cells, but has since been identified on a number of cell types including cells of the CNS and PNS [213-217]. This is in contrast to previous studies describing the absence of JAM-C expression in the CNS [218, 219]. To date, a role for JAM-C in CNS function has been increasingly accepted as an important regulator of brain development and CSF homeostasis. In addition to the fertility issues, *JAM-C*$^{-/-}$ mice develop hydrocephalus in addition to disrupted cortical layering and a deficiency in pyramidal cell differentiation. However, the hydrocephalus is not a consequence of the vascular function of JAM-C as re-introduction of endothelial specific JAM-C does not rescue the defect [217]. Interestingly, an autosomal recessive disordered caused by a JAM-C mutation was found in a family from the United Arab Emirates. Affected family members develop similar problems as those observed in the *JAM-C*$^{-/-}$ mice, namely, hemorrhagic destruction of the brain. This finding suggests a role for JAM-C in cerebrovascular function [220].

A functional role for JAM-C was identified in cerebellar granule neuron (CGN) exit from their germinal zone in the external granular layer (EGL). Famulski and colleagues found that Pard3A recruits JAM-C to the neuronal cell surface as the neuronal progenitors leave the EGL and migrate though the molecular layer to their final residence in the internal granule layer [221]. Over-expression of Pard3A leads to precocious exit from the granular zone while silencing of JAM-C promoted CGN retention in the EGL [221]. This study highlighted a functional role for JAM-C in CNS niches.

Furthermore, Stelzer and colleagues identify JAM-C as an apical stem cell marker in both embryonic and adult mice. They show polarized JAM-C enrichment at the apical surface of NSCs. This polarized expression is only observed in vivo, whereas, in vitro JAM-C is expressed homogenously on the surface of NSCs [222]. NSC self-renewal can occur via either symmetric divisions to generate daughter cells with the same fate or asymmetric divisions where one daughter cell will maintain the same fate as the mother cell while the other undergos a neurogenic fate. In particular, partitioning of fate determinants at the apical membrane is a determining factor in mode of division [105]. Stelzer and colleagures, suggest that partitioning of JAM-C during cell divisions is asymmetric and only retained by the daughter cell maintaining contact with the ventricular wall [222]. A well-characterized apical membrane component that is asymetrically distributed is the “cadherin hole” [105]. Stelzer and colleagues identify JAM-C as a marker of this cadherin hole and speculate that neural stem cell characteristics are maintained by JAM-C adhesional contacts with the ventricular wall [222]. This study implicated JAM-C in NSC maintenance in the apical SVZ domain.

The full-length form of JAM-C has a molecular weight of approximately 43 kDa in CHO cells [203, 222]. Previous reports studying JAM-C in human microvascular endothelial cells (HMVEC) identify a 50 kDA full length form and a 40 kDa soluble form (sJAM-C) [223]. Release of sJAM-C was increased following TNF-alpha stimulation in the absence of an increase in mRNA suggesting an increased release of membrane bound JAM-C from the plasma membrane. Silencing of the protease activity of ADAM10

and ADAM17 prevented shedding of sJAM-C in response to TNF-alpha. Functionally, the sJAM-C fragment was reported to increase angiogenesis in vitro [223]. This study identified ADAM10 as a critical regulator of JAM-C cleavage.

1.11 JAM-C Regulates Rap1 Activity

As mentioned, JAM-C was shown to interact with and regulate Cdc42 activity during spermatid polarization [213]. Considering Cdc42 is a small GTPase, Orlova and colleagues studied whether JAM-C altered the activity of other small GTPases. In primary human dermal microvascular endothelial cells (HDMECs), JAM-C knockdown had no affect on the activity of Cdc42, Rac, or Ras. However, JAM-C down-regulation produced a significant up-regulation in endogenous Rap1 activity [224]. In accordance, over-expression of JAM-C decreased Rap1 activity [225]. Rap1 is part of the Ras family of proteins that cycle between GDP- and GTP-bound forms. Based on differences in only a few amino acids, two isoforms of Rap1 have been described, Rap1a and Rap1b. Rap1 represents a molecular on/off switch as it cycles between a GTP or GDP bound state. Guanine nucleotide-exchange factors (GEFs) allow GTP to bind and promote the "on" form. On the other hand, GTPase-activating proteins (GAPs) lead to hydrolysis of the bound GTP to turn Rap1 "off" [226].

1.12 Rap1 in Stem Cell Niches

A role for Rap1 and the molecules that participate in cycling between the GTP and GDP forms has been identified in stem cell niches. For example, Rap1 functions in directing stem cell self-renewal in *Drosophila* testes. Loss of function of Rap-Gef

(Gef26) prevents the active GTP bound Rap1 and leads to “drifting away” of stem cells from their niche. Lack of stem cell contact with niche cells leads to loss of stem cell identity and subsequent decline in germline and somatic stem cells [227]. Thus, Rap1-GTP maintains stem cell identify via anchoring to the niche. In an earlier study, Rap1 was reported to regulate the distribution of adherens junctions. Cells mutant for Rap1 had adherens junctions dispersed unevenly and into neighboring cells [228]. Therefore, it was proposed that Rap-Gef/Rap1 leads to proper assembly of adherens junctions and positioning of stem cells within their niche. Proper positioning allows for signal transduction pathway activation to regulate key stem cell properties such as self-renewal or differentiation [227]. These findings were similar to those observed following loss of adhesion molecules. Considering these findings in drosophila stem cells, Rap1 involvement in mammalian stem cell regulation would be noteworthy.

Indeed, it has been demonstrated that in mouse embryonic NSCs, Rap1 activity is higher in stem cells while Rap1Gap expression is higher in cells undergoing differentiation and leaving the niche. Rap1Gap (GTPase-activating protein), a negative regulator of active Rap1-GTP, is co-induced with DCX following NSC commitment towards a migrating neuroblast fate in the post natal (P4) mouse brain [131]. In the mouse embryonic ventricular zone, Rap1Gap is induced as apical progenitors lose their contact with the ventricular wall and give rise to basal progenitors. Upon removal of growth factors to promote NSC differentiation in vitro, analysis of the NSC expression marker Nestin is lost as Rap1Gap expression is induced and Rap1 activity (Rap1-GTP) is inhibited. Furthermore, acute expression of lentivirally delivered Rap1Gap impairs

adhesion to laminin and fibronectin substrates. However, under these conditions Rap1Gap did not have any significant effect on neuronal or glial differentiation programs [131]. Similar to growth factor removal, induced differentiation following acute deletion of *Id* genes in the presence of growth factors results in Rap1Gap induction [131]. Niola and colleagues showed that Id proteins repress *Rap1Gap* in vivo and that their interactions are necessary for proper anchoring of NSCs in the neurovascular niche. Despite the lack of effect on differentiation following Rap1Gap over-expression, disruption of adhesive contacts in vivo is associated with the initiation of differentiation. The authors comment that loss of adhesion following Id deletion is invariably associated with the onset of differentiation [131].

Therefore, in multiple biologic settings Rap1 acts as a key regulator of cell adhesion. Several lines of evidence, have suggested that Rap1 is important for integrin-mediated cell adhesion. While identification of the effector molecule has remained uncertain, evidence indicates that Rap1 could acts as an “inside-out” regulator of integrin activation. Introduction of constitutively active Rap1 promotes integrin-mediated cell adhesion, while over-expression of Rap1Gap to inhibit Rap1 signaling inhibits inside-out integrin activation [229].

In a human fibrosarcoma cell line, JAM-C was shown to promote metastasis via increased adhesion, migration, and invasion. Increased JAM-C was additionally identified in several cancer cell lines where it mediated their metastatic potential as evidenced by siRNA knockdown of JAM-C. JAM-C knockdown decreased adhesion and

tumor spreading [230]. Based on recent findings, the effect on metastasic potential could be mediated via adhesion molecule activation. In a different study, over-expression of JAM-C in endothelial cells increased activation of αvβ3 integrin via association with JAM-C, which controlled localization and activity of the integrin. In the same study, a link between JAM-C, Rap1, and β1 integrin was identified. JAM-C was demonstrated to inhibit active β1 integrin, although it did not associate with it. Rather, the change in β1 integrin activation was mediated by Rap1 activity [225]. Moreover, Rap1 has been demonstrated to regulate α3β1-dependent adhesion. siRNA mediated reduction of JAM-C expression resulted in VE-cadherin–mediated interendothelial adhesion. Again, the stabilization of VE-cadherin was dependent on Rap1 activity [224]. Clearly, JAM-C and Rap1 play a role in adhesion molecule dependent cellular processes. Additionally, it has been suggested that Rap1 mediates crosstalk between cadherins and integrins, and in doing so, modulates a number of cellular responses [231]. However, it is also possible that Rap1 induces actin remodeling or expression of different classes of cell-surface adhesion proteins.

For example, a role for Rap1 and N-Cadherin was identified during rodent neurogenesis during development. In response to reelin encountered in the middle intermediate zone, Rap1 increased surface N-Cadherin levels on multipolar neurons to promote radial migration into the upper intermediate zone. The authors of this study suggest that low levels of N-cadherin allow neurons to sense directional cues in the environment [69]. Once a bipolar morphology is achieved, locomotion to the cortical plate becomes independent of Rap1 and N-cadherin. Imaging studies showed that

inhibition of Rap1 in neurons resulted in ectopic accumulation as a result of deficient polarization rather than defective motility. This study identified a role for Rap1 in the initial polarization of neurons. Following inhibition of Rap1, expression of N-cadherin at low levels was able to rescue the polarization defect. This result was interesting considering that N-cadherin is normally down-regulated in neurons leaving the ventricular zone [232]. However, the authors agree that high levels of N-cadherin do block neuronal migration while low levels may be necessary to respond to stimuli in the local environment. These studies demonstrate that expression of cell surface receptors is finely tuned and that polarized migration is controlled by the integration of multiple signals.

A role for Rap1 in cortical development was further solidified following experiments using C3G (Rap-Gef1) mutants. C3G is important for adding the GTP to Rap1 to activate signaling. Mice mutant for C3G, were embryonic lethal (by E14.5) and demonstrated neuronal migration defects due to loss of radial glial basement membrane anchoring and disorganized processes. In this study, the hypomorphic *Rapgef1* allele lead to neuronal arrest in the multipolar phase. The migration arrest resulted in the accumulation of neurons below the preplate [233]. Moreover, experiments deleting RA-GEF-1 in the dorsal telencephalon to prevent Rap1-GTP signaling displayed abnormal cortical myeloarchitecture and cytoarchitecture. This study utilized a conditional knockout of *Rapgef2* using *Emx1-Cre* to target neuronal progenitors. Similar to the C3G mutants, disruption of RA-GEF led to neuronal accumulation [234]. Development of a disorganized, heterotopic cortex corroborated a role for the Rap-associated enzymes in

cortical development. More recently, conditional *Rapgef1* (C3G) inactivation to avoid the early embryonic lethality of hypomorphic *Rapgef1* in the developing mouse cortex showed defects in neuronal migration, axon formation and cortical lamination [235]. Use of *Emx1-Cre* to target progenitors in the cortex starting at E9.5 demonstrated that C3G is required for the multipolar to bipolar (MTB) transition as was observed with the Rap1 GTPases [69, 235]. However, the effect of C3G is time dependent. Inactivation of *Rapgef1* using a Nex-Cre to target bipolar neurons did not show any defects because the inactivation occurred after the MTB transition [235] .

The apical plasma membrane of NSCs seems crucial for self-renewal of neural stem cells, and lack of these apically localized constituents has been associated with neuronal differentiation. Identification of signaling pathways that originate at the apical plasma membrane before transduction to the cell interior will provide a mechanism for NSC maintenance, leading us to further explore ADAM10 and JAM-C function. Similarities in Rap1, JAM-C, and ADAM10 disruption were identified in cortical organization and niche exist. A link between JAM-C and Rap1 was previously identified, as was an association between ADAM10 and JAM-C processing. However, these signaling elements were not examined in the adult SVZ. Therefore, the purpose of this project is to test our hypothesis that ADAM10 regulates NSC lineage progression by mediating shedding and signalling activation of the adhesion molecule JAM-C. We test this hypothesis by 1.) Characterizing the SVZ niche in WT and Nestin:ADAM10$^{fl/fl}$ mice. 2.) Defining the role of ADAM10 in instructing NSC properties and 3) Determining the mechanism regulating NSC properties via an ADAM10-JAMC-Rap1 pathway.

Chapter 2: Materials and Methods

Animals

Animal experiments were performed in accordance with the *Guide for the Care and Use of Laboratory Animals* and approved by the *Institutional Animal Care and Use Committee of Division of Laboratory Animal Resources*, State University of New York Stony Brook School of Medicine. The transgenic mouse strains Nestin-Cre^{ER};$ADAM10^{fl/fl}$/Rosa26YFP and GFAP-GFP were previously described by our lab [155, 189]. Nestin-Cre (stock no. 012906) was obtained from Jackson Laboratories. The $ADAM10^{fl/fl}$ was donated by Dr. Dempsey (Mayo Clinic Jacksonville, Florida). Mouse genotyping was conducted by digesting mice tails in Solution A (25mM NaOH, .2mM EDTA) for 45 min. at $98.^{0}$ The DNA digestion mixture was mixed with an equal amount of Solution B (45mM Tris-HCL). Mouse DNA was genotyped with the following primers:

ADAM10F: 5'cgtatctcaaaactaccctccc3'

ADAM10R:5'gttggacataactttggatctcc3'

CreF:5'gcggtctggcagtaaaaactatc3'

CreR:5'cgttttcgttctgccaatatgg3'

YFPF:5'gacgacggcaactacaagac3'

YFPR:5'atgtgatcgcgcttctcgt3'

Genomic DNA was mixed with primers and Phusion® High-Fidelity PCR Master Mix (New England BioLabs).

RNA Isolation

RNA was purified from FACS-sorted YFP+ populations with the RNeasy Kit (QIAGEN). cDNA was synthesized with qScript cDNA SuperMix (Quanta BioSciences). Primers spanning exons 9-10 to monitor deletion of the protease domain of *ADAM10* are available on request.

Tamoxifen and BrdU Administration:

Nestin-Cre^{ER};ADAM10$^{fl/fl}$ mice (4–6 weeks old) were administered tamoxifen (TAM) at 100 mg/kg/d for 3 days 48 hrs apart (intraperitoneally (IP); dissolved in 10% EtOH/90% sunflower oil). Littermate mice wild-type for ADAM10 or negative for Nestin-Cre were used as controls and were also treated with tamoxifen concurrent with ADAM10$^{fl/fl}$ mice. For in vitro experiments, hydroxy-tamoxifen (4-OHT; Sigma) was added at 1uM to the media for the duration of the experiment unless otherwise indicated.

BrdU (Sigma; 10mg/ml solution) was injected intraperitoneally (100 mg/kg). For the BrdU-LRC assay, BrdU was injected (IP) 5X every 3 hrs into ADAM10$^{fl/fl}$ and WT control mice following tamoxifen administration. Mice were sacrificed 30 days after the final BrdU injection. For cell cycle analysis BrdU was injected intraperitoneally 2 hours before mice were sacrificed and SVZ tissue harvested. In vitro short term BrdU analysis involved BrdU administration (10uM) 2 hours before fixation.

Acitretin:

For in vivo experiments, mice were injected with Acitretin (Sigma, IP; 5 mg/kg) 18 hrs and 4 hrs before tissue harvest (or BrdU administration for cell cycle analysis). In vitro, acitretin (10uM) was added at the same time points. Increased SVZ ADAM10 activity was demonstrated following IP acitretin injections with SensoLyte® 520 ADAM10 Activity Assay Kit performed per manufacturers instructions (AnaSpec).

Neurosphere cultures and culture based assays

Adult SVZ tissue was dissected into HBSS containing 26 mM HEPES, 0.3% glucose, and 0.75% sucrose (D1 medium). Tissue was dissociated into single cell suspensions using papain (10mg/mL), 0.1% trypsin and 100 U/ml DNase I (Sigma-Aldrich) in D1 medium for 25 min. at room temperature (RT). For self-renewal assays, single cell suspensions were plated in floating cultures at clonal density in stem-cell medium (SCM; 1:1 DMEM:F12 medium, 1x B27 supplement, 1% penicillin/streptomycin with addition of EGF (Millipore Bioscience Research Reagents, 20 ng/ml; and bFGF2, Millipore Bioscience Research Reagents,10 ng/ml)) as previously described [155]. Quantification of sphere formation occurred 7 days after plating. For differentiation experiments, secondary neurospheres were dissociated after 7 days in vitro (DIV) using TrypLE (Invitrogen) and single cells were plated onto poly-L-lysine (100 µg/ml) coated coverslips or 6 well plates. These cultures were maintained for 7 DIV in SCM without EGF or FGF, and then processed for immunofluorescence analysis with stem cell or neural lineage-specific antibodies. Western blot analysis of differentiated secondary

neurospheres was performed similarly but cells were plated in 6-well PLL coated dishes. All neurosphere, cell, and tissue explant cultures were performed in a humidified incubator maintained at 37°C and 5% CO_2.

Transfections

The pcDNA-JAM3 plasmid was a kind gift from Dr. Santoso (Justus-Liebig-University, Giessen, Germany) and its production previously described [236]. pcDNA-dsRED vector was used as a control for transfection effects on endogenous gene expression. Transfection was performed using PolyJet (SignaGen Laboratories) in a 3:1 ratio as per manufacturer's instructions.

Lentivirus Production

pGFP-C-shLenti expression vectors carrying shRNAs to mJAM-C or scramble control were purchased from OriGene. pLOC–GFP–Rap1GAP and control lentivirus were purchased from Sigma and provided by Lewis Kaufman (previously described in [117]). Lentivirus was generated using the lentiviral transfer vector co-transfected with the vesicular stomatitis virus G (pCMV-VSV-G) viral envelope and gag-pol (pCMV-dR8.2 dvpr) into HEK293 cells using Calcium Phosphate Transfection kit (Clontech). Growth medium was added to cells after 12 h, and supernatant was harvested 24-72 hrs. after transfection.

FACS

GFAP::GFP and YFP^+ cells were sorted on a FACStar plus instrument (Beckton Dickinson, Franklin Lakes, NJ). The GFP and YFP were detected using 490 long-pass and 510/20 filters. Cell aggregates and small debris were excluded on the basis of side scatter (measuring cell granularity) and forward scatter (measuring cell size). Gating parameters were set using positive and negative cell populations to measure background fluorescence. Positive cell populations were either used for cell culture experiments or fixed for cell cycle analysis.

Cell cycle analysis

48 hrs after the final TAM injection mice were injected with BrdU 2 hours before SVZ tissue was dissected and dissociated. Single cells were fixed in ice-cold ethanol for at least 30 minutes before antigen retrieval. After pelleting (5 min; 500 rcf), cells were incubated with 2NHCl for 30 minutes at room temperature, pelleted, and resuspended in of 0.1 M $Na_2B_4O_7$ (pH 8.5) to neutralize the sample. Cells were washed with .1M PBS and incubated in primary rat anti-BrdU antibody overnight. The next day cells were washed, pelleted, and incubated in FITC conjugated goat ant-rat secondary for 1 hr at RT before incubation with Propidium Iodide/RNAse staining buffer (with .2% triton-X added the same day; BD Pharmingen) 1 hour before cell cycle analysis. For sorted GFAP-GFP cell cycle analysis, cells were immediately fixed following cell sorting and processed as above. In the acitretin goup, mice were injected (IP; 5 mg/kg) at 18 hrs and 6 hrs (4 hrs. before BrdU) before tissue dissection and processing. Cells were analyzed using a fluorescence-activated cell sorting (FACS) Calibur flow cytometer (BD

Biosciences). Data were acquired from comparably gated events and staining was compared with PI only and secondary only stained cells. The number of gated events was lower than the standard 10,000 events from sorted cells because biologic replicates were analyzed separately.

SVZ Slice culture/SVZ Explant cultures

Adult brains were dissected, washed in HBSS, then transferred to fresh ice-cold D1 medium. Brains were sectioned into 200-300 μm-thick coronal sections using a tissue chopper (McIlwian) before careful dissection of the SVZ. SVZ pieces were transferred to 12-well polycarbonate transwell inserts (.4 μm pore, Corning Incorporated) containing peptide hydrogel (BD PuraMatrix) with the ventricular side facing up. 700 ul of SCM was added to each well and supplemented with growth factors. For analysis of the JAM-C cleavage product, hydoxy-tamoxifen (1uM) was added along with EGF (20 ng/mL) and FGF (10 ng/mL) for the duration of the experiment (4DIV). An anti-JAM-C antibody (R&D) to the N-terminal domain was used to detect the extracellular product following acitretin addition on days 3 and 4 *in vitro*.

For cell plating experiments, single cells obtained from YFP sorted secondary neurospheres were dissociated (4000 cells in 10ul SCM per explant), gently pipetted onto the surface of SVZ explants, and maintained for 4 DIV before fixation and analysis. For Rap1Gap over-expression analysis, cells were infected with control or Rap1Gap lentivirus and maintained in culture for 7 days before dissociation (TrypLE) and plating as before. A minimum of 4 slice cultures were analyzed per experiment.

Scratch Test/Migration Assay

WT and ADAM10$^{fl/fl}$ secondary neurospheres grown in the presence of hydroxy-tamoxifen were plated in 6 well poly-L-lysine (PLL) coated dishes or PLL coated coverslips and maintained to confluency. In monolayers, a cross was created in the cell layer by scratching a pipette tip across the bottom of the well to create a line followed by a second scratch perpendicular to the first line. The wells were washed to remove detached cells and the cross was imaged using a Zeiss Microscope. 24 hrs later the cross was re-imaged to analyze migration by capturing an image at the same spot as time 0. By overlaying images from time 0 and 24 hrs, individual cell migration from the edge of the scratch was quantified using the ImageJ64 line measure tool [237]. Experiments were performed by analyzing multiple wells and repeated with three biologic replicates.

Short-term Adhesion Assay

50,000 WT or ADAM10$^{fl/fl}$ were incubated with Calcein-AM (Life Technologies; 4 ug/mL) for 20 min at 37°C and 5% CO_2. The fluorescence-labeled cells were incubated with JAM-C blocking antibody (.01 ug/ul R&D) or IgG control for 45 minutes. The cells were added onto PLL (100 µg/mL), laminin (10 µg/mL), or fibronectin (1mg/mL) coated 96-well plates and allowed to adhere for 20 minutes. Non-adherent calcein-labeled cells were removed by gently washing twice with 1X PBS. Adherent cells were calculated as a percentage of total fluorescence before washing. For adhesion experiments with the Rap1 activator, 8-CPT-2-O-Me-cAMP (60 uM; Sigma), small molecule ADAM10 inhibitor

GI245023X (40uM, Sigma), or DMSO control, cells were incubated for 15 min. with the small molecule before addition to PLL, laminin, or fibronectin coated 96 well plates. Adhesion was calculated as above. Experiments were performed in triplicate and repeated 3 times.

Rap1 Activation assay

The rap-binding domain of ral-GDS binds only the active form of Rap1 serving as the basis for the Rap-GTP binding assay [238]. The levels of active GTP-bound RAP1 were determined using the Active RAP1 Pull-Down and Detection Kit (Thermo Fisher Scientific) according to the manufacturer's instruction using WT and ADAM10$^{fl/fl}$ NSCs cultured in hydoxy-tamoxifen. For over-expression of JAM-C, cells were transfected 48 hrs. before collection. Lentiviral mediated Rap1GAP over-expression occurred 7 days following initial transduction. Proteins were analyzed by immunoblotting using anti-RAP1 antibody.

Immunohistochemistry

Animals were transcardially perfused with PBS (20ml) followed by fixative solution (4% paraformaldehyde; 50ml). Brains were dissected and post-fixed for 4-24 hours before transferring to cryoprotective solution (30% sucrose) for at least 24 hours. Tissue sectioning was performed using a frozen microtome. Brain sections (30-50μm thick) of the region of interest were collected in .1M PBS. Immunostaining was performed using free-floating coronal or sagittal brain slices blocked in 10% normal goat serum (Invitrogen) containing 0.3-0.5% TritonX-100 and 1% albumin (SIGMA) in .1M PBS for 1 hr. at RT. Tissue sections were incubated overnight at 4^{0}C in blocking

solution containing primary antibodies including the following: anti-bromodeoxyuridine (BrdU; rat Accurate Chemical and Scientific Corporation, mouse Becton Dickinson), anti-Nestin (Chemicon), anti-GFAP (BD Biosciences, abcam), anti-Ki67 (Novocastra), anti EGFR (abcam), anti-VCAM1 (R&D), anti-Rap1gap (abcam), anti-GFP (Aves), anti-Lex (MMA clone, BD Biosciences), anti-JAM-C (goat R&D; rabbit Novus Biologicals), anti-ADAM10 (rabbit abcam, rat R&D), anti-doublecortin (abcam), CD133 (eBioScience), anti-laminin (Sigma), anti-Sox2 (Chemicon), and Anti-Map2 (abcam). The appropriate secondary antibodies were purchased from Jackson ImmunoResearch and used at 1:500 dilutions in blocking solution for 1 hour at RT.

For BrdU staining, sections were incubated with 2N hydrochloric acid (HCl) for 20 min at 37°C then washed with 0.1 M $Na_2B_4O_7$ 2x for 10 min before standard staining protocol. Rat anti-BrdU (Accurate) and mouse anti-BrdU (Becton Dickinson) was used for 5-chloro-2-deoxyuridine (CldU) and 5-iodo-2-deoxyuridine (IdU) detection, respectively. The CldU/IdU staining was done as described previously [239].

Coverglass staining was performed by blocking for 10 min at RT before addition of primary antibody mixture for 1 hr. at RT. Coverglasses were gently washed 3x5min. before addition of the appropriate fluorescent conjugated secondary antibody (1:500) for 1hr at RT. Coverglasses were washed 3x5min. and incubated with DAPI to visualize the cell nuclei before mounting with MOWIOL mounting media.

SVZ wholemount dissection and staining

SVZ wholemounts of striatal lateral wall were dissected from adult mice [240]. A 2-4 mm-long strip of SVZ tissue covering the striatum was dissected from under the

corpus callosum to the ventral tip of the lateral ventricle in ice-cold PBS. The SVZ wholemounts were fixed in cold 4% paraformaldehyde in 0.1M PBS overnight, washed with PBS, blocked with 10% normal goat serum in PBS/0.3% Triton X-100 for 60 min. at RT then incubated with primary antibodies diluted in blocking buffer for 48 hrs. at 4°C. Tissues were washed 3X in PBS/0.3% Triton 15 min. on a rocker, and incubated with appropriate secondary antibodies at RT for 1 hr. After washing, DAPI was added and the wholemounts transferred to a glass slide and coverslipped with MOWIOL mounting media for confocal imaging.

Antibodies used: GFAP, Chicken IgG, 1:500 (abcam), Laminin, rabbit IgG, 1:1000 (Sigma), β-catenin mouse IgG1, 1:200 (BD Bioscience), VCAM1, Rat IgG, 1:500 (R&D). Primary antibodies were visualized using fluorescent conjugate secondary antibodies (Jackson).

Microscopic analysis and quantification

A confocal laser-scanning microscope TCS-SP5 (Leica DMI6000 B instrument) was used for image localization of FITC (488-nm laser line excitation; 522/35 emission filter), CY3 (570-nm excitation; 605/32 emission filter) and Cy5 (647 excitation; 680/32 emission filter). Optical sections (*z* ranging from 0.5 to 1μm) of confocal epifluorescence images were sequentially acquired using a 20-63x objectives with LAS AF software. NIH ImageJ software was then used to merge images. Merged images were processed in Photoshop CS4 software with minimal manipulations of contrast. Cell counting was performed from each experimental condition and compared with respective control. Tissue sections containing the SVZ niche region were matched across samples in each

experimental condition and compared with their respective control. An average of 4 sections containing the SVZ niche were used to collect serial confocal images for each individual condition (n=3-6) using unbiased stereological morphometric to obtain an estimate of the total number cells in question. For cells in monolayer, 5-10 images were taken per condition. For GFAP-GFP cellular distribution from the ventricular wall and blood vessels, the distance from the center of the cell body to the nearest vessel surface or lateral ventricle as demarcated by DAPI staining was measured. An average of 200 cells from 3 pairs of mice in each 40X z-stack were included.

Western blots and immunoprecipitation.

For Western blots, SVZ tissue was dissected at the end of the experiments or cells harvested and used for protein extraction using lysis buffer (50 mM Tris-HCl, pH 7.5, 1 mM EDTA, 1 mM EGTA, 1 mM sodium orthovanadate, 50 mM sodium fluoride, 0.1% 2-mercaptoethanol, 1% Triton X-100, plus proteases inhibitor cocktail; Sigma). Proteins were quantified using a standard BCA assay (Pierce), and 20–50 µg of protein/lane was loaded on 10% SDS-PAGE and transferred to PVDF membranes (Millipore) to perform Western blot analysis. The membranes were blocked in 2% BSA and incubated with primary antibodies overnight at 4°C. Primary antibodies not listed elsewhere include anti-N-Cadherin (BD Transduction Labs) and anti-cleaved caspase3 (Santa Cruz Biotech). Proteins were detected using horseradish peroxidase conjugated secondary antibody (1:5000; Santa Cruz). Bands were visualized by chemiluminescence.

For immunoprecipitation experiments, SVZ tissue from three wild-type mice was lysed with RIPA buffer to obtain protein extracts. Aliquots of 200 µg (for *in vivo* studies) of protein extract were incubated with antibodies against JAM-C (R&D; 1 µg) and 10 µl of Protein-A-conjugated agarose beads (Santa Cruz Biotechnology) for 12–16 h at 4°C. Proteins associated with JAM-C were concentrated by centrifugation at 10,000 × *g* for 3 min at 4°C and washed twice with cold RIPA buffer to remove nonspecific binding partners. JAM-C complexes were resolved on acrylamide gels and detected as described above. Immunoprecipitation experiment was performed three times with SVZ tissue pooled from three mice for each experiment.

Behavioral Tests

Behavioral testing began 2 weeks following the final TAM administration (3x 48 hrs apart). Three days before the behavioral experiments began, mice were housed singly in the behavioral testing room. 24 hrs before behavioral testing, animals were habituated by exposure (ten min) to an empty open-field arena to familiarize them with the procedure. Odors were presented by placing an odor stimulus or control odor (mineral oil in water) on a cotton tip suspended from a thin cord above the arena so that the tip was ~8cm from the floor. A test session consisted of two 5 min odor presentations of the same odor with a 30 or 60 min interval between presentations. These different intervals were tested in separate sessions spaced at least 24 hr. apart with different odors used in each test. Odors and control swab were randomly placed to control for behaviors related to memory. All odors were dissolved in water (10^{-3}) and freshly prepared before each experiment. Examples of odors used were isoamyl

acetate, citrate, and benzaldehyde. We recorded the time animals spent investigating the swab by defining an equal area directly surrounding the odor or control swab. Mouse tracking was recorded using EthoVision XT9 software (Noldus). A significant decrease in investigation time during the second presentation indicates that mice were able to recognize an odor that had been presented previously. Paired t-test was used to analyze odor investigation.

For the object placement test of spatial and learning and memory, mice were tested 30 days following TAM administration. The test took place on 3 consecutive days. On day1, mice were habituated for 10 min to the open-field arena. On day2, mice were exposed to two identical objects placed in specific locations. Day 3 consisted of the test trial where one object was moved to a different location within the arena. The amount of time spent investigating both objects were recorded and discrimination ratios were calculated by subtracting the time spent investigating the familiar object (T_f) from time spent investigating the novel object position (T_N) and dividing by total exploration of both objects (T_N-T_F/T_N+T_F). Ratios near 0 indicate no preference while ratios >.5 indicate a preference for the novel position [241].

Statistics and Data analysis

Data are presented as means ± standard error of the mean (s.e.m.) and were analyzed by Student's t-test (two groups), paired-test when analyzing fold change (two groups), or ANOVA (multiple groups) with multiple comparison test as indicated in the figure legends (Prism 6 , GraphPad Software, La Jolla and Mac OS X). Experiments were completed with at least thee biologic replicates unless indicated. (* p≤0.05, **p≤0.01, or ***p≤0.001)

Chapter 3: Results

ADAM10 is Expressed in the Apical SVZ

The adult SVZ microenvironment has two critical compartments referred to as the apical and basal niches [103]. In the apical niche, ependymal cells form pinwheel structures with B1 cells intercalated among them. Recent studies revealed that this unique cytoarchitecture is fundamental in directing NSC function [101]. Previously, we reported ADAM10 expression in the cell membrane of GFAP-GFP+ NSCs and EGFR+ progenitors using coronal tissue sections of the SVZ [242]. We verified this staining pattern in GFAP-GFP+ cells and observed increased density of ADAM10 positive cells within the SVZ when compared to adjacent striatal tissue (Fig.6 A). Next, we checked whether ADAM10 expression was confined to particular sites of interaction between NSCs and niche structures. Using wholemount preparations, which allow for an en face view of the ependymal cell layer, we observed ADAM10 expression at sites of NSC contact with the ventricular wall. In particular, ADAM10 co-expressed at the center of pinwheels suggesting a role for ADAM10 in directing NSC adhesion to the apical niche (Fig. 6B; arrow). The ADAM10 staining appeared punctate in places, suggesting a subcellular localization. Perhaps ADAM10 is expressed in exosomes allowing for quick trafficking to the cell membrane.

ADAM10 is Required to Maintain NSC Lineage Progression and Neurogenesis

Considering the expression of ADAM10 at unique sites within the SVZ, we sought to determine the role ADAM10 plays in directing NSC properties. Due to the embryonic lethality in ADAM10-/- and Nestin::ADAM10$^{-/-}$ mice [169, 185], we made an inducible mouse line to delete ADAM10 in neural stem and progenitor cells following Cre induction with tamoxifen (Nestin-CRE^{ER};ADAM10$^{fl/fl}$/R26R-YFP denoted as ADAM10$^{fl/fl}$ or fl/fl; characterized in [189]), allowing us to determine the role of ADAM10 in the adult SVZ. The mice also contained a floxed YFP reporter gene in the Rosa26 locus to facilitate the monitoring of recombined NSCs and NPCs and infer lineage of the NSC progeny after ADAM10 deletion. We verified deletion of the protease domain of ADAM10 in YFP-sorted cells following tamoxifen administration via western blotting and RT-PCR (Fig 6C). Using this mouse line and the tamoxifen (TAM) paradigm (3 injections x 48 hrs.) we characterized NSCs and lineages at different time points after ADAM10 deletion. At 5 days after the last TAM injection (10 days after first injection), our data reveled a decreased density of GFAP+Sox2+ NSCs in the ADAM10$^{fl/fl}$ SVZ (7.73±1.16 vs. 3.3±.51 cells per mm^3; Fig. 6 D-E). It has been suggested this population might represent early neural stem cell/precursor cell types [243]. Therefore, the GFAP+Sox2+ population serves as a readout of the neural stem and early progenitor (NSPC) populations. Considering the impact of deletion on NSPCs, we wondered if their progeny would also be affected. Interestingly, the reduction of NSCs in the SVZ was also reflected in the number of their lineage cells as numbers of both NPCs (EGFR+ progenitors, 49.12± 9.03% reduction in ADAM10$^{fl/fl}$ sample vs. WT) and neuroblasts (43.17±1.89% in WT vs. 33.42±3.02% in ADAM10$^{fl/fl}$ samples) were reduced in the

acutely dissociated WT and ADAM10$^{fl/fl}$ SVZ tissue (Fig. 6 F-I). These findings suggest a decrease in lineage progression of NSCs into activated progenitors and neuroblasts.

To determine whether changes in neuroblast proliferation could account for the differences in DCX+ cells observed, we analyzed BrdU incorporation in DCX+ neuroblasts following TAM administration. Acutely dissociated SVZ tissue (48 hrs after the final TAM) was administered BrdU in vitro for 2 hrs before analysis. BrdU incorporation in the remaining DCX+ cells in the ADAM10$^{fl/fl}$ conditions were similar to WT controls (BrdU+DCX+/Total DCX; Fig.6 J-K). Alternatively, increased cell death following ADAM10 deletion could factor in. However, cleaved-caspase3 immunoblotting of WT and ADAM10$^{fl/fl}$ NSC lysates after the onset of differentiation in vitro (Day2 in differentiating conditions) did not detect significant cell death in NSCs or their lineages (Fig. 6 L-M). These findings suggest the changes in the progenitor populations are due to alterations in NSC properties and not decreased neuroblast proliferation or increased cell death.

ADAM10 Directs Olfactory Bulb Neurogenesis

To detect the outcome of decreased neuroblast (DCX+) number in the SVZ of ADAM10$^{fl/fl}$ mice, we investigated neurogenesis to the olfactory bulb (OB) and mouse behavior. To investigate OB neurogeneisis, mice were injected with tamoxifen (as above) and 30 days later mice were processed for immunofluorescence (IF). At this time point, we observed decreased YFP+ cells in the RMS and OB of ADAM10$^{fl/fl}$ mice compared to WT (Fig. 7A). Additionally, the number of YFP+ cells entering the granule

cell layer (GCL) of the OB was significantly reduced in the ADAM10$^{fl/fl}$ mice (53.56±1.74 vs. 24.98±2.09 cells per mm^3; Fig.7 A-C). To characterize the YFP+ cells, we analyzed the co-expression of YFP+ cells that reached the OB with the mature neuronal marker, NeuN. This analysis demonstrated a significant decrease in the total YFP+NeuN+ cells in the GCL of ADAM10$^{fl/fl}$ mice (29± 1.76 vs. 15±1.52 per mm^3; Fig.7 B-C). However, the percentage of double positive cells (YFP+NeuN+/Total YFP) was unchanged, indicating an intact differentiation program in YFP+ cells reaching the OB (55.09±2.66% vs. 49.21±2.71%; Fig. 7B-C).

In addition to the YFP lineage tracking, we also analyzed newly generated neurons in the SVZ using a BrdU labeling paradigm (BrdU injection 5 times every 3 hours following tamoxifen administration). Tissue was processed 30 days after BrdU administration to detect neurogenesis in the SVZ-OB axis. Consistent with our YFP data, BrdU lineage tracing following ADAM10 deletion showed a reduced number of mature neurons in the GCL of the OB (BrdU+NeuN+ cells; not shown).

Adult neurogenesis is important for complex forms of olfactory behavior such as short-term olfactory memory [58, 244-246]. To determine whether the cellular phenotype lead to a behavioral outcome, we analyzed short-term olfactory memory using the cotton- tip based short-term olfactory memory test [58]. The test of olfactory memory is based on the idea that mice generally spend more time investigating an odor they do not remember having encountered [58]. When presented with the same odor at a short interval, mice spend significantly less time investigating the odor on the second

presentation that they remember having encountered. Both WT and ADAM10$^{fl/fl}$ mice were injected with tamoxifen as above and 2 weeks after TAM we assayed for short-term olfactory memory. We did not observe significant differences in time spent investigating a cotton swab versus a presented odor between WT and ADAM10$^{fl/fl}$ animals, suggesting that preference for odor vs. control swab is not affected, yet, we did observe differences in short term olfactory memory. A significant reduction in odor investigation was observed in the WT group at 30 minutes and 60 minutes. However, we did not see a significant reduction in odor investigation in the ADAM10$^{fl/fl}$ mice at the same time points (Fig. 7D). These observations suggest that olfaction is normal in ADAM10$^{fl/fl}$ mice, but that short-term olfactory memory is impaired. The behavioral output of reduced OB neurogenesis demonstrates a phenotypic effect mediated by ADAM10 deletion in NSCs. Altogether our data here indicates that a shortage of NPC and neuroblast populations result in decreased neurogenesis in the ADAM10$^{fl/fl}$ mice.

ADAM10 Activity Regulates NSC Cell Cycle Status

NSCs balance multiple signaling cues sensed by the single primary cilium at the ventricular surface and large basal process contacting the adjacent vasculature to regulate cell cycle status and prevent massive proliferation and exhaustion [101, 103, 108]. The extracellular matrix, adhesion molecules, and growth factors also provide significant regulation of cell cycle status. These elements preserve NSC positioning within the niche and as a consequence regulate intrinsic cell cycle programs. Interestingly, several of these proteins serve as ADAM10 substrates [247] [88, 97, 109, 123, 124, 135, 142]. The reduced number of both NSCs and lineages in the SVZ

suggests that ADAM10 may regulate NSC lineage progression and proliferation. Therefore, we analyzed cell cycle dynamics of NSCs. Five days following the final TAM administration, characterization of quiescent NSCs ($GFAP^{+}EGFR^{neg}$/Total GFAP), activated NSCs ($GFAP^{+}EGFR^{+}$/Total GFAP) and NPC ($GFAP^{neg}EGFR^{+}$) populations showed trends toward a more quiescent niche as changes were observed in the different populations (quiescent: 75.44±3.48% vs. 88.94±3.02%, activated: 25.82±4.6% vs. 15.33±3.2%, NPCs: 17.39±1.19 vs. 12.15±1.24 cells/mm^3, in WT and $ADAM10^{fl/fl}$, respectively; Fig. 8 A-B). To further explore NSC cycling dynamics in WT and $ADAM10^{fl/fl}$ mice, we analyzed NSC retention within the SVZ niche after ADAM10 deletion. At 30 days after the final TAM, in situ characterization of YFP+ cells revealed an increased percentage of NSCs (YFP+Sox2+/Total YFP cells) in the SVZ of $ADAM10^{fl/fl}$ mice (58.65±2.86% vs. 75.16±5.44% in WT vs. $ADAM10^{fl/fl}$ SVZ; Fig.8 C,E). Analysis of DCX+ cells in the SVZ at this time point demonstrated decreased expression in the $ADAM10^{fl/fl}$ SVZ. Together, these results point to a shortage of lineage commitment and higher self-renewal capacity (Fig. 8 D). To further corroborate this idea, we analyzed BrdU label-retaining cells (LRCs) [248]. This assay relies on the fact that slowly cycling NSCs retain a BrdU label, whereas dividing cells dilute the BrdU and leave the niche within the chase period [249]. For this experiments, we injected P45 mice with TAM (3x48 hrs apart) followed by BrdU (5x every 3 hours). Analysis was performed at P75 after a 30-day chase (Fig. 8F). On average, we observed 1-2 LTR-BrdU+ cells in the WT vs. 4-5 LTR-BrdU+ cells in the $ADAM10^{fl/fl}$ SVZ. To characterize the LTR-BrdU+ cells as stem cells vs. terminally differentiated cells, we analyzed the co-expression of LTR-BrdU+ cells with the NSC marker, Sox2+. Our data revealed an

increased number of slowly cycling NSCs (BrdU+Sox2+) in the ADAM10$^{fl/fl}$ SVZ, further demonstrating that NSCs are retained in the SVZ as opposed to differentiating and leaving the niche (Fig.8 G-H). These results demonstrate that deleting ADAM10 results in a more quiescent niche, with decreased activation of quiescent NSCs to a more active proliferative state.

To verify the decrease in actively proliferating cells, we examined Ki67 expression. Ki67, a marker of late G1, S, G2, and M phases of the cell cycle identifies actively dividing progenitors. Immunostaining for Ki67 further corroborated a decrease in dividing progenitors in the ADAM10$^{fl/fl}$ SVZ (30.27±4.62 vs. 16.45±2.54 cells per mm^3; Fig. 9A-B). Moreover, the increase in slowly cycling LRC-BrdU+ NSCs, implies differences in cell cycle kinetics in the ADAM10$^{fl/fl}$ compared to the WT prompting us to evaluate the impact of ADAM10 deletion on rate of cell cycle withdrawal and length of the cell cycle. We examined cell cycle re-entry *in vivo* following TAM by labeling cells in S phase with CldU and IdU [239]. CldU was administered followed by IdU at varying intervals between the two injections, termed Δt. At a Δt of 24 hours, analysis of CldU+ NSCs that had exited S phase of the cell cycle 24 hrs. after CldU labeling (CldU+IdU−/Total CldU) revealed that ADAM10$^{fl/fl}$ NSCs had a decreased probability of exiting from active proliferation relative to controls. At the same time the ADAM10$^{fl/fl}$ NSCs demonstrated an increased probability of re-entry (CldU+IdU+/Total CldU; Fig. 9 C-E). Comparison of tissue from mice treated with a Δt of 6 hours suggests ADAM10$^{fl/fl}$ mice have a prolonged cell-cycle timing as less S-phase re-entry (CldU+IdU+/CldU+ Total) was observed at t=6 in the ADAM10$^{fl/fl}$ compared to WT. (Fig 9 A-C). These

results agree with the increase in LRC-BrdU+ cells in the ADAM10$^{fl./fl}$ SVZ, indicating an increase in slowly cycling NSCs maintained within the cell cycle.

To evaluate cell cycle withdrawal, we used an in vitro system allowing temporal control over BrdU incorporation and deletion of ADAM10. For this experiment, we plated secondary neurospheres obtained from WT and ADAM10$^{fl/fl}$ SVZ tissue on PLL coated coverslips before administering BrdU for 24 hours to label cells in S phase. The cells were washed then incubated with hydroxy-tamoxifen (4-OHT) for 3 days to delete ADAM10 in floxed cells followed by growth factor removal. This paradigm allowed us control for BrdU incorporation and recombination to analyze cell cycle status following ADAM10 deletion. Subsequently, cells were analyzed for co-expression with Ki67 to quantify the number of BrdU labeled cells remaining in the cell cycle after ADAM10 deletion. Using this paradigm, we observed a higher number of cycling stem cells (BrdU+ Ki67+/Total BrdU) in the ADAM10$^{fl/fl}$ (2.92±.30% vs. 4.52±.05% ,in WT and fl/fl cells, respectively) condition suggesting an increased probability that the cells remain in the cell cycle rather than exiting (BrdU+Ki67-/Total BrdU; 97.08±.30% vs. 95.52±.09%, in WT and fl/fl cells respectively; Fig. 9 F-G). Cell cycle exit is associated with terminal differentiation unless cells revert to quiescence (G0) which is unlikely in culture conditions [250]. Moreover, maintenance of cells within the cell cycle indicates retention of stem cell properties, as slow cell cycle progression could be involved in sustaining self-renewal [251]. These studies corroborate the increase in LRC-BrdU cells, and indicate ADAM10$^{fl/fl}$ NSCs are retained in the cell cycle while dividing slowly rather than actively proliferating.

To directly study proliferation, we performed cell cycle analysis to examine the effects of ADAM10 deletion on SVZ cells and GFAP-GFP sorted cells using flow cytometry. Mice were injected with TAM (3x 24 hrs.) and 48hrs after the final TAM, they received a single BrdU injection. At 2hrs after the BrdU injection, a single cell suspension was prepared from SVZ tissue, fixed, and processed for BrdU and propidium iodide (PI) staining. For GFAP-GFP experiments, SVZ tissue was similarly prepared for FAC sorting and collected cells were fixed for BrdU/PI staining. We found that the fraction of cells in S phase was decreased in ADAM10$^{fl/fl}$ SVZ tissue and GFAP-GFP+ sorted cells when compared with WT samples (73.75±9.11% of controls for SVZ tissue and 44.42±19.22% of controls for GFAP-GFP sorted cells ; Fig. 10 A).

To further investigate the biologic role of ADAM10 in NSC cell cycle status, we examined the effect of ADAM10 gain-of-function using acitretin (AC), a pharmacologic activator of ADAM10 transcription. First, we verified an increase in SVZ ADAM10 activity *in vivo* following acitretin administration using an ADAM10 activity assay kit as per manufacturer's instructions (SensoLyte® 520 ADAM10 Activity Assay Kit; Fig. 10B). Additionally, acitretin injections increased levels of the cleaved (C-terminal fragment, CTF) form of the established substrate, N-cadherin, a biologic readout of increased ADAM10 activity (Fig. 10C) [189, 252]. To this end, WT mice were injected with AC twice before SVZ tissue was processed for cell cycle analysis as above. Activation of ADAM10 by AC, increased the percentage of SVZ cells in S phase as compared with control samples (1.32±.078 of controls; Fig. 10E). Interestingly, fewer cells were

collected in the GFAP-GFP sorted cells in the AC treated group suggesting lineage progression and subsequent loss of GFP expression which could explain the decrease in S phase fraction observed in the acitretin treated GFAP-GFP+ sorted group**.** Collectively, these results suggest ADAM10 regulates proliferation and lineage progression of NSCs in the SVZ. The overall decrease in proliferation in the ADAM10$^{f/lfl}$ SVZ suggests a decrease in NSC differentiation into rapidly dividing progenitors while the decreased proliferation in the FACs experiments points to the neural stem cell population as the origin.

ADAM10 Directs NSC Properties *In Vitro*

Given the effect of ADAM10 in vivo, we investigated the impact of ADAM10 deletion on essential features of NSCs, including self-renewal, proliferation, and the ability to produce differentiated progeny in vitro. In the appropriate culture conditions, NSCs form free-floating non-adherent spherical clusters of cells termed neurospheres [12]. After passaging, re-formation of neurospheres indicates retention of the self-renewal potential of stem cells whereas progenitors lose the ability for sphere formation. Deletion of ADAM10 increased formation of secondary neurospheres (1.99 ± 0.32 of control) and tertiary neurospheres (1.54± 0.20 of controls; Fig. 10 D-E). Furthermore, analysis of neurosphere size from FAC-sorted WT and ADAM10$^{fl/fl}$ YFP+ cells showed that on average, ADAM10$^{fl/fl}$ YFP+ sorted cells had a smaller diameter (57.81±5.09 vs. 36.20±2.67 um in WT vs. fl/fl YFP sorted cells, respectively; Fig. 10F). Bins of neurosphere size demonstrated that the majority of ADAM10$^{fl/fl}$ neurospheres were more likely to be less than 30μm while WT neurospheres were 50μm or greater,

indicating decreased proliferation (Fig. 10G). We confirmed the proliferation defect in ADAM10$^{fl/fl}$ YFP cells vs. WT YFP cells by short term (2 hr) BrdU administration *in vitro* to identify the rapidly dividing cells (35.83±1.79% vs. 7.15±6.77% YFP+BrdU+/Total YFP; Fig. 10 I). These results showed that the recombined cells were responsible for the decreased proliferation and further demonstrated retention of self-renewal properties as previously indicated by the increased LTR-BrdU cells (Fig. 8C-H).

In vivo we observed a reduced number of NSC progeny in the ADAM10$^{fl/fl}$ mice. To investigate lineage progression in vitro, we differentiated WT and ADAM10$^{fl/fl}$ NSCs on PLL coated coverglasses for 6 days in vitro (DIV) before analysis with markers of the differentiated and undifferentiated state. Dissociated cultures of secondary neurospheres from YFP-sorted SVZ cells demonstrated increased Nestin+ stem and progenitor cells but fewer Map2+ neurons in the ADAM10$^{fl/fl}$ compared to WT cells (Nestin counts were 2.17±0.48 of controls and Map2 counts were 0.51±0.08 of controls Fig. 11A-E). These findings are consistent with ADAM10 deletion maintaining NSC properties as the ADAM10$^{fl/fl}$ NSCs retain Nestin expression. We confirmed this finding with GFAP-GFP NSCs, which showed a similar phenotype. Namely, an increase in ADAM10$^{fl/fl}$ GFAP-GFP+ NSCs co-expressing with Nestin (arrows) once exposed to differentiation conditions compared to WT NSCs (Fig. 11C-D).

ADAM10 Directs NSC Positioning and Morphology

Considering the defective differentiation of NSCs, we investigated whether deletion of ADAM10 in adult NSCs would have any effect on NSC morphology or

positioning within the SVZ. Wholemount analysis of the ADAM10$^{fl/fl}$ SVZ revealed normal pinwheel architecture with GFAP+ NSCs located at the center and a normal vascular plexus. Interestingly, we observed a very different morphology in ADAM10$^{fl/fl}$ GFAP+ NSCs at 5 days following TAM administration. Namely, ADAM10$^{fl/fl}$ NSCs extended long basal processes to contact the vasculature reminiscent of a ”radial glial-like” morphology, whereas WT NSCs were found both away from and making direct cell body contact with the vessels (Fig 12B-C). To facilitate the identification of NSCs in situ, we crossed the Nestin-CRE^{ER};ADAM10$^{fl/fl}$ mice with a transgenic mouse in which GFP is specifically expressed in the cell body of NSCs (GFAP-GFP). Next, we quantified positioning by analyzing the relationship of GFAP-GFP+ NSCs with niche structures using SVZ coronal tissue sections. To quantify the positioning of NSCs within the SVZ we measured the shortest distance between the NSC cell body and their closest blood vessel as visualized by laminin staining. At the same time, we measured the distance from the ventricular wall. On average, the ADAM10$^{fl/fl}$ GFAP-GFP+ NSCs were closer to the ventricular wall and farther from the blood vessels measured using coronal sections (21.1±1.3μm vs. 12.22±0.68 μm and 16.08±0.88 vs. 24.98±1.38μm, respectively. Additionally, frequency analysis of the total GFAP-GFP cells analyzed showed ADAM10$^{fl/fl}$ NSCs were distributed closer to the ventricular wall. The majority of ADAM10$^{fl/fl}$ NSCs were within 5μm of the ventricular wall and farther from the blood vessels while WT NSCs demonstrated an even distribution (Fig.12 D-F). Our data was further validated using SVZ wholemount preparations (13.73±.38μm vs. 31.46±6.1μm; distance from blood vessels; not shown). These results suggest ADAM10 regulates NSC translocation from the apical to the basal niche.

After observing the tendency for ADAM10$^{fl/fl}$ NSCs to remain in the apical niche, we examined adhesion molecules known to regulate neurogenesis. An interesting candidate was VCAM-1, which specifically co-expresses in the apical endfeet of NSCs at the ventricular wall. VCAM-1 is a surface molecule known to regulate niche architecture and neural stem cell function [123]. Immunoblotting for VCAM-1 expression in both SVZ tissue and NSCs cultured in vitro revealed an 8.61 fold increase (0.32± 0.16 vs. 1.17±.12 AU) in VCAM-1 expression in the ADAM10 $^{fl/fl}$ compared to WT lysates (Fig12 G-H). This result is consistent with the idea that ADAM10$^{fl/fl}$ NSCs retain contacts with the ventricular wall and an undifferentiated state. Similarly, immunofluorescence analysis revealed an increase in VCAM-1 spots in ADAM10$^{fl/fl}$ tissue compared to WT controls (Fig. 12I). Taken together, these experiments suggest increased NSC adhesion to the apical SVZ niche results in reduced translocation and, as a result, reduced lineage progression in the ADAM10$^{fl/fl}$ compared to the WT animals.

ADAM10 Directs NSC Properties in a Cell Autonomous Manner

ADAM10 can act via autocrine, paracrine, or juxtacrine signals, prompting us to examine whether our observed phenotype was cell autonomous or non-autonomous. To this end, FAC sorted WT and ADAM10$^{f/lfl}$ Nestin-YFP+ secondary neurospheres were dissociated, and single cells in suspension were seeded on top of WT SVZ explants for 3DIV (Fig. 13A). While WT Nestin-YFP+ cells displayed a rounded morphology with fewer processes (resembling NPCs), ADAM10$^{fl/fl}$ YFP+ cells displayed a radial glial-like morphology with few cells displaying NPC morphology in the explants (Fig. 13B-F).

Note that ADAM10$^{fl/fl}$ YFP+Nestin+ cells in WT explants revealed a similar morphology as observed in situ in the ADAM10$^{fl/fl}$ GFAP+ wholemounts (compare Fig. 13B to Fig. 12B). We further characterized Nestin-YFP+ cells after seeding with markers for stem and progenitor cells. Interestingly, a higher percentage of YFP+ cells co-expressing with the stem cells markers CD133 and Nestin were observed in ADAM10$^{fl/fl}$ cells as compared to WT, suggesting that WT NSCs underwent lineage progression from NSCs to NPCs. Analysis of the percentage of YFP+CD133+/Total YFP+ cells showed 16.15±12.21% vs. 70.20±6.59% and YFP+Nestin+/Total YFP were 14.05±5.62% vs. 56.19±9.11% in WT and ADAM10$^{fl/fl}$ samples, respectively (Fig. 13C-D, H-G). Furthermore, there was no significant difference in the distance of YFP+ cells from blood vessels indicating ADAM10$^{fl/fl}$ NSCs are able to respond to endothelial-derived cues similar to WT NSCs (11.02±2.09 μm vs. 16.15±4.48 μm in WT and ADAM10$^{fl/fl}$ YFP+ cells, respectively). These experiments validated our earlier finding that deletion of ADAM10 in NSCs maintains the undifferentiated state. Altogether, our observations suggest that ADAM10 works in a cell autonomous fashion in NSCs to regulate positioning within the niche and lineage progression.

ADAM10 Cleaves JAM-C

To define a mechanism by which ADAM10 regulates NSC lineage progression and positioning within the SVZ niche, we performed a micro-array analysis where we observed that several canonical ADAM10 substrates were down regulated including Eph Receptors, ephrins, neuropilin, and netrins in addition to the tight junction molecule junctional adhesion molecule C (JAM-C). Pathway analysis further highlighted

alterations in the tight-junction signaling pathway. In this study, we focused on JAM-C as a molecular substrate for ADAM10 in NSCs by investigating expression levels of the full length/cleaved forms as well as downstream signaling partners. JAM-C served as an interesting candidate due to its identification as an apical surface marker of neural stem cells and a substrate for ADAM10 cleavage in two endothelial cell lines, HMVEC and HMEC-1s [222, 223]. In SVZ wholemount preps, we identified JAM-C expression in the apical niche co-expressing with GFAP+ NSCs and, of particular interest, at the center of pinwheels (Fig.14 A). We verified JAM-C expression using coronal sections where it co-expressed with GFAP+ NSCs in the apical SVZ (arrows; Fig. 14B). Additionally, we identified JAM-C co-expression in Nestin and Lex positive neural stem and progenitor cells from acutely dissociated preparations of WT SVZ tissue (Fig. 14C-D). Immunoblotting of WT SVZ protein lysates revealed both JAM-C and ADAM10 expression in the SVZ, with JAM-C expression enriched in the SVZ compared to the cortex (Fig. 14E-G). The specific expression of JAM-C to the SVZ suggests a unique role in directing NSC properties. To identify whether ADAM10 and JAM-C interact in the SVZ, we performed immunoprecipitation experiments with JAM-C, and blotted for ADAM10 expression, which demonstrated an association between the two (Fig. 15G).

To determine whether ADAM10 sheds JAM-C, we used SVZ explants from WT and ADAM10$^{fl/fl}$ mice as well as ADAM10 gain of function experiments using AC. First, we induced deletion of ADAM10 in vitro by administering 4-OHT in WT and ADAM10$^{fl/fl}$ SVZ explant cultures. 48 hrs. after the first 4-OHT administration, explants were treated with AC (18hrs and 4 hrs before harvest) and processed for western blot analysis. Using

an antibody targeted to the N-terminal region, we observed the full length JAM-C at 42 kDA in protein lysates from all SVZ explants. However, the JAM-C N-terminal fragment (25kDa) was only detected in AC treated WT samples but not in ADAM10$^{fl/fl}$ explants (Fig.14 H-I). Moreover, a significant difference in the full-length and cleaved form was observed between WT and ADAM10$^{fl/fl}$ AC treated samples. This analysis indicates that ADAM10 specifically expressed in NSCs promotes JAM-C shedding by the fact that the shed form was not present in ADAM10$^{fl/fl}$ samples treated with AC. To confirm our hypothesis that ADAM10 regulates JAM-C signaling in NSCs, we analyzed WT and ADAM10$^{fl/fl}$ NSC lysates. Consistent with our hypothesis that NSC derived ADAM10 processes JAM-C, ADAM10$^{fl/fl}$ NSCs expressed higher levels of the full-length form of JAM-C (1.98±.35 of controls; Fig. 14 J-K).

Previous studies demonstrated decreased Rap1 activity (Rap1-GTP) following JAM-C over expression as well as increased Rap1 activity following JAM-C ablation, indicating Rap1 is a downstream target of JAM-C signaling activation [224, 225]. To test whether this mechanism is conserved in other cell lines, we examined the response of HEK293 cells to plasmid mediated JAM-C overexpression. We observed a similar decrease in Rap1-GTP following JAM-C over expression. Interestingly, immunoblotting for the negative regulator of active Rap1, Rap1-GAP, in cells over-expressing JAM-C showed increased expression (not shown). Previous studies did not identify a molecular mediator for the decrease in Rap1-GTP following JAM-C over-expression, indicating Rap1Gap is downstream of JAM-C and mediates the changes in active Rap1.

In support of our hypothesis that ADAM10 regulates JAM-C signaling in NSCs, we detected increased Rap1-GTP in conjunction with decreased Rap1Gap expression in ADAM10$^{fl/fl}$ vs. WT NSCs by western blot. Rap1Gap expression in ADAM10$^{fl/fl}$ NSC lysates was 0.48±0.12 of controls and Rap1-GTP was 4.39±.1.27 of controls (Fig. 14J-K). Similarly, treatment with the small molecule ADAM10 inhibitor GI 254023X (GI), showed a trend towards a decrease in Rap1Gap and an increase in the full-length form of JAM-C. JAM-C expression in GI254023X treated NSC lysates was 1.77±.14 of controls and Rap1Gap was 0.72±.09 of controls (Fig. 14L). These findings suggest that processing of JAM-C is necessary for signal activation as we observed a decrease in Rap1Gap in the ADAM10$^{fl/fl}$ NSCs in conjunction with increased full length JAM-C.

In the context of the SVZ and development, it has been suggested that at both embryonic (E18.5) and postnatal (P4) stages Rap1 activity is higher in stem cells while Rap1Gap expression is higher in cells undergoing differentiation. Rap1Gap is co-induced with DCX in cells leaving the niche following commitment towards a migratory fate [131]. Similarly, we observed this same increase in Rap1Gap expression in cells exposed to differentiating conditions, demonstrating that this mechanism is preserved in adult NSCs of the SVZ (Fig. 15A). Immunostaining of SVZ tissue showed Rap1Gap expression highest in cells displaced from the ventricular wall (Fig. 15B-C). High magnification analysis revealed Rap1Gap expression in cells located in the basal niche whereas apical SVZ cells are devoid of any substantial expression (Fig. 15B). Additionally, ADAM10$^{fl/fl}$ GFAP-GFP+ NSCs found adjacent to the ventricular wall rarely express Rap1Gap, while WT GFAP-GFP+ NSCs are found leaving the ventricular wall

and up-regulating Rap1Gap expression (arrow; Fig. 15C). This staining pattern is consistent with a role for Rap1Gap in apical to basal translocation and vascular niche residence.

In further support of an ADAM10/JAM-C signaling axis, we examined Nestin-YFP+ WT and ADAM10$^{fl/fl}$ cells in vitro by IF. We observed a trend towards a decrease in Rap1Gap staining in the ADAM10$^{fl/fl}$ (YFP+) cells compared to WT YFP+ cells 6.74±0.52% vs. 18.39±4.27% (Fig. 16A-B). When both WT and ADAM10$^{fl/fl}$ cells were treated with AC, Rap1Gap expression increased in the WT cells and ADAM10$^{fl/fl}$ cells that did not recombine (YFP-), but not cells deleted of ADAM10 activity (YFP+). Co-expression of Rap1Gap in WT YFP+ cells increased to 70.98±15.98: following acitretin administration whereas the percentage of double positive ADAM10$^{fl/fl}$ YFP+ cells only increased to 30.34±2.48% (Fig 16A-B). We confirmed this finding in vivo by immmunoblotting SVZ tissue for Rap1Gap, which showed a decrease in Rap1Gap expression in ADAM10$^{fl/fl}$ SVZ tissue (0.35±.08 of WT controls; Fig. 16C). Similar to the in vitro experiments, over-expression of ADAM10 by administering acitretin (IP injections) increased Rap1Gap expression in both WT and ADAM10$^{fl/fl}$ SVZ tissue. WT SVZ tissue treated with acitretin increased to 3.64±.94 of controls and the ADAM10$^{fl/fl}$ SVZ increased 3.71±.92 of controls; Fig. 16C). The increased Rap1Gap in the ADAM10$^{fl/fl}$ SVZ following AC injections is likely due to lower recombination in vivo or a non-NSC response. However, in vitro we did not observe an increase in Rap1Gap following AC administration in ADAM10$^{fl/fl}$ YFP+ cells (see Fig. 16A). This experiment placed Rap1Gap downstream of ADAM10 initiated signaling.

Based on previous literature, we hypothesized that JAM-C over expression would recover Rap1Gap expression in ADAM10$^{fl/fl}$ NSCs. Indeed, plasmid mediated JAM-C over expression 48 hrs. after transfection recovered Rap1Gap in the ADAM10$^{fl/fl}$ cells to WT levels (Fig. 16D-E). To determine whether Rap1Gap levels inversely correlate with Rap1 activity as predicted, we performed active Rap1-GTP pulldown assays in WT, ADAM10$^{fl/fl}$, and JAM-C over-expressing NSCs, as per manufacturer's instructions (ThermoFisher). We observed a 4.39±1.26 fold increase in active Rap1 (Rap1-GTP) in the ADAM10$^{fl/fl}$ compared to WT NSCs. Increased Rap1-GTP is associated with increased adhesion and the NSC state [131]. In our model, ADAM10$^{fl/fl}$ NSCs retain adhesion to the apical niche, therefore, increased Rap1-GTP could mediate this phenotype. Moreover, the increased Rap1-GTP was rescued to WT levels by JAM-C over-expression (Fig 16D-E). To prove that Rap1Gap acts downstream of JAM-C in NSCs, we lentivirally delivered shRNA targeted against JAM-C in vitro. After infection, the shRNA decreased JAM-C expression to 0.33± .08 of controls (Fig. 16G). Similar to the ADAM10$^{fl/fl}$ NSCs, we observed a decrease in Rap1Gap expression after JAM-C knockdown (0.16±.05 of controls; Fig 16F-G). This result demonstrates that the decrease in Rap1Gap observed in the ADAM10$^{fl/fl}$ NSCs is due to decreased signaling in an axis that includes JAM-C (Fig 10H). These results place Rap1Gap downstream of both ADAM10 and JAM-C.

To correlate JAM-C and Rap1 signaling with NSC lineage progression, we characterized expression levels of Rap1Gap in NSCs in either proliferating or differentiation conditions. As expected, our data showed lower levels of Rap1Gap in proliferating WT NSCs and higher levels during differentiation. In WT NSCs, Rap1Gap expression increased from 0.86±.11 on day 0 (D0) in differentiation conditions to 2.02±.41 after 4 days (D4) in differentiating conditions (Fig. 16H). However, differentiation of ADAM10$^{fl/fl}$ cells did not demonstrate the same increase in Rap1Gap. Not only was Rap1Gap expression lower at each time point analyzed, in ADAM10$^{fl/fl}$ vs. WT cells, no significant difference was observed between ADAM10$^{fl/fl}$ cells at day 0 (D0) and after four days in differentiating conditions (D4). Rap1Gap expression did not significantly increase (0.48±.08 to 0.71±.26 from D0 to D4) (Fig16. H-J). Interestingly, we observed a correlation between JAM-C and Rap1Gap during lineage progression. JAM-C expression increased from D0 to D4 of differentiation (Fig. 16H). This observation is in line with a previous study implicating JAM-C recruitment to the cell surface in the adhesion-dependent exit of neuronal progenitors from their germinal zone [221].

Consistent with VCAM-1 promoting adhesion and the undifferentiated NSC state, the increase in VCAM-1 expression observed in the ADAM10$^{fl/fl}$ cell lysates was similarly recovered to WT levels by the increase in Rap1Gap following JAM-C over-expression (Fig. 16K-L). This result agrees with earlier data demonstrating higher ADAM10$^{fl/fl}$ NSC adhesion within the niche and places the increased adhesion downstream of ADAM10/JAM-C signaling. Taken together, these results suggest that

ADAM10 regulates niche adhesion through JAM-C shedding in NSCs resulting in increased Rap1Gap and a concurrent decrease in Rap1-GTP.

Rap1-GTP has been associated with increased N-cadherin, integrin and cadherin activation [69]. To determine whether Rap1-GTP is responsible for the increased VCAM-1 or the increase is a consequence of the phenotype, we treated WT cells with the Rap1 activator 8-Cpt-2Me-cAMP [253]. Treatment of WT NSCs with the Rap1 activator demonstrated a trend towards an increase in VCAM-1 expression suggesting VCAM-1 expression may be regulated by this signaling mechanism (Fig. 16M-N). In our model, deletion of ADAM10, produces a decrease in Rap1Gap expression resulting in elevated active Rap1-GTP and increased adhesion to the apical SVZ. Taken together, these results suggest that deletion of ADAM10 regulates apical-basal translocation and maintenance of stem cell properties.

ADAM10 and Rap1 Direct Adhesion and Translocation

To investigate, the role of ADAM10-JamC-Rap1GAP-Rap1-GTP signaling in NSC positioning within the niche, we examined the adhesive and migratory properties of WT and ADAM10$^{fl/fl}$ NSCs in vitro. To study the effect of ADAM10 on migration/translocation, we performed in vitro scratch/wound assays [254]. When cells reached 80-90% confluence, a pipette tip was used to create a scratch in the monolayer. Migration distances of individual cells were analyzed 24 hours later. We observed a significant decrease in the number of NSCs that migrated from the scratch edge in ADAM10$^{fl/fl}$ NSCs as compared with WT NSCs and a decrease in the distance

migrated. On average, WT NSCs migrated 104.7±2.76μm while ADAM10$^{fl/fl}$ NSCs migrated 63.45±1.65μm from the scratch edge (Fig. 18A-B). Furthermore, we noticed that WT NSCs displayed a collective migration phenotype as we observed an average of 9 cells per stream while in the ADAM10$^{fl/fl}$ samples single cells tended to migrate alone. To verify that the NSCs themselves had an impaired migration phenotype we analyzed GFAP-GFP derived NSCs cultures. When only GFP+ cells were analyzed, a similar decrease in migration distance was observed in the ADAM10$^{fl/fl}$ GFAP-GFP+ cells. On average WT GFP+ cells migrated 145.80±9.42 μm while ADAM10$^{fl/fl}$ GFP+ cells migrated 82.13±9.58 μm (Fig. 18C-D). This data suggested a defect in cell adhesion in ADAM10$^{fl/fl}$ NSCs, which could affect collective migration.

Short-term adhesion assays using Calcein AM were used to test WT and ADAM10$^{fl/fl}$ NSC adhesion to a laminin, PLL, and fibronectin substrate. To investigate whether JAM-C is downstream of ADAM10 mediated NSC adhesion, we used a JAM-C blocking antibody in ADAM10$^{fl/fl}$ NSCs to prevent adhesion and signaling. Briefly, calcein-stained WT and ADAM10$^{fl/fl}$ cells were plated in the presence of JAM-C blocking antibody or isotype control IgG and allowed to adhere. After a 20-minute incubation, non-adherent cells were gently washed away and the remaining fluorescence was calculated as a percentage of total fluorescence before washing. We observed a 1.53±0.09 fold increase in ADAM10$^{fl/fl}$ NSC adhesion to laminin only, and this increase was rescued to WT levels after incubation with JAM-C blocking antibody indicating the increased adhesion in ADAM10$^{fl/fl}$ cells is JAM-C dependent (Fig. 17A). In further support, the adhesion experiments were repeated in the presence of the small molecule

inhibitor of ADAM10, GI 254023X, as well at the small molecule Rap1 activator 8-CPT-2-O- Me-cAMP [253]. As before, inhibition of ADAM10 activity with GI 254023X increased adhesion of treated cells to a laminin substrate only (1.62±0.20 of controls), while treatment with the Rap1 activator showed a trend towards an increase in adhesion when plated on laminin (1.39±0.15 of controls; Fig. 17B). These results demonstrate that inhibition of ADAM10 activity promotes increased NSC adhesion and correlates the increase in Rap1 to the increase in adhesion.

Rap1 Acts Downstream of JAM-C

Both ADAM10$^{fl/fl}$ and JAM-C knockdown produced a decrease in Rap1Gap, therefore, we wondered whether a similar decrease in migration would be observed in the JAM-C knockdown condition as in the ADAM10$^{fl/fl}$. We investigated migration, using the scratch test/migration assay in WT and ADAM10$^{fl/fl}$ monolayers treated with either lentivirus delivered scramble or shRNA targeting JAM-C. As before, ADAM10$^{fl/fl}$+ Scramble NSCs migrated less from the edge of the scratch when compared to WT+ Scramble NSCs. Interestingly, a similar decrease was observed between WT+shRNA NSCs compared to WT+Scramble cells. On average, ShRNA treated cells migrated 87.71±4.72μm and control cells migrated 118.12±5.26μm (18F-G). Decreased Rap1Gap expression was observed in WT+shRNA compared to WT+scramble NSCs (refer to Fig. 16F) implying the decreased migratory potential of ADAM10$^{fl/fl}$ NSCs is due to a decrease in the ADAM10-JamC-Rap1Gap-Rap1 pathway. To verify that Rap1Gap acts downstream of ADAM10 and is responsible for the migration defect in ADAM10$^{fl/fl}$ NSCs, we lentivirally overexpressed Rap1Gap which increased Rap1Gap expression

13.64±4.65 fold compared to control lentivirus. As expected, lentiviral over expression of Rap1Gap rescued the elevated Rap1-GTP in ADAM10$^{fl/fl}$ NSCs to WT levels (Fig. 18H). Moreover, migration was increased in ADAM10$^{fl/fl}$ NSCs over-expressing Rap1Gap when compared to ADAM10$^{fl/fl}$ NSCs treated with control lentivirus (82.09±3.19 μm vs. 140.57±11.32 μm; Fig. 18 I-J). Therefore, the deficit in Rap1Gap was responsible for the decreased migration in ADAM10$^{fl/fl}$ NSCs.

To investigate the effect of Rap1Gap over-expression on morphology and differentiation, control and Rap1Gap lentivirus transduced ADAM10$^{fl/fl}$ NSCs were plated on top of WT SVZ explants as before. Cells transduced by either control or Rap1Gap lentivirus expressed fluorescent protein, allowing for controlled co-expression analysis with neural stem and progenitor markers. Co-expression analysis demonstrated a decrease in Rap1Gap infected ADAM10$^{fl/fl}$ NSCs co-expressing with CD133 (prominin) compared to control infected ADAM10$^{fl/fl}$ NSCs (GFP+CD133+/Total GFP+ cells). 93.98±6.02% of ADAM10$^{fl/fl}$ GFP+ cells compared to 30.21±11.17% of ADAM10$^{fl/fl}$ GFP+ cells over-expressing Rap1Gap co-expressed with CD133 (Fig. 18K-L). However, no significant changes were observed in Nestin double-labeled cells between groups (GFP+Nestin/Total GFP+ cells). On average, 87.83±0.33% vs. 82.5±2.1% of control and Rap1Gap ADAM10$^{fl/fl}$ GFP+ cells co-expressed with Nestin, respectively (Fig. 18K-L). CD133 is expressed in quiescent and activated NSCs whereas Nestin identifies activated NSCs and progenitors. This result indicates a lineage progression induced by Rap1Gap and agrees with the higher Rap1Gap expression observed in SVZ neural

progenitors vs. apical NSCs. Morphologically, the control ADAM10$^{fl/fl}$ NSCs were “radial-glial” like as before, whereas the Rap1Gap GFP+ cells appeared rounder (Fig. 18K).

Analysis of Additional Substrates

ADAM10 has a number of identified substrates that are expressed in the SVZ. Two of the major substrates include N-cadherin and Notch, prompting us to explore the full length and cleaved forms in WT and ADAM10$^{fl/fl}$ NSC protein lysates isolated from secondary neurospheres. Examination of N-cadherin expression showed a similar result to one previously reported by our group using WT and ADAM10$^{fl/fl}$ SVZ explants [189]. Namely, both the full length and the CTF expression were down regulated in the ADAM10$^{fl/fl}$ NSCs. ADAM deletion decreased expression of the CTF from 0.74±0.12 to 0.43±0.11 in ADAM10$^{fl/fl}$ NSCs (Fig. 19A). The decrease in the CTF (cleavage fragment) is in-line with ADAM10 cleaving N-Cadherin. Since the full-length form was not increased, it is unlikely N-cadherin is mediating the effects seen following ADAM10 deletion. Moreover, western blot analysis of Notch processing did not reveal any significant difference in release of the Notch intracellular domain (NICD; Fig. 19B). However, a more in depth analysis of downstream gene targets would be necessary to rule this out. Based on this brief analysis, neither of these substrates seems like likely candidates.

ADAM10 in the Hippocampus

As mentioned, two stem cell niches exist in the CNS. Nestin expression has been identified in the SVZ as well as the dentate gyrus [255]. We chose to focus on the

SVZ in this study. However, brief analysis of YFP+ cells in the dentate gyrus showed an interesting pattern of distribution 30 days following TAM administration. In the WT dentate gyrus, the majority of cells were found in the outer subgranular zone layer while YFP+ cells in the ADAM10$^{fl/fl}$ animal were found dispersed throughout the granular zone. Quantification of cells shows 2.34±1.41% of WT YFP vs. 29.27±2.03% of ADAM10$^{fl/fl}$ YFP+ cells in the inner subgranular zone (Fig. 19C-D).

We tested one aspect of hippocampal spatial memory, the object location test. This test relies on the fact that mice spend more time investigating an object in a novel location. After habituation, mice are presented with the same object in two corners of the open field arena. The next day, mice are presented with the same two objects, however, one object is moved to a new location on the opposite corner of the arena. The moved object represents the novel location [256]. Analysis of time spent investigating the objects on the third day of the trial compared to the second day of the trial did not show any significant difference between the groups (Fig. 19E).

Chapter 4: Discussion

Retention of NSCs within the SVZ-niche is critical for NSC maintenance. The functional properties of stem cells, namely, their ability to self-renew and differentiate are important for the continuous generation of neurons and the production of cells for tissue repair. Currently, the diverse array of cues that regulate both NSC-NSC and NSC-niche interactions remain largely undefined. Identification of specific molecules that mediate the balance between NSC maintenance and lineage progression will facilitate the development of novel therapies for the purposes of cell replacement. Our data here show that the protease, ADAM10, maintains the pool of NSCs and their lineage cells by regulating adhesion to the apical SVZ domain upstream of a JAM-C/Rap1 axis.

ADAM10 Regulates NSC Self-Renewal and Lineage Progression in the Adult SVZ Niche

Extrinsic and intrinsic signaling pathways maintain NSC properties and the production of lineage cells throughout life. Several signals have been identified in promoting these properties. For example, the adhesion molecule, VCAM-1, found on qNSCs at sites of contact with the ventricular wall mediates NSC identity. Disruption of VCAM-1 leads to loss of the pinwheel architecture within the apical niche, lineage progression, and ultimately, depletion of the NSC pool [123]. Moreover, Noggin, the

bone morphogenetic protein (BMP) antagonist may best exemplify niche regulation of NSC maintenance. Due to its close proximity, ependymal cell derived Noggin has immediate access to inhibit BMPs before the tightly associated B1 cells can gain access. As a consequence, a restricted neurogenic microenvironment for SVZ cells is created [257]. Therefore, residence within the apical SVZ domain is necessary for maintenance of NSC properties.

Our data showed that ADAM10 maintains NSC number and the production of YFP+ cells that integrate into the OB. A lower number of DCX+ neural lineage cells were observed in the SVZ. These findings suggest that the sheddase is key to maintaining NSC biology in the adult SVZ niche, by regulating self-renewal and lineage progression. In the SVZ, Notch mediates cell-cell interactions and signaling activation to maintain NSC identity and self-renewal [155]. Several studies have identified a role for ADAM10 in the S2 cleavage necessary for Notch activation, whereas others name ADAM17 as the major sheddase. It appears that ADAM10 may be important for ligand-independent Notch activation whereas ADAM17 may be the primary protease in ligand-dependent signaling [177]. However, one may be able to compensate for loss of the other. During embryonic development, ADAM10 deletion in neural stem and progenitor cells leads to progenitor depletion due to premature neuronal differentiation. Additionally, neurosphere formation is affected due to decreased NICD1 production and activation of its downstream gene targets [185]. Interestingly, in the adult we observed a decrease in neurogenesis in the olfactory bulb and an increase in NSC self-renewal after ADAM10 deletion. These disparities could be attributed to differences in the timing

of ADAM10 deletion during embryogenesis vs. the adult. While many of the key mediators in the embryo continue to direct neurogenesis in the adult, critical differences exist in the cellular response profile. For example, BMP signaling maintains NSC proliferation in the embryo whereas in the adult, it promotes quiescence to prevent NSC exhaustion [258]. Distinctions in embryonic neurogenesis vs. adult neurogenesis have been attributed to the number of cell types produced during each period of life. At early time points, the entire brain is populated by a diverse number of neuronal and glial cell types, whereas neurogenesis in the adult is restricted to the production of granule and periglomerular cells of the olfactory bulb [66, 259]. Moreover, differences exist in the experimental design of our study vs. *Adam10*cKO during embryonic development [185]. For example, our mouse model targets exon 9 (floxed region), the protease domain, whereas Jorissen et al targeted exon 2 [185]. Moreover, in vitro differentiation by Jorissen et. al. was performed using primary neurospheres, whereas we differentiated secondary neurospheres. Primary neurospheres consist of a larger proportion of committed cells than secondary neurospheres, making the study of NSC fate decision or lineage progression difficult to interpret in the primary spheres. However, one could hypothesize that in the event of premature neuronal differentiation, this phenomenon would be lost when studying secondary neurospheres, whereas the primary neurospheres would contain increased numbers of neuronal progenitors and capture these differences. Additionally, later time points (E17.5) analyzed by Jorissen et al. showed a decrease in NeuN staining in the VZ and GE of Adam10 cKO, similar to the neurogenesis defect observed in our study. Only at E15.5 were more post-mitotic NeuN positive cells identified in the cortex and GE of Adam10 cKO. Hence, timing of analysis

can result in striking differences. Finally, the authors suggest that the premature differentiation results in progenitor depletion, similar to the decrease in progenitors we observed [185].

To date, ADAM10 has over 100 identified substrates [260]. As a result, functional changes following deletion of ADAM10 could arise due to altered signaling originating from one substrate or a collection of substrates. A recent study demonstrated that deletion of ADAM10 in neurons results in mis-targeted axons to the olfactory bulb and diffuse glomeruli due to altered NrCAM processing [260]. In the present study, defects in NSC lineage progression were evident when we analyzed neurogenesis in the OB by BrdU and YFP lineage tracing**.** We detected fewer YFP+ neurons in the granular cell layer of the OB. While the total number of YFP+NeuN+ neurons was significantly decreased by deletion of ADAM10, we did not observe significant changes in the percentage of YFP+NeuN+/Total YFP+ cells. These findings indicate that maturation of recombined cells reaching the olfactory bulb is not affected. Additionally, nestin expression is found in both neural stem and progenitor cells, therefore, deletion of ADAM10 in different stages could result in recombined cell emergence in the OB with an in tact differentiation program [30].

The defective neurogenesis in the OB can result from deficits in survival, migration, or lineage progression of NSCs. Cell death as measured by cleaved-caspase-3 immunoblotting was not statistically different between WT and ADAM10$^{fl/fl}$

protein lysates after the onset of differentiation. NSC lineages arising from the SVZ are continuously added to the OB after migrating the length of the RMS to finally emerge in the OB. This is in contrast to the dentate gyrus where newly generated neurons only migrate a short distance to integrate into the local circuitry [30]. Therefore, migration can significantly affect OB neurogenesis. Previously, we showed that deletion of ADAM10 in NPCs delayed progenitor migration into the subcortical white matter[189]. Since migration defects were observed in oligodendrocyte precursors in a mouse model of demyelination, we cannot exclude that in our system, migration of neuroblasts is also affected and could partly explain the reduction of Nestin lineage cell entry into the OB. Additionally, several molecules involved in cell migration are substrates of ADAM10 including discoidin domain receptor 1 (DDR1), cadherins, and Eph/Ephrins [189, 261, 262]. Interestingly, gene array analysis of transcripts altered in the SVZ of WT and ADAM10$^{fl/fl}$ samples showed changes in molecules associated with migration including Eph/ephrins and members of the cadherin family. Considering the observed decrease in DCX+ cells in the ADAM10$^{fl/fl}$ SVZ, the defective neurogenesis in the OB likely arises in the SVZ due to changes in NSC properties.

In vitro, we observed an increase in secondary neurosphere formation in FAC-sorted ADAM10$^{fl/fl}$ vs. WT NSCs demonstrating their neural stem cell capacity and ability for self-renewal. The neurospheres formed in the ADAM10$^{fl/fl}$ condition were smaller in size due to a decrease in proliferation. Sphere size is mainly related to the proliferation of the type C cells indicating a decrease in the number of intermediate progenitors within the secondary neurospheres [99]. In further support,

immunofluorescence demonstrated a decrease in Ki67+ progenitors in the ADAM10$^{fl/fl}$ SVZ. In conjunction with in vitro evidence demonstrating retention of Nestin+ cells following exposure to differentiation conditions, deletion of ADAM10 appears to promote maintenance of NSC properties. Consistent with the increased self-renewal observed in vitro, we observed an increase in BrdU label retaining cells (LRC-BrdU) in the ADAM10$^{fl/fl}$ SVZ. LRC-BrdU identify the slowly cycling NSC populations, and when co-expressed with NSC markers, demarcate cells maintained in the cell cycle vs. those that have locally differentiated and thus retain the BrdU signal [248]. Altogether, our data demonstrates maintenance of “stemness” and decreased lineage progression following deletion of ADAM10 in neural stem and progenitor cells.

The phenotypic output of these cellular and molecular changes was a decrease in newborn neurons reaching the olfactory bulb resulting in impaired short- term olfactory memory. The working model for signaling in the OB is that ongoing neurogenesis supplies the interneurons necessary to maintain proper inhibitory strength within the OB network [59]. Short-term memory formation, then, is driven by this feedback inhibition. Previous studies demonstrated that ablation of neurogenesis following infusion of the anti-mitotic drug AraC resulted in decreased short -term olfactory memory [58]. On the other hand, others demonstrated that enhanced neurogenesis via ERK5 activation in Nestin+ cells promoted short-term olfactory memory in the presence of normal olfactory discrimination and detection [246]. These studies validated a role for adult neurogenesis in mediating short-term memory. Of note, while we did observe some YFP+ cells in the OB of ADAM10$^{fl/fl}$ mice, those present

were not able to compensate for the overall decrease as demonstrated by the defective short-term olfactory memory. In the future, experiments studying other aspects of olfactory behaviors such as object discrimination and odor threshold will be important in determining the role of ADAM10 in olfaction.

ADAM10 Regulates the Anchorage and Apical Polarity of NSCs to Maintain Stemness

Wholemount analysis of SVZ tissue from WT and ADAM10$^{fl/fl}$ mice stained for GFAP showed NSCs with a very different morphology and contacts with niche structures. While the ependymal niche and blood vessels appeared unaffected, GFAP+ ADAM10$^{fl/fl}$ NSCs made contacts with the vasculature via long basal extending processes and rarely made cell body contact. Interestingly, the same “radial-glia” like morphology was observed when plating ADAM10$^{fl/fl}$ YFP sorted cells on top of WT slice cultures, indicating these changes occur in a cell-autonomous manner. Moreover, YFP+ cells from ADAM10$^{fl/fl}$ derived mice were more likely to co-express with the NSC markers Nestin and CD133 than the WT derived cells. These results demonstrate that the in vivo phenotype following loss of ADAM10 activity are not due to changes in signals originating from the vasculature. If NSC derived ADAM10 was responsible for the release of factors promoting lineage progression, the radial-glia phenotype would not be observed after plating ADAM10$^{fl/fl}$ NSCs on the WT explants. Moreover, this experiment demonstrates that ADAM10$^{fl/fl}$ NSCs are able to respond to endothelial-derived cues similar to WT NSCs. For example, ADAM10 could inactivate receptors to growth factors or chemokines, however no significant differences were observed in WT and ADAM10$^{fl/fl}$ NSC distance from the vasculature in the explant cultures. Of note, this

assay has previously been used to study chemotaxis [102]. However, it is also useful to study cell autonomous properties of NSCs in their native environment [124].

NSCs interact with their niche by spanning the apical and basal domains through adhesive interactions with ependymal cells on one side and the vasculature on the other. Apical adhesion junctions at NSC processes direct functional properties not only via adhesive contacts but also by directing signaling cascades and mode of division [105, 247]. Expression of cell surface proteins mediates positioning of NSCs within the niche to direct "stemness" properties such as self-renewal and multipotency [98]. Therefore, association with niche structures is necessary for NSC residence and stem cell characteristics. One mechanism that could mediate these observations is an increase in anchorage to the apical SVZ domain. Additionally, protease activity within the SVZ directs either signaling activation or maintenance of adhesion in the stem cell niche such as in the case of Notch or N-cadherin [248]. Porlan et al recently demonstrated a role for MT5-MMP mediated processing of N-Cadherin in directing NSC residence within the SVZ [135]. Therefore, NSC molecular expression patterns modulate NSC stemness, and these intrinsic programs can be modified by protease activity.

Our data suggests that inhibition of ADAM10 initiated pathways maintains the undifferentiated state of NSCs in the adult SVZ. This prompted us to examine positioning within the SVZ. Deletion of the protease domain of ADAM10 in Nestin+ NSCs resulted in retention of NSCs within the apical SVZ domain. Frequency analysis,

in the ADAM10$^{fl/fl}$ mice, showed GFAP-GFP+ NSCs were distributed closer to the ventricular wall than the vasculature while WT NSCs showed a more even distribution within both the apical and basal SVZ domains. In further support, a recent study demonstrated cells detained in the ventricular zone/ subventricular zone following *in utero* electroporation of ADAM10 shRNA. Moreover, they observed a decrease in DCX expression following shRNA mediated ADAM10 knockdown in cortical neurons and in ADAM10-cKO in cortical tissue at E18. However, this group attributed the decrease to disrupted microtubule stability downstream of Notch signaling [186].

Consistent with ADAM10$^{fl/fl}$ NSCs retaining contacts with the ventricular wall and maintaining an undifferentiated state, immunoblotting for VCAM-1 revealed increased expression in ADAM10$^{fl/fl}$ NSCs and SVZ tissue compared to WT. In conjunction with the in vitro evidence where ADAM10$^{fl/fl}$ NSCs were more likely to maintain Nestin expression after exposure to differentiation conditions, these findings indicate a retention of NSC characteristics. A possible explanation, for the disturbed lineage progression can be explained by altered translocation from the apical to the basal niche.

ADAM10 Cleaves JAM-C

We identified the apical stem cell marker, JAM-C as a substrate for ADAM10, where it regulates NSC anchorage to the ventricular wall. SVZ explants revealed a 25 kDa cleavage fragment following treatment with the ADAM10 transcriptional activator, acitretin, in WT slice cultures but not in ADAM10$^{fl/fl}$ explants. We additionally observed an increase in the full-length form of JAM-C in ADAM10$^{fl/fl}$ NSCs. Previous reports

identified ADAM10 as the protease responsible for shedding a soluble JAM-C fragment in endothelial cells [223]. This is the first time JAM-C was identified as a substrate for ADAM10 in NSCs. Earlier studies not only identified JAM-C as an apical stem cell marker, they suggested that during asymmetric divisions, neural stem cell characteristics are maintained by the daughter cell retaining JAM-C adhesional contacts with the ventricular wall [222]. Based on this report, it is tempting to suggest that ADAM10 plays a role in this process. By cleaving JAM-C, ADAM10 could provide the means for daughter cell detachment and exit from the ventricular wall. Additional experiments would be necessary to confirm this hypothesis.

Investigation of molecules known to act downstream of JAM-C highlighted Rap1, a small molecule GTPase able to switch between an inactive Rap1-GDP form and an active Rap1-GTP. Action of the GTPase activating protein, Rap1Gap mediates exchange of the GTP to the GDP bound inactive form, thus, serving as a negative regulator of Rap1 activity [229]. Previous reports showed an increase in active Rap1-GTP following inhibition of JAM-C and a decrease in Rap1-GTP following over-expression of JAM-C [204, 224]. Similarly, in our system, deletion of the protease domain of ADAM10 decreased JAM-C signaling in ADAM10$^{fl/fl}$ NSCs as revealed by increased expression of the downstream target of JAM-C, Rap1-GTP. In addition we observed decreased Rap1GAP expression. Moreover, cleavage of JAM-C following acitretin treatment correlated with an increase in Rap1Gap, placing Rap1Gap downstream of ADAM10 initiated JAM-C signaling.

Evidence in embryonic neural stem cells has demonstrated Rap1Gap involvement in the molecular machinery promoting niche exit as it is co-induced with the neuroblast marker, DCX. Niola et. al., described an increase in Rap1Gap during embryonic NSC differentiation whereas repression of Rap1Gap has been shown to modulate residency within the niche [131]. We observed the same increase in WT adult NSCs during differentiation. However, we report that deletion of ADAM10 activity prevents the elevation of Rap1Gap normally observed, thereby maintaining active GTP bound Rap1. Moreover, increased Rap1 activity, a key mediator of cell adhesion, in ADAM10$^{fl/fl}$ NSCs is rescued by over expression of JAM-C, placing Rap1 activity downstream of ADAM10 initiated JAM-C signaling. The over expression of JAM-C in ADAM10$^{fl/fl}$ cells likely targets recombined and non-recombined cells. Therefore, by over expressing JAM-C, we are able to push the system towards signaling activation by promoting the non-recombined cells to cleave JAM-C or saturating the system enough that another protease is able to cleave JAM-C. Alternatively, over expression of JAM-C is able to recruit the intracellular signaling partners.

Taken together, these findings suggest ADAM10 mediates a pathway essential to regulation of NSC anchorage to the ventricular wall. We hypothesize that if we knockout ADAM10 activity then JAM-C is no longer cleaved resulting in decreased Rap1Gap and loss of NSC translocation/neural lineage progression. To study NSC translocation, we substituted in the in vitro scratch wound assay. When we analyzed NSC migration with the in vitro scratch test assay, ADAM10$^{fl/fl}$ NSCs were less likely to migrate from the edge of the scratch than WT NSCs. This decrease in migration was

rescued by lentiviral over expression of Rap1Gap demonstrating the decrease in Rap1Gap is responsible for the translocation/migration defect in ADAM10$^{fl/fl}$ NSCs. Interestingly, we also observed a decrease in Rap1Gap expression and migration following lentivirally delivered shRNA to JAM-C in WT NSCs, phenocopying the ADAM10$^{fl/fl}$ NSCs. This experiment demonstrated that decreased signaling downstream of JAM-C mediates NSC migration. Also, this result indicates the increased extracellular JAM-C is not mediating the migration defect by promoting adhesion.

It is possible that JAM-C maintains NSC polarity via Rap1 and that the increase in Rap1Gap mediated by ADAM10 activity abolishes this polarization. Phalloidin immuno-staining of WT and ADAM10$^{fl/fl}$ NSCs, to visualize the F-actin filaments in migrating NSCs, showed WT NSCs exhibit a polarized migration by extending a long leading processes. However, the leading process in ADAM10$^{fl/fl}$ NSCs was blunted in shape. As mentioned, Rap1 regulates inside-out integrin activation [231]. In addition, a role for Rap1 has been demonstrated in paxillin positive focal adhesions [263], suggesting the elevated Rap1-GTP in ADAM10$^{fl/fl}$ NSCs is responsible for the migration and morphologic changes by altering focal adhesion and/or the actin reorganization necessary for proper migration. Moreover, we observed an increase in ADAM10fl/fl NSC adhesion to laminin substrates and not fibronectin. Not only did this result imply the increased adhesion is integrin dependent, it implied the changes in adhesion are Rap1 dependent. This is interesting when considering the elevated VCAM-1 whose substrate is fibronectin. As such, it follows that VCAM-1 is a consequence of the phenotype and not the mechanism mediating adhesion to the apical niche. Our results

are consistent with Rap1 serving as a positive regulator of integrin mediated adhesion and the associated signaling events [264]. Further studies into the integrins or cadherins regulated by Rap1 in ADAM10$^{fl/fl}$ NSCs would identify additional downstream targets of this pathway.

.

We used the in vitro migration assay as a substitute for in vivo translocation. Interestingly, NSCs rarely migrate in vivo. It is the progenitors that migrate from the niche to the OB. Our observation that GFAP+ NSCs migrate from the scratch edge suggests NSCs have a potential to migrate but are normally inhibited from doing so, perhaps by their apical and basal attachments. Additionally, further investigation into WT-WT and ADAM10$^{fl/fl}$-ADAM10$^{fl/fl}$ NSC interactions with one another would determine whether the streams observed in the migrating WT cells are due to changes adhesion. By performing the same short-term adhesion assays as before but plating calcein-labeled cells on WT and ADAM10$^{fl/fl}$ NSC monolayers would determine their adhesive interactions.

Rap1Gap over-expressing ADAM10$^{fl/fl}$ NSCs were less likely to co-express with the NSC marker CD133 compared to control infected cells when plated on SVZ explants. This rescue identified the decrease in Rap1Gap as responsible for the retention of NSC characteristics in the ADAM10$^{fl/fl}$ NSCs (increased CD133 expression). The mediator between JAM-C and Rap1 has not been identified, however, our evidence shows a correlation between ADAM10 in initiating Rap1Gap via JAM-C processing.

The mechanism in which JAM-C directs NSC properties is likely due to establishment of cell polarity and regulation of the cytoskeleton. As mentioned, the C-terminal domain of JAM-C contains a PDZ-binding domains as well as multiple phosphorylation sites [208]. This c-terminal domain recruits a cell polarity complex downstream of JAM-C to direct apical-basal polarity as evidenced during spermatid differentiation. This complex includes Par6, Cdc42, and atypical PKC [213]. Additionally, JAM-C interacts with ZO-1 and Par3 in epithelial and endothelial cells [207]. However, the mechanism in which JAM-C directs Rap1 activity has not been identified. In this study we identified Rap1Gap as a mediator, but the link between JAM-C and Rap1Gap is yet to be determined. Previous studies suggested JAM-A dimerization facilitates formation of a complex with PDZ-GEF2 to activated Rap1A [207]. In our model, it is possible JAM-C homophillic interactions in the apical SVZ similarly regulates NSC Rap1 activity by binding Rap1Gap or other upstream regulators. To test this hypothesis, it would be interesting to examine Rap1 activity in NSCs allowed to adhere to immobilized JAM-C in the presence of JAM-C blocking antibody to prevent adhesion or control IgG. The role of ADAM10 in this process has not been elucidated, however, it appears that ADAM10 cleavage of JAM-C plays a role in this process. Two possibilities are i) ADAM10 promotes conformational changes in the JAM-C structure that expose or hide cytoplasmic binding sites or ii) ADAM10 disrupts NSC-JAM-C interactions with extracellular binding partners to prevent the dimerization necessary for molecules with PDZ binding motifs to associate with the c-terminal domain of JAM-C. To test this hypothesis, we could first immuno-precipitate established polarity complex members with JAM-C to identify the proteins that interact with JAM-C. Following the identification

of binding partners, we could examine whether interaction of these proteins is affected by ADAM10 by performing the same immuno-precipitation experiment using WT and ADAM10$^{fl/fl}$ NSCs to determine the role of ADAM10 in this process.

In summary, JAM-C located at the apical plasma membrane of NSCs is processed by ADAM10. Without ADAM10 activity, Rap1Gap expression decreases and Rap1-GTP is high, promoting adhesion and retention in the apical SVZ. ADAM10 processing of JAM-C or Rap1Gap over-expression promotes translocation to the basal SVZ and subsequent lineage progression (summarized in Fig. 20).

ADAM10 Cleaves Additional Substrates Present in the SVZ

As mentioned, ADAM10 has a number of substrates. Our Investigation did not reveal any significant changes in Notch processing which was one of the substrates identified in embryonic analysis of ADAM10 deletion [185]. Additionally, a recent report identified N-cadherin in maintenance of NSCs at the ventricular wall [135]. While N-cadherin has been identified as a substrate for ADAM10 [252], we observed a trend towards a decrease in expression of the full- length form in addition to the CTF. However, other studies have demonstrated an increase in the full-length form following ADAM10 deletion [158]. If N-cadherin was responsible for NSC adhesion to the apical SVZ, we would expect an increase in the full length form. Our results suggest that these two substrates are not responsible for the phenotype observed in the adult following deletion of the protease domain of ADAM10 in Nestin+ cells.

ADAM10 Directs Nestin+ Cells in the Dentate Gyrus

Finally, we observed changes in the dentate gyrus, however, more precise co-expression analysis with markers for NSCs and differentiated cell types would need to be performed to determine the effect. Overall, there appeared to be a migration or differentiation defect. The ADAM10$^{fl/fl}$ YFP+ cells were found scattered throughout the dentate gyrus, similar to the cortical layering defect observed following ADAM10 deletion in newborn neurons [186].

A more thorough understanding of ADAM10 initiated cellular changes and the underlying molecular mechanisms are crucial to enhance SVZ neurogenesis as a means of curing neurologic disorders. Here, we provide evidence that ADAM10 regulates NSC lineage progression and translocation within the SVZ niche acting upstream of a JAM-C/ Rap1 axis.

Future Directions

To investigate the role of ADAM10 in NSCs, it would be of interest to target ADAM10 under a GFAP-CreER promotor. In our study we target Nestin+ stem and progenitors, then visualized the NSCs using a GFAP-GFP transgenic mouse line. By specifically targeting the NSCs we may see a more pronounced effect, or a very different effect following ADAM10 deletion. Additionally, in vivo experiments using JAM-C and Rap1 over-expression or shRNA vectors in our mouse models would be interesting. We showed recovery of migration and CD133 expression in the ADAM10$^{fl/fl}$ NSCs following Rap1Gap over-expression. In vivo evidence would take into account the entire SVZ milieu of factors that influence NSC properties.

Moreover, we show evidence of Rap1Gap rescue following JAM-C over-expression. This study suggests that by over-expressing JAM-C we are able to activate JAM-C signal transduction. Identification of the cleavage form in the supernatant following JAM-C over-expression in the ADAM10$^{fl/fl}$ NSCs would verify this correlation. Alternatively, over-expressing a mutant form of JAM-C that leaves it unable to be processed by ADAM10 followed by analysis of downstream signaling partners, would determine whether JAM-C signal transduction relies on sheddase activity.

Finally, a recent lab member identified a role for JAM-C in CNS injury models. At 3 days post demyelinating injury, it was observed that expression levels of JAM-C along with the other adhesion molecules, E-Cadherin and N-Cadherin, were reduced in apical GFAP+ NSCs (not published). This evidence was in the context of a decrease in NSCs in the apical compartment and a reduction in LRC-BrdU + NSCs. Further identification of a role for ADAM10 or JAM-C in stem cell activation during injury could have consequences for the field of stem cell regeneration.

1. Rakic, P., *Limits of neurogenesis in primates.* Science, 1985. **227**(4690): p. 1054-6.
2. Leblond, C.P., *CLASSIFICATION OF CELL POPULATIONS ON THE BASIS OF THEIR PROLIFERATIVE BEHAVIOR.* Natl Cancer Inst Monogr, 1964. **14**: p. 119-50.
3. Altman, J. and G.D. Das, *Postnatal changes in the concentration and distribution of cholinesterase in the cerebellar cortex of rats.* Exp Neurol, 1970. **28**(1): p. 11-34.
4. Altman, J. and G.D. Das, *Autoradiographic and histological studies of postnatal neurogenesis. I. A longitudinal investigation of the kinetics, migration and transformation of cells incorporating tritiated thymidine in neonate rats, with special reference to postnatal neurogenesis in some brain regions.* J Comp Neurol, 1966. **126**(3): p. 337-89.
5. Altman, J., *Autoradiographic investigation of cell proliferation in the brains of rats and cats.* Anat Rec, 1963. **145**: p. 573-91.
6. Altman, J. and G.D. Das, *Autoradiographic and histological evidence of postnatal hippocampal neurogenesis in rats.* J Comp Neurol, 1965. **124**(3): p. 319-35.
7. Kuhn, H.G., H. Dickinson-Anson, and F.H. Gage, *Neurogenesis in the dentate gyrus of the adult rat: age-related decrease of neuronal progenitor proliferation.* J Neurosci, 1996. **16**(6): p. 2027-33.
8. Seki, T. and Y. Arai, *Distribution and possible roles of the highly polysialylated neural cell adhesion molecule (NCAM-H) in the developing and adult central nervous system.* Neurosci Res, 1993. **17**(4): p. 265-90.
9. Luskin, M.B., *Restricted proliferation and migration of postnatally generated neurons derived from the forebrain subventricular zone.* Neuron, 1993. **11**(1): p. 173-89.
10. Goldman, S.A. and F. Nottebohm, *Neuronal production, migration, and differentiation in a vocal control nucleus of the adult female canary brain.* Proc Natl Acad Sci U S A, 1983. **80**(8): p. 2390-4.
11. Alvarez-Buylla, A., D.R. Buskirk, and F. Nottebohm, *Monoclonal antibody reveals radial glia in adult avian brain.* J Comp Neurol, 1987. **264**(2): p. 159-70.
12. Reynolds, B.A. and S. Weiss, *Generation of neurons and astrocytes from isolated cells of the adult mammalian central nervous system.* Science, 1992. **255**(5052): p. 1707-10.
13. Reynolds, B.A., W. Tetzlaff, and S. Weiss, *A multipotent EGF-responsive striatal embryonic progenitor cell produces neurons and astrocytes.* J Neurosci, 1992. **12**(11): p. 4565-74.
14. Gage, F.H., *Mammalian neural stem cells.* Science, 2000. **287**(5457): p. 1433-8.
15. Alvarez-Buylla, A. and D.A. Lim, *For the long run: maintaining germinal niches in the adult brain.* Neuron, 2004. **41**(5): p. 683-6.
16. Gage, F.H., et al., *Multipotent progenitor cells in the adult dentate gyrus.* J Neurobiol, 1998. **36**(2): p. 249-66.
17. Kornack, D.R. and P. Rakic, *The generation, migration, and differentiation of olfactory neurons in the adult primate brain.* Proc Natl Acad Sci U S A, 2001. **98**(8): p. 4752-7.
18. Lois, C. and A. Alvarez-Buylla, *Long-distance neuronal migration in the adult mammalian brain.* Science, 1994. **264**(5162): p. 1145-8.
19. Corotto, F.S., J.A. Henegar, and J.A. Maruniak, *Neurogenesis persists in the subependymal layer of the adult mouse brain.* Neurosci Lett, 1993. **149**(2): p. 111-4.

20. van Praag, H., et al., *Functional neurogenesis in the adult hippocampus.* Nature, 2002. **415**(6875): p. 1030-4.
21. Markakis, E.A. and F.H. Gage, *Adult-generated neurons in the dentate gyrus send axonal projections to field CA3 and are surrounded by synaptic vesicles.* J Comp Neurol, 1999. **406**(4): p. 449-60.
22. Kornack, D.R. and P. Rakic, *Continuation of neurogenesis in the hippocampus of the adult macaque monkey.* Proc Natl Acad Sci U S A, 1999. **96**(10): p. 5768-73.
23. Doetsch, F., J.M. Garcia-Verdugo, and A. Alvarez-Buylla, *Cellular composition and three-dimensional organization of the subventricular germinal zone in the adult mammalian brain.* J Neurosci, 1997. **17**(13): p. 5046-61.
24. Doetsch, F., et al., *Subventricular zone astrocytes are neural stem cells in the adult mammalian brain.* Cell, 1999. **97**(6): p. 703-16.
25. Ponti, G., et al., *Cell cycle and lineage progression of neural progenitors in the ventricular-subventricular zones of adult mice.* Proc Natl Acad Sci U S A, 2013. **110**(11): p. E1045-54.
26. Doetsch, F., J.M. García-Verdugo, and A. Alvarez-Buylla, *Regeneration of a germinal layer in the adult mammalian brain.* Proc Natl Acad Sci U S A, 1999. **96**(20): p. 11619-24.
27. Alvarez-Buylla, A., J.M. Garcia-Verdugo, and A.D. Tramontin, *A unified hypothesis on the lineage of neural stem cells.* Nat Rev Neurosci, 2001. **2**(4): p. 287-93.
28. Abrous, D.N., M. Koehl, and M. Le Moal, *Adult Neurogenesis: From Precursors to Network and Physiology.* Physiological Reviews, 2005. **85**(2): p. 523-569.
29. Nagayama, S., R. Homma, and F. Imamura, *Neuronal organization of olfactory bulb circuits.* Frontiers in Neural Circuits, 2014. **8**(98).
30. Lagace, D.C., et al., *Dynamic contribution of nestin-expressing stem cells to adult neurogenesis.* J Neurosci, 2007. **27**(46): p. 12623-9.
31. Ninkovic, J., T. Mori, and M. Gotz, *Distinct modes of neuron addition in adult mouse neurogenesis.* J Neurosci, 2007. **27**(40): p. 10906-11.
32. Lledo, P.M. and A. Saghatelyan, *Integrating new neurons into the adult olfactory bulb: joining the network, life-death decisions, and the effects of sensory experience.* Trends Neurosci, 2005. **28**(5): p. 248-54.
33. Imayoshi, I., et al., *Roles of continuous neurogenesis in the structural and functional integrity of the adult forebrain.* Nat Neurosci, 2008. **11**(10): p. 1153-61.
34. Whitman, M.C. and C.A. Greer, *Synaptic integration of adult-generated olfactory bulb granule cells: basal axodendritic centrifugal input precedes apical dendrodendritic local circuits.* J Neurosci, 2007. **27**(37): p. 9951-61.
35. Carlen, M., et al., *Functional integration of adult-born neurons.* Curr Biol, 2002. **12**(7): p. 606-8.
36. Magavi, S.S., et al., *Adult-born and preexisting olfactory granule neurons undergo distinct experience-dependent modifications of their olfactory responses in vivo.* J Neurosci, 2005. **25**(46): p. 10729-39.
37. Kaplan, M.S., N.A. McNelly, and J.W. Hinds, *Population dynamics of adult-formed granule neurons of the rat olfactory bulb.* J Comp Neurol, 1985. **239**(1): p. 117-25.
38. Lemasson, M., et al., *Neonatal and adult neurogenesis provide two distinct populations of newborn neurons to the mouse olfactory bulb.* J Neurosci, 2005. **25**(29): p. 6816-25.

39. Petreanu, L. and A. Alvarez-Buylla, *Maturation and death of adult-born olfactory bulb granule neurons: role of olfaction.* J Neurosci, 2002. **22**(14): p. 6106-13.
40. Carleton, A., et al., *Becoming a new neuron in the adult olfactory bulb.* Nat Neurosci, 2003. **6**(5): p. 507-18.
41. Saghatelyan, A., et al., *Local neurons play key roles in the mammalian olfactory bulb.* J Physiol Paris, 2003. **97**(4-6): p. 517-28.
42. Mori, K., *Membrane and synaptic properties of identified neurons in the olfactory bulb.* Prog Neurobiol, 1987. **29**(3): p. 275-320.
43. Peretto, P., et al., *Glial tubes in the rostral migratory stream of the adult rat.* Brain Res Bull, 1997. **42**(1): p. 9-21.
44. Peretto, P., et al., *The subependymal layer in rodents: a site of structural plasticity and cell migration in the adult mammalian brain.* Brain Res Bull, 1999. **49**(4): p. 221-43.
45. Lagier, S., A. Carleton, and P.M. Lledo, *Interplay between local GABAergic interneurons and relay neurons generates gamma oscillations in the rat olfactory bulb.* J Neurosci, 2004. **24**(18): p. 4382-92.
46. Mason, H.A., S. Ito, and G. Corfas, *Extracellular signals that regulate the tangential migration of olfactory bulb neuronal precursors: inducers, inhibitors, and repellents.* J Neurosci, 2001. **21**(19): p. 7654-63.
47. Zerlin, M., S.W. Levison, and J.E. Goldman, *Early patterns of migration, morphogenesis, and intermediate filament expression of subventricular zone cells in the postnatal rat forebrain.* J Neurosci, 1995. **15**(11): p. 7238-49.
48. Suzuki, S.O. and J.E. Goldman, *Multiple cell populations in the early postnatal subventricular zone take distinct migratory pathways: a dynamic study of glial and neuronal progenitor migration.* J Neurosci, 2003. **23**(10): p. 4240-50.
49. Doetsch, F. and A. Alvarez-Buylla, *Network of tangential pathways for neuronal migration in adult mammalian brain.* Proc Natl Acad Sci U S A, 1996. **93**(25): p. 14895-900.
50. Anderson, S.A., et al., *Interneuron migration from basal forebrain to neocortex: dependence on Dlx genes.* Science, 1997. **278**(5337): p. 474-6.
51. Wonders, C.P. and S.A. Anderson, *The origin and specification of cortical interneurons.* Nat Rev Neurosci, 2006. **7**(9): p. 687-96.
52. Ventura, R.E. and J.E. Goldman, *Dorsal radial glia generate olfactory bulb interneurons in the postnatal murine brain.* J Neurosci, 2007. **27**(16): p. 4297-302.
53. Kosaka, K., et al., *Chemically defined neuron groups and their subpopulations in the glomerular layer of the rat main olfactory bulb.* Neurosci Res, 1995. **23**(1): p. 73-88.
54. Merkle, F.T., Z. Mirzadeh, and A. Alvarez-Buylla, *Mosaic organization of neural stem cells in the adult brain.* Science, 2007. **317**(5836): p. 381-4.
55. PRICE, J.L. and T.P.S. POWELL, *The Synaptology of the Granule Cells of the Olfactory Bulb.* Journal of Cell Science, 1970. **7**(1): p. 125-155.
56. Kelsch, W., et al., *Distinct mammalian precursors are committed to generate neurons with defined dendritic projection patterns.* PLoS Biol, 2007. **5**(11): p. e300.
57. Parrish-Aungst, S., et al., *Quantitative analysis of neuronal diversity in the mouse olfactory bulb.* J Comp Neurol, 2007. **501**(6): p. 825-36.
58. Breton-Provencher, V., et al., *Interneurons produced in adulthood are required for the normal functioning of the olfactory bulb network and for the execution of selected olfactory behaviors.* J Neurosci, 2009. **29**(48): p. 15245-57.

59. Arenkiel, B.R., *Adult neurogenesis supports short-term olfactory memory.* J Neurophysiol, 2010. **103**(6): p. 2935-7.
60. Rochefort, C., et al., *Enriched odor exposure increases the number of newborn neurons in the adult olfactory bulb and improves odor memory.* J Neurosci, 2002. **22**(7): p. 2679-89.
61. Chae, C.H., et al., *Swimming exercise stimulates neuro-genesis in the subventricular zone via increase in synapsin I and nerve growth factor levels.* Biol Sport, 2014. **31**(4): p. 309-14.
62. Ma, D.K., G.L. Ming, and H. Song, *Glial influences on neural stem cell development: cellular niches for adult neurogenesis.* Curr Opin Neurobiol, 2005. **15**(5): p. 514-20.
63. Kikuta, S., et al., *Sensory Deprivation Disrupts Homeostatic Regeneration of Newly Generated Olfactory Sensory Neurons after Injury in Adult Mice.* The Journal of Neuroscience, 2015. **35**(6): p. 2657-2673.
64. Rawson, N.E. and A.S. LaMantia, *A speculative essay on retinoic acid regulation of neural stem cells in the developing and aging olfactory system.* Exp Gerontol, 2007. **42**(1-2): p. 46-53.
65. Villeda, S.A., et al., *The ageing systemic milieu negatively regulates neurogenesis and cognitive function.* Nature, 2011. **477**(7362): p. 90-4.
66. Ming, G. and H. Song, *Adult Neurogenesis in the Mammalian Brain: Significant Answers and Significant Questions.* Neuron, 2011. **70**(4): p. 687-702.
67. Sanai, N., et al., *Unique astrocyte ribbon in adult human brain contains neural stem cells but lacks chain migration.* Nature, 2004. **427**(6976): p. 740-4.
68. Gonzalez-Perez, O., *Neural stem cells in the adult human brain.* Biol Biomed Rep, 2012. **2**(1): p. 59-69.
69. Jossin, Y. and J.A. Cooper, *Reelin, Rap1 and N-cadherin orient the migration of multipolar neurons in the developing neocortex.* Nat Neurosci, 2011. **14**(6): p. 697-703.
70. Lendahl, U., L.B. Zimmerman, and R.D. McKay, *CNS stem cells express a new class of intermediate filament protein.* Cell, 1990. **60**(4): p. 585-95.
71. Imayoshi, I., M. Sakamoto, and R. Kageyama, *Genetic methods to identify and manipulate newly born neurons in the adult brain.* Front Neurosci, 2011. **5**: p. 64.
72. Hendrickson, M.L., et al., *Expression of nestin by neural cells in the adult rat and human brain.* PLoS One, 2011. **6**(4): p. e18535.
73. Eng, L.F. and R.S. Ghirnikar, *GFAP and astrogliosis.* Brain Pathol, 1994. **4**(3): p. 229-37.
74. Frederiksen, K. and R.D. McKay, *Proliferation and differentiation of rat neuroepithelial precursor cells in vivo.* J Neurosci, 1988. **8**(4): p. 1144-51.
75. Park, D., et al., *Nestin is required for the proper self-renewal of neural stem cells.* Stem Cells, 2010. **28**(12): p. 2162-71.
76. Kang, H., et al., *Regulation of the intermediate filament protein nestin at rodent neuromuscular junctions by innervation and activity.* J Neurosci, 2007. **27**(22): p. 5948-57.
77. Frojdman, K., et al., *The intermediate filament protein nestin occurs transiently in differentiating testis of rat and mouse.* Differentiation, 1997. **61**(4): p. 243-9.
78. Terling, C., et al., *Expression of the intermediate filament nestin during rodent tooth development.* Int J Dev Biol, 1995. **39**(6): p. 947-56.

79. Mokry, J. and S. Nemecek, *Cerebral angiogenesis shows nestin expression in endothelial cells.* Gen Physiol Biophys, 1999. **18 Suppl 1**: p. 25-9.
80. Suzuki, S., et al., *The neural stem/progenitor cell marker nestin is expressed in proliferative endothelial cells, but not in mature vasculature.* J Histochem Cytochem, 2010. **58**(8): p. 721-30.
81. Lin, R.C., et al., *Re-expression of the intermediate filament nestin in reactive astrocytes.* Neurobiol Dis, 1995. **2**(2): p. 79-85.
82. Cho, J.M., et al., *Characterization of nestin expression in astrocytes in the rat hippocampal CA1 region following transient forebrain ischemia.* Anat Cell Biol, 2013. **46**(2): p. 131-40.
83. Uchida, N., et al., *Direct isolation of human central nervous system stem cells.* Proc Natl Acad Sci U S A, 2000. **97**(26): p. 14720-5.
84. Marzesco, A.M., et al., *Release of extracellular membrane particles carrying the stem cell marker prominin-1 (CD133) from neural progenitors and other epithelial cells.* J Cell Sci, 2005. **118**(Pt 13): p. 2849-58.
85. Pfenninger, C.V., et al., *CD133 is not present on neurogenic astrocytes in the adult subventricular zone, but on embryonic neural stem cells, ependymal cells, and glioblastoma cells.* Cancer Res, 2007. **67**(12): p. 5727-36.
86. Kriegstein, A. and A. Alvarez-Buylla, *The Glial Nature of Embryonic and Adult Neural Stem Cells.* Annu Rev Neurosci, 2009. **32**: p. 149-84.
87. Graham, V., et al., *SOX2 functions to maintain neural progenitor identity.* Neuron, 2003. **39**(5): p. 749-65.
88. Doetsch, F., et al., *EGF converts transit-amplifying neurogenic precursors in the adult brain into multipotent stem cells.* Neuron, 2002. **36**(6): p. 1021-34.
89. Pastrana, E., L.C. Cheng, and F. Doetsch, *Simultaneous prospective purification of adult subventricular zone neural stem cells and their progeny.* Proc Natl Acad Sci U S A, 2009. **106**(15): p. 6387-92.
90. Parras, C.M., et al., *Mash1 specifies neurons and oligodendrocytes in the postnatal brain.* Embo j, 2004. **23**(22): p. 4495-505.
91. Francis, F., et al., *Doublecortin is a developmentally regulated, microtubule-associated protein expressed in migrating and differentiating neurons.* Neuron, 1999. **23**(2): p. 247-56.
92. Rousselot, P., C. Lois, and A. Alvarez-Buylla, *Embryonic (PSA) N-CAM reveals chains of migrating neuroblasts between the lateral ventricle and the olfactory bulb of adult mice.* J Comp Neurol, 1995. **351**(1): p. 51-61.
93. Gusel'nikova, V.V. and D.E. Korzhevskiy, *NeuN As a Neuronal Nuclear Antigen and Neuron Differentiation Marker.* Acta Naturae, 2015. **7**(2): p. 42-7.
94. Codega, P., et al., *Prospective identification and purification of quiescent adult neural stem cells from their in vivo niche.* Neuron, 2014. **82**(3): p. 545-59.
95. Deleyrolle, L.P. and B.A. Reynolds, *Isolation, expansion, and differentiation of adult Mammalian neural stem and progenitor cells using the neurosphere assay.* Methods Mol Biol, 2009. **549**: p. 91-101.
96. Pastrana, E., V. Silva-Vargas, and F. Doetsch, *Eyes Wide Open: A Critical Review of Sphere-Formation as an Assay For Stem Cells.* Cell Stem Cell, 2011. **8**(5): p. 486-98.
97. Lathia, J.D., et al., *The microenvironment of the embryonic neural stem cell: lessons from adult niches?* Dev Dyn, 2007. **236**(12): p. 3267-82.

98. Gattazzo, F., A. Urciuolo, and P. Bonaldo, *Extracellular matrix: a dynamic microenvironment for stem cell niche.* Biochim Biophys Acta, 2014. **1840**(8): p. 2506-19.
99. Campos, L.S., *Neurospheres: insights into neural stem cell biology.* J Neurosci Res, 2004. **78**(6): p. 761-9.
100. Kazanis, I. and C. ffrench-Constant, *Extracellular matrix and the neural stem cell niche.* Dev Neurobiol, 2011. **71**(11): p. 1006-17.
101. Mirzadeh, Z., et al., *Neural stem cells confer unique pinwheel architecture to the ventricular surface in neurogenic regions of the adult brain.* Cell stem cell, 2008. **3**(3): p. 265-278.
102. Shen, Q., et al., *Adult SVZ stem cells lie in a vascular niche: a quantitative analysis of niche cell-cell interactions.* Cell Stem Cell, 2008. **3**(3): p. 289-300.
103. Fuentealba, L.C., K. Obernier, and A. Alvarez-Buylla, *Adult neural stem cells bridge their niche.* Cell Stem Cell, 2012. **10**(6): p. 698-708.
104. Gotz, M. and W.B. Huttner, *The cell biology of neurogenesis.* Nat Rev Mol Cell Biol, 2005. **6**(10): p. 777-788.
105. Kosodo, Y., et al., *Asymmetric distribution of the apical plasma membrane during neurogenic divisions of mammalian neuroepithelial cells.* Embo j, 2004. **23**(11): p. 2314-24.
106. Hartmann, U. and P. Maurer, *Proteoglycans in the nervous system--the quest for functional roles in vivo.* Matrix Biol, 2001. **20**(1): p. 23-35.
107. Zimmermann, D.R. and M.T. Dours-Zimmermann, *Extracellular matrix of the central nervous system: from neglect to challenge.* Histochem Cell Biol, 2008. **130**(4): p. 635-53.
108. Cheung, T.H. and T.A. Rando, *Molecular regulation of stem cell quiescence.* Nat Rev Mol Cell Biol, 2013. **14**(6): p. 329-40.
109. Loulier, K., et al., *beta1 integrin maintains integrity of the embryonic neocortical stem cell niche.* PLoS Biol, 2009. **7**(8): p. e1000176.
110. Johansson, P.A., S. Cappello, and M. Gotz, *Stem cells niches during development--lessons from the cerebral cortex.* Curr Opin Neurobiol, 2010. **20**(4): p. 400-7.
111. Nakayama, K.H., et al., *Decellularized rhesus monkey kidney as a three-dimensional scaffold for renal tissue engineering.* Tissue Eng Part A, 2010. **16**(7): p. 2207-16.
112. Kurtz, A. and S.J. Oh, *Age related changes of the extracellular matrix and stem cell maintenance.* Prev Med, 2012. **54 Suppl**: p. S50-6.
113. Urtasun, R., L. Conde de la Rosa, and N. Nieto, *Oxidative and nitrosative stress and fibrogenic response.* Clin Liver Dis, 2008. **12**(4): p. 769-90, viii.
114. Wang, H., X. Luo, and J. Leighton, *Extracellular Matrix and Integrins in Embryonic Stem Cell Differentiation.* Biochem Insights, 2015. **8**(Suppl 2): p. 15-21.
115. Barros, C.S., S.J. Franco, and U. Muller, *Extracellular matrix: functions in the nervous system.* Cold Spring Harb Perspect Biol, 2011. **3**(1): p. a005108.
116. McClenahan, F.K., et al., *Dystroglycan Suppresses Notch to Regulate Stem Cell Niche Structure and Function in the Developing Postnatal Subventricular Zone.* Dev Cell, 2016. **38**(5): p. 548-66.
117. Kerever, A., et al., *Novel extracellular matrix structures in the neural stem cell niche capture the neurogenic factor fibroblast growth factor 2 from the extracellular milieu.* Stem Cells, 2007. **25**(9): p. 2146-57.

118. Kerever, A., et al., *Perlecan is required for FGF-2 signaling in the neural stem cell niche.* Stem Cell Research, 2014. **12**(2): p. 492-505.
119. Xiong, A., S. Kundu, and K. Forsberg-Nilsson, *Heparan sulfate in the regulation of neural differentiation and glioma development.* Febs j, 2014. **281**(22): p. 4993-5008.
120. Sirko, S., et al., *Chondroitin sulfate glycosaminoglycans control proliferation, radial glia cell differentiation and neurogenesis in neural stem/progenitor cells.* Development, 2007. **134**(15): p. 2727-38.
121. Akita, K., et al., *Expression of multiple chondroitin/dermatan sulfotransferases in the neurogenic regions of the embryonic and adult central nervous system implies that complex chondroitin sulfates have a role in neural stem cell maintenance.* Stem Cells, 2008. **26**(3): p. 798-809.
122. Sirko, S., et al., *Chondroitin sulfate glycosaminoglycans control proliferation, radial glia cell differentiation and neurogenesis in neural stem/progenitor cells.* Development, 2007. **134**(15): p. 2727-2738.
123. Kokovay, E., et al., *VCAM1 is essential to maintain the structure of the SVZ niche and acts as an environmental sensor to regulate SVZ lineage progression.* Cell Stem Cell, 2012. **11**(2): p. 220-30.
124. Kokovay, E., et al., *Adult SVZ lineage cells home to and leave the vascular niche via differential responses to SDF1/CXCR4 signaling.* Cell Stem Cell, 2010. **7**(2): p. 163-73.
125. Falcão, A.M., et al., *The path from the choroid plexus to the subventricular zone: go with the flow!* Front Cell Neurosci, 2012. **6**.
126. Thouvenot, E., et al., *The proteomic analysis of mouse choroid plexus secretome reveals a high protein secretion capacity of choroidal epithelial cells.* Proteomics, 2006. **6**(22): p. 5941-52.
127. Keep, R.F. and H.C. Jones, *A morphometric study on the development of the lateral ventricle choroid plexus, choroid plexus capillaries and ventricular ependyma in the rat.* Brain Res Dev Brain Res, 1990. **56**(1): p. 47-53.
128. Vescovi, A.L., et al., *bFGF regulates the proliferative fate of unipotent (neuronal) and bipotent (neuronal/astroglial) EGF-generated CNS progenitor cells.* Neuron, 1993. **11**(5): p. 951-66.
129. Lehtinen, M.K., *The cerebrospinal fluid provides a proliferative niche for neural progenitor cells.* 2011. **69**(5): p. 893-905.
130. Chen, S., M. Lewallen, and T. Xie, *Adhesion in the stem cell niche: biological roles and regulation.* Development, 2013. **140**(2): p. 255-65.
131. Niola, F., et al., *Id proteins synchronize stemness and anchorage to the niche of neural stem cells.* Nat Cell Biol, 2012. **14**(5): p. 477-87.
132. Kosodo, Y., et al., *Asymmetric distribution of the apical plasma membrane during neurogenic divisions of mammalian neuroepithelial cells.* Embo j, 2004. **23**(11): p. 2314-24.
133. Kim, S.A., et al., *Calcium-dependent dynamics of cadherin interactions at cell-cell junctions.* Proc Natl Acad Sci U S A, 2011. **108**(24): p. 9857-62.
134. Luccardini, C., et al., *N-Cadherin Sustains Motility and Polarity of Future Cortical Interneurons during Tangential Migration.* J Neurosci, 2013. **33**(46): p. 18149-60.
135. Porlan, E., et al., *MT5-MMP regulates adult neural stem cell functional quiescence through the cleavage of N-cadherin.* Nat Cell Biol, 2014. **16**(7): p. 629-38.

136. Kadowaki, M., et al., *N-cadherin mediates cortical organization in the mouse brain.* Developmental Biology, 2007. **304**(1): p. 22-33.
137. Long, K.R. and C. Ffrench-Constant, *Neural stem cell quiescence comes to an un-sticky end.* Nat Cell Biol, 2014. **16**(7): p. 625-7.
138. Kawauchi, T., et al., *Rab GTPases-dependent endocytic pathways regulate neuronal migration and maturation through N-cadherin trafficking.* Neuron, 2010. **67**(4): p. 588-602.
139. Song, X., et al., *Germline Stem Cells Anchored by Adherens Junctions in the Drosophila Ovary Niches.* Science, 2002. **296**(5574): p. 1855-1857.
140. Jin, Z., et al., *Differentiation-defective stem cells outcompete normal stem cells for niche occupancy in the Drosophila ovary.* Cell Stem Cell, 2008. **2**(1): p. 39-49.
141. Emsley, J.G. and T. Hagg, *alpha6beta1 integrin directs migration of neuronal precursors in adult mouse forebrain.* Exp Neurol, 2003. **183**(2): p. 273-85.
142. Aguirre, A., et al., *Overexpression of the epidermal growth factor receptor confers migratory properties to nonmigratory postnatal neural progenitors.* J Neurosci, 2005. **25**(48): p. 11092-106.
143. Maslov, A.Y., et al., *Neural stem cell detection, characterization, and age-related changes in the subventricular zone of mice.* J Neurosci, 2004. **24**(7): p. 1726-33.
144. Enwere, E., et al., *Aging results in reduced epidermal growth factor receptor signaling, diminished olfactory neurogenesis, and deficits in fine olfactory discrimination.* J Neurosci, 2004. **24**(38): p. 8354-65.
145. Gritti, A., et al., *Epidermal and fibroblast growth factors behave as mitogenic regulators for a single multipotent stem cell-like population from the subventricular region of the adult mouse forebrain.* J Neurosci, 1999. **19**(9): p. 3287-97.
146. Kuhn, H.G., et al., *Epidermal growth factor and fibroblast growth factor-2 have different effects on neural progenitors in the adult rat brain.* J Neurosci, 1997. **17**(15): p. 5820-9.
147. Reynolds, B.A. and S. Weiss, *Clonal and population analyses demonstrate that an EGF-responsive mammalian embryonic CNS precursor is a stem cell.* Dev Biol, 1996. **175**(1): p. 1-13.
148. Piccin, D., F. Yu, and C.M. Morshead, *Notch signaling imparts and preserves neural stem characteristics in the adult brain.* Stem Cells Dev, 2013. **22**(10): p. 1541-50.
149. Varela-Nallar, L. and N.C. Inestrosa, *Wnt signaling in the regulation of adult hippocampal neurogenesis.* Front Cell Neurosci, 2013. **7**: p. 100.
150. Faigle, R. and H. Song, *Signaling mechanisms regulating adult neural stem cells and neurogenesis.* Biochim Biophys Acta, 2013. **1830**(2): p. 2435-48.
151. Schwarz, T.J., B. Ebert, and D.C. Lie, *Stem cell maintenance in the adult mammalian hippocampus: a matter of signal integration?* Dev Neurobiol, 2012. **72**(7): p. 1006-15.
152. Suh, H., W. Deng, and F.H. Gage, *Signaling in adult neurogenesis.* Annu Rev Cell Dev Biol, 2009. **25**: p. 253-75.
153. Lu, P., et al., *Extracellular Matrix Degradation and Remodeling in Development and Disease.* Cold Spring Harb Perspect Biol. **3**(12).
154. Tropepe, V., et al., *Transforming growth factor-alpha null and senescent mice show decreased neural progenitor cell proliferation in the forebrain subependyma.* J Neurosci, 1997. **17**(20): p. 7850-9.

155. Aguirre, A., M.E. Rubio, and V. Gallo, *Notch and EGFR pathway interaction regulates neural stem cell number and self-renewal.* Nature, 2010. **467**(7313): p. 323-7.
156. Saftig, P. and S.F. Lichtenthaler, *The alpha secretase ADAM10: A metalloprotease with multiple functions in the brain.* Prog Neurobiol, 2015. **135**: p. 1-20.
157. Solanas, G., et al., *Cleavage of E-cadherin by ADAM10 mediates epithelial cell sorting downstream of EphB signalling.* Nat Cell Biol, 2011. **13**(9): p. 1100-7.
158. Reiss, K., et al., *ADAM10 cleavage of N-cadherin and regulation of cell-cell adhesion and beta-catenin nuclear signalling.* Embo j, 2005. **24**(4): p. 742-52.
159. Weber, S. and P. Saftig, *Ectodomain shedding and ADAMs in development.* Development, 2012. **139**(20): p. 3693-709.
160. Dreymueller, D., S. Uhlig, and A. Ludwig, *ADAM-family metalloproteinases in lung inflammation: potential therapeutic targets.* American Journal of Physiology - Lung Cellular and Molecular Physiology, 2015. **308**(4): p. L325-L343.
161. Wong, E., et al., *The Functional Maturation of A Disintegrin and Metalloproteinase (ADAM) 9, 10, and 17 Requires Processing at a Newly Identified Proprotein Convertase (PC) Cleavage Site.* J Biol Chem, 2015. **290**(19): p. 12135-46.
162. Hitoshi, S., et al., *Notch pathway molecules are essential for the maintenance, but not the generation, of mammalian neural stem cells.* Genes Dev, 2002. **16**(7): p. 846-58.
163. Bai, G. and S.L. Pfaff, *Protease regulation: the Yin and Yang of neural development and disease.* Neuron, 2011. **72**(1): p. 9-21.
164. Hattori, M., M. Osterfield, and J.G. Flanagan, *Regulated cleavage of a contact-mediated axon repellent.* Science, 2000. **289**(5483): p. 1360-5.
165. Janes, P.W., et al., *Adam meets Eph: an ADAM substrate recognition module acts as a molecular switch for ephrin cleavage in trans.* Cell, 2005. **123**(2): p. 291-304.
166. Alfandari, D., et al., *Xenopus ADAM 13 is a metalloprotease required for cranial neural crest-cell migration.* Curr Biol, 2001. **11**(12): p. 918-30.
167. Tsai, Y.H., et al., *ADAM10 regulates Notch function in intestinal stem cells of mice.* Gastroenterology, 2014. **147**(4): p. 822-834.e13.
168. Kwon, J., et al., *ADAM10 Is Involved in Cell Junction Assembly in Early Porcine Embryo Development.* PLoS One, 2016. **11**(4): p. e0152921.
169. Hartmann, D., et al., *The disintegrin/metalloprotease ADAM 10 is essential for Notch signalling but not for alpha-secretase activity in fibroblasts.* Hum Mol Genet, 2002. **11**(21): p. 2615-24.
170. Yavari, R., et al., *Human metalloprotease-disintegrin Kuzbanian regulates sympathoadrenal cell fate in development and neoplasia.* Hum Mol Genet, 1998. **7**(7): p. 1161-7.
171. Karkkainen, I., et al., *Metalloprotease-disintegrin (ADAM) genes are widely and differentially expressed in the adult CNS.* Mol Cell Neurosci, 2000. **15**(6): p. 547-60.
172. Kuhn, P.H., et al., *ADAM10 is the physiologically relevant, constitutive alpha-secretase of the amyloid precursor protein in primary neurons.* Embo j, 2010. **29**(17): p. 3020-32.
173. Zhuang, J., et al., *Effects of ADAM10 deletion on Notch-1 signaling pathway and neuronal maintenance in adult mouse brain.* Gene, 2015. **555**(2): p. 150-8.
174. Imayoshi, I., et al., *Essential roles of Notch signaling in maintenance of neural stem cells in developing and adult brains.* J Neurosci, 2010. **30**(9): p. 3489-98.

175. Louvi, A. and S. Artavanis-Tsakonas, *Notch signalling in vertebrate neural development.* Nat Rev Neurosci, 2006. **7**(2): p. 93-102.
176. Yoon, K. and N. Gaiano, *Notch signaling in the mammalian central nervous system: insights from mouse mutants.* Nat Neurosci, 2005. **8**(6): p. 709-15.
177. van Tetering, G., *Proteolytic Cleavage of Notch: "HIT and RUN".* 2011. **11**(4): p. 255-69.
178. Qi, H., et al., *Processing of the notch ligand delta by the metalloprotease Kuzbanian.* Science, 1999. **283**(5398): p. 91-4.
179. LaVoie, M.J. and D.J. Selkoe, *The Notch ligands, Jagged and Delta, are sequentially processed by alpha-secretase and presenilin/gamma-secretase and release signaling fragments.* J Biol Chem, 2003. **278**(36): p. 34427-37.
180. Six, E., et al., *The Notch ligand Delta1 is sequentially cleaved by an ADAM protease and gamma-secretase.* Proc Natl Acad Sci U S A, 2003. **100**(13): p. 7638-43.
181. Mumm, J.S., et al., *A ligand-induced extracellular cleavage regulates gamma-secretase-like proteolytic activation of Notch1.* Mol Cell, 2000. **5**(2): p. 197-206.
182. Brou, C., et al., *A novel proteolytic cleavage involved in Notch signaling: the role of the disintegrin-metalloprotease TACE.* Mol Cell, 2000. **5**(2): p. 207-16.
183. Murphy, G., *The ADAMs: signalling scissors in the tumour microenvironment.* Nat Rev Cancer, 2008. **8**(12): p. 929-41.
184. Prox, J., et al., *Postnatal disruption of the disintegrin/metalloproteinase ADAM10 in brain causes epileptic seizures, learning deficits, altered spine morphology, and defective synaptic functions.* J Neurosci, 2013. **33**(32): p. 12915-28, 12928a.
185. Jorissen, E., et al., *The disintegrin/metalloproteinase ADAM10 is essential for the establishment of the brain cortex.* J Neurosci, 2010. **30**(14): p. 4833-44.
186. Yang, Z., et al., *ADAM10-Initiated Release of Notch Intracellular Domain Regulates Microtubule Stability and Radial Migration of Cortical Neurons.* Cereb Cortex, 2017: p. 1-14.
187. Schmid, R.S. and E.S. Anton, *Role of integrins in the development of the cerebral cortex.* Cereb Cortex, 2003. **13**(3): p. 219-24.
188. Senturk, A., et al., *Ephrin Bs are essential components of the Reelin pathway to regulate neuronal migration.* Nature, 2011. **472**(7343): p. 356-60.
189. Klingener, M., et al., *N-cadherin promotes recruitment and migration of neural progenitor cells from the SVZ neural stem cell niche into demyelinated lesions.* J Neurosci, 2014. **34**(29): p. 9590-606.
190. Bittman, K., et al., *Cell coupling and uncoupling in the ventricular zone of developing neocortex.* J Neurosci, 1997. **17**(18): p. 7037-44.
191. Karpowicz, P., et al., *E-Cadherin regulates neural stem cell self-renewal.* J Neurosci, 2009. **29**(12): p. 3885-96.
192. Belvindrah, R., et al., *Beta1 integrins control the formation of cell chains in the adult rostral migratory stream.* J Neurosci, 2007. **27**(10): p. 2704-17.
193. Bittman, K.S. and J.J. LoTurco, *Differential regulation of connexin 26 and 43 in murine neocortical precursors.* Cereb Cortex, 1999. **9**(2): p. 188-95.
194. Vangipuram, S.D., et al., *Ethanol increases fetal human neurosphere size and alters adhesion molecule gene expression.* Alcohol Clin Exp Res, 2008. **32**(2): p. 339-47.
195. Feldman, G.J., J.M. Mullin, and M.P. Ryan, *Occludin: structure, function and regulation.* Adv Drug Deliv Rev, 2005. **57**(6): p. 883-917.

196. Persidsky, Y., et al., *Blood-brain barrier: structural components and function under physiologic and pathologic conditions.* J Neuroimmune Pharmacol, 2006. **1**(3): p. 223-36.
197. Huber, J.D., R.D. Egleton, and T.P. Davis, *Molecular physiology and pathophysiology of tight junctions in the blood-brain barrier.* Trends Neurosci, 2001. **24**(12): p. 719-25.
198. Watters, A.K., et al., *Identification and dynamic regulation of tight junction protein expression in human neural stem cells.* Stem Cells Dev, 2015. **24**(12): p. 1377-89.
199. Palmeri, D., et al., *Vascular endothelial junction-associated molecule, a novel member of the immunoglobulin superfamily, is localized to intercellular boundaries of endothelial cells.* J Biol Chem, 2000. **275**(25): p. 19139-45.
200. Cunningham, S.A., et al., *A novel protein with homology to the junctional adhesion molecule. Characterization of leukocyte interactions.* J Biol Chem, 2000. **275**(44): p. 34750-6.
201. Aurrand-Lions, M.A., et al., *Cloning of JAM-2 and JAM-3: an emerging junctional adhesion molecular family?* Curr Top Microbiol Immunol, 2000. **251**: p. 91-8.
202. Aurrand-Lions, M., et al., *JAM-2, a novel immunoglobulin superfamily molecule, expressed by endothelial and lymphatic cells.* J Biol Chem, 2001. **276**(4): p. 2733-41.
203. Arrate, M.P., et al., *Cloning of human junctional adhesion molecule 3 (JAM3) and its identification as the JAM2 counter-receptor.* J Biol Chem, 2001. **276**(49): p. 45826-32.
204. Liang, T.W., et al., *Vascular endothelial-junctional adhesion molecule (VE-JAM)/JAM 2 interacts with T, NK, and dendritic cells through JAM 3.* J Immunol, 2002. **168**(4): p. 1618-26.
205. Williams, A.F. and A.N. Barclay, *The immunoglobulin superfamily--domains for cell surface recognition.* Annu Rev Immunol, 1988. **6**: p. 381-405.
206. Barclay, A.N. and M.H. Brown, *Heterogeneity of interactions mediated by membrane glycoproteins of lymphocytes.* Biochem Soc Trans, 1997. **25**(1): p. 224-8.
207. Ebnet, K., et al., *Junctional adhesion molecules (JAMs): more molecules with dual functions?* Journal of Cell Science, 2004. **117**(1): p. 19-29.
208. Ebnet, K., et al., *Junctional adhesion molecules (JAMs): more molecules with dual functions?* J Cell Sci, 2004. **117**(Pt 1): p. 19-29.
209. Follis, Rose M. and Bruce D. Carter, *Myelin Avoids the JAM.* Neuron, 2016. **91**(4): p. 713-716.
210. Redmond, Stephanie A., et al., *Somatodendritic Expression of JAM2 Inhibits Oligodendrocyte Myelination.* Neuron, 2016. **91**(4): p. 824-836.
211. Arcangeli, M.L., et al., *JAM-B regulates maintenance of hematopoietic stem cells in the bone marrow.* Blood, 2011. **118**(17): p. 4609-19.
212. Arcangeli, M.L., et al., *Function of Jam-B/Jam-C interaction in homing and mobilization of human and mouse hematopoietic stem and progenitor cells.* Stem Cells, 2014. **32**(4): p. 1043-54.
213. Gliki, G., et al., *Spermatid differentiation requires the assembly of a cell polarity complex downstream of junctional adhesion molecule-C.* Nature, 2004. **431**(7006): p. 320-4.
214. Zen, K., et al., *JAM-C Is a Component of Desmosomes and a Ligand for CD11b/CD18-mediated Neutrophil Transepithelial Migration.* Mol Biol Cell, 2004. **15**(8): p. 3926-37.

215. Morris, A.P., et al., *Junctional Adhesion Molecules (JAMs) are differentially expressed in fibroblasts and co-localize with ZO-1 to adherens-like junctions.* Cell Commun Adhes, 2006. **13**(4): p. 233-47.
216. Keiper, T., et al., *The role of junctional adhesion molecule-C (JAM-C) in oxidized LDL-mediated leukocyte recruitment.* Faseb j, 2005. **19**(14): p. 2078-80.
217. Wyss, L., et al., *Junctional adhesion molecule (JAM)-C deficient C57BL/6 mice develop a severe hydrocephalus.* PLoS One, 2012. **7**(9): p. e45619.
218. Scheiermann, C., et al., *Expression and function of junctional adhesion molecule-C in myelinated peripheral nerves.* Science, 2007. **318**(5855): p. 1472-5.
219. Aurrand-Lions, M., et al., *Heterogeneity of endothelial junctions is reflected by differential expression and specific subcellular localization of the three JAM family members.* Blood, 2001. **98**(13): p. 3699-707.
220. Mochida, G.H., et al., *A homozygous mutation in the tight-junction protein JAM3 causes hemorrhagic destruction of the brain, subependymal calcification, and congenital cataracts.* Am J Hum Genet, 2010. **87**(6): p. 882-9.
221. Famulski, J.K., et al., *Siah regulation of Pard3A controls neuronal cell adhesion during germinal zone exit.* Science, 2010. **330**(6012): p. 1834-8.
222. Stelzer, S., et al., *JAM-C is an apical surface marker for neural stem cells.* Stem Cells Dev, 2012. **21**(5): p. 757-66.
223. Rabquer, B.J., et al., *Junctional adhesion molecule-C is a soluble mediator of angiogenesis.* J Immunol, 2010. **185**(3): p. 1777-85.
224. Orlova, V.V., et al., *Junctional adhesion molecule-C regulates vascular endothelial permeability by modulating VE-cadherin-mediated cell-cell contacts.* J Exp Med, 2006. **203**(12): p. 2703-14.
225. Li, X., et al., *JAM-C induces endothelial cell permeability through its association and regulation of {beta}3 integrins.* Arterioscler Thromb Vasc Biol, 2009. **29**(8): p. 1200-6.
226. Bos, J.L., J. de Rooij, and K.A. Reedquist, *Rap1 signalling: adhering to new models.* Nat Rev Mol Cell Biol, 2001. **2**(5): p. 369-77.
227. Wang, H., et al., *Rap-GEF signaling controls stem cell anchoring to their niche through regulating DE-cadherin-mediated cell adhesion in the Drosophila testis.* Dev Cell, 2006. **10**(1): p. 117-26.
228. Knox, A.L. and N.H. Brown, *Rap1 GTPase regulation of adherens junction positioning and cell adhesion.* Science, 2002. **295**(5558): p. 1285-8.
229. Bos, J.L., et al., *The role of Rap1 in integrin-mediated cell adhesion.* Biochem Soc Trans, 2003. **31**(Pt 1): p. 83-6.
230. Fuse, C., et al., *Junctional adhesion molecule-C promotes metastatic potential of HT1080 human fibrosarcoma.* J Biol Chem, 2007. **282**(11): p. 8276-83.
231. Retta, S.F., F. Balzac, and M. Avolio, *Rap1: a turnabout for the crosstalk between cadherins and integrins.* Eur J Cell Biol, 2006. **85**(3-4): p. 283-93.
232. Zhang, J., et al., *Cortical neural precursors inhibit their own differentiation via N-cadherin maintenance of beta-catenin signaling.* Dev Cell, 2010. **18**(3): p. 472-9.
233. Voss, A.K., et al., *C3G regulates cortical neuron migration, preplate splitting and radial glial cell attachment.* Development, 2008. **135**(12): p. 2139-49.

234. Bilasy, S.E., et al., *Dorsal telencephalon-specific RA-GEF-1 knockout mice develop heterotopic cortical mass and commissural fiber defect.* Eur J Neurosci, 2009. **29**(10): p. 1994-2008.
235. Shah, B., et al., *C3G/Rapgef1 Is Required in Multipolar Neurons for the Transition to a Bipolar Morphology during Cortical Development.* PLoS One, 2016. **11**(4).
236. Santoso, S., et al., *The Junctional Adhesion Molecule 3 (JAM-3) on Human Platelets is a Counterreceptor for the Leukocyte Integrin Mac-1.* The Journal of Experimental Medicine, 2002. **196**(5): p. 679-691.
237. Schneider, C.A., W.S. Rasband, and K.W. Eliceiri, *NIH Image to ImageJ: 25 years of image analysis.* Nat Methods, 2012. **9**(7): p. 671-5.
238. Franke, B., J.W. Akkerman, and J.L. Bos, *Rapid Ca2+-mediated activation of Rap1 in human platelets.* Embo j, 1997. **16**(2): p. 252-9.
239. Tuttle, A.H., et al., *Immunofluorescent detection of two thymidine analogues (CldU and IdU) in primary tissue.* J Vis Exp, 2010(46).
240. Lois, C. and A. Alvarez-Buylla, *Proliferating subventricular zone cells in the adult mammalian forebrain can differentiate into neurons and glia.* Proc Natl Acad Sci U S A, 1993. **90**(5): p. 2074-7.
241. Tuscher, J.J., et al., *Regulation of object recognition and object placement by ovarian sex steroid hormones.* Behav Brain Res, 2015. **285**: p. 140-57.
242. Mirzadeh, Z., et al., *The subventricular zone en-face: wholemount staining and ependymal flow.* J Vis Exp, 2010(39).
243. Ferri, A.L.M., et al., *Sox2 deficiency causes neurodegeneration and impaired neurogenesis in the adult mouse brain.* Development, 2004. **131**(15): p. 3805-3819.
244. Moreno, M.M., et al., *Olfactory perceptual learning requires adult neurogenesis.* Proc Natl Acad Sci U S A, 2009. **106**(42): p. 17980-5.
245. Kageyama, R., I. Imayoshi, and M. Sakamoto, *The role of neurogenesis in olfaction-dependent behaviors.* Behav Brain Res, 2012. **227**(2): p. 459-63.
246. Wang, W., et al., *Inducible Activation of ERK5 MAP Kinase Enhances Adult Neurogenesis in the Olfactory Bulb and Improves Olfactory Function.* J Neurosci, 2015. **35**(20): p. 7833-49.
247. Marthiens, V., et al., *Adhesion molecules in the stem cell niche – more than just staying in shape?* Journal of Cell Science, 2010. **123**(10): p. 1613-1622.
248. Johansson, C.B., et al., *Neural stem cells in the adult human brain.* Exp Cell Res, 1999. **253**(2): p. 733-6.
249. Johansson, C.B., et al., *Identification of a neural stem cell in the adult mammalian central nervous system.* Cell, 1999. **96**(1): p. 25-34.
250. Järvinen, E., et al., *Timing of the Cell Cycle Exit of Differentiating Hippocampal Neural Stem Cells.* Int J Stem Cells, 2010. **3**(1): p. 46-53.
251. Bradford, G.B., et al., *Quiescence, cycling, and turnover in the primitive hematopoietic stem cell compartment.* Exp Hematol, 1997. **25**(5): p. 445-53.
252. Reiss, K., et al., *ADAM10 cleavage of N-cadherin and regulation of cell–cell adhesion and β-catenin nuclear signalling.* Embo j, 2005. **24**(4): p. 742-52.
253. Bryn, T., et al., *The cyclic AMP-Epac1-Rap1 pathway is dissociated from regulation of effector functions in monocytes but acquires immunoregulatory function in mature macrophages.* J Immunol, 2006. **176**(12): p. 7361-70.

254. Liang, C.C., A.Y. Park, and J.L. Guan, *In vitro scratch assay: a convenient and inexpensive method for analysis of cell migration in vitro.* Nat Protoc, 2007. **2**(2): p. 329-33.
255. Fukuda, S., et al., *Two distinct subpopulations of nestin-positive cells in adult mouse dentate gyrus.* J Neurosci, 2003. **23**(28): p. 9357-66.
256. Vogel-Ciernia, A. and M.A. Wood, *Examining Object Location and Object Recognition Memory in Mice.* Curr Protoc Neurosci, 2014. **69**: p. 8.31.1-8.31.17.
257. Lim, D.A., et al., *Noggin antagonizes BMP signaling to create a niche for adult neurogenesis.* Neuron, 2000. **28**(3): p. 713-26.
258. Urbán, N. and F. Guillemot, *Neurogenesis in the embryonic and adult brain: same regulators, different roles.* Front Cell Neurosci, 2014. **8**.
259. Zhao, C., W. Deng, and F.H. Gage, *Mechanisms and functional implications of adult neurogenesis.* Cell, 2008. **132**(4): p. 645-60.
260. Kuhn, P.H., et al., *Systematic substrate identification indicates a central role for the metalloprotease ADAM10 in axon targeting and synapse function.* eLife, 2016. **5**.
261. Atapattu, L., M. Lackmann, and P.W. Janes, *The role of proteases in regulating Eph/ephrin signaling.* Cell Adh Migr, 2014. **8**(4): p. 294-307.
262. Shitomi, Y., et al., *ADAM10 controls collagen signaling and cell migration on collagen by shedding the ectodomain of discoidin domain receptor 1 (DDR1).* Mol Biol Cell, 2015. **26**(4): p. 659-73.
263. Voss, A.K., P. Gruss, and T. Thomas, *The guanine nucleotide exchange factor C3G is necessary for the formation of focal adhesions and vascular maturation.* Development, 2003. **130**(2): p. 355-67.
264. Reedquist, K.A., et al., *The small GTPase, Rap1, mediates CD31-induced integrin adhesion.* J Cell Biol, 2000. **148**(6): p. 1151-8.

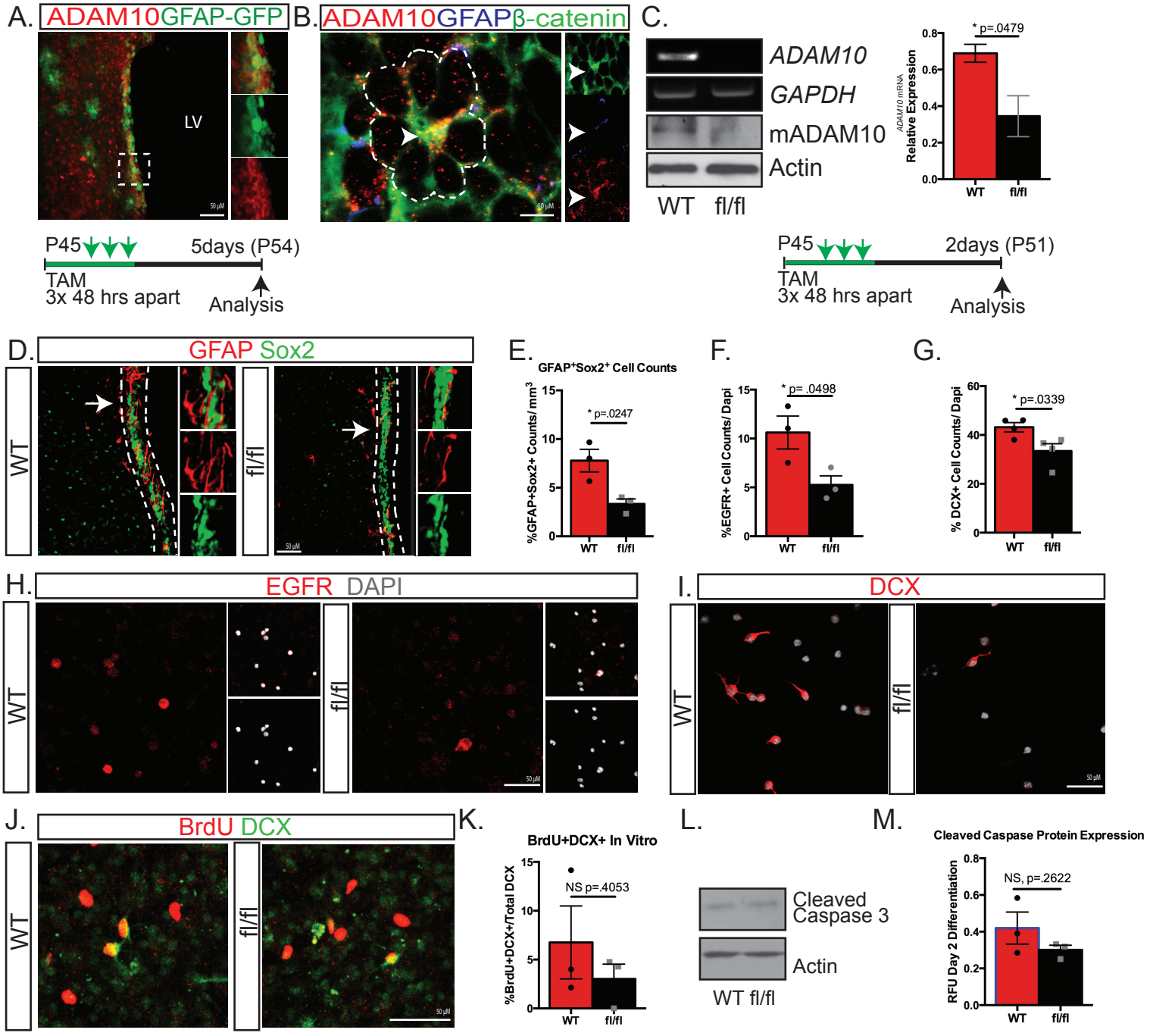

Figure 6. GFAP+ stem cells in the subventricular zone (SVZ) interact with their niche through ADAM10 initiated contacts. A) Immunostaining for ADAM10 in coronal SVZ sections shows ADAM10 (red) expression in the SVZ co-localizing with GFAP-GFP+ (green) NSCs. B) SVZ wholemount preparations show ADAM10 (red) expression at the ventricular surface co-localizing with GFAP+ (blue) NSC apical membranes at the center (arrowhead) of pinwheels (demarcated by β-catenin in green). Dotted line outlines pinwheel. C) Top panel: representative RT PCR of the ADAM10 protease domain, from YFP-sorted WT and ADAM10fl/fl cells. Bottom panel: Representative immunoblots for mADAM10 in YFP sorted cell protein extracts. Quantification shows RT PCR analysis for *ADAM10*. D) Representative coronal SVZ sections immunostained for GFAP (red) and Sox2 (green) 5 day after the final TAM injection. Inserts show high magnification of arrow. E) Quantification of GFAP+Sox2+ double positive cells. F-I) Immunostaining for transit amplifying EGFR+ cells and DCX+ neuroblasts in acutely dissociated SVZ tissue from wild-type and ADAM10 fl/fl animals. Quantification of the percentage of EGFR+cells/Total DAPI (from 417 WT and 453 fl/fl cells) and DCX+ cells/ Total DAPI cell counts (from 1339 WT and 1348 fl/fl cells). J) Acutely dissociated SVZ tissue was administered BrdU for 2 hrs. in vitro before immunostaining for BrdU and DCX K.) Quantification of DCX+BrdU+ cells per total DCX cell counts (435 WT and 349 fl/fl cells). L.) Immunoblotting for cleaved caspase 3 (19kDA) in WT and and ADAM10fl/fl NSCs differentiated in vitro for two days. M) Quantification of cleaved caspase western blots. F) Paired t-test. All others unpaired t-test. Error bars represent the mean ± s.e.m. Dots represent biologic replicates.

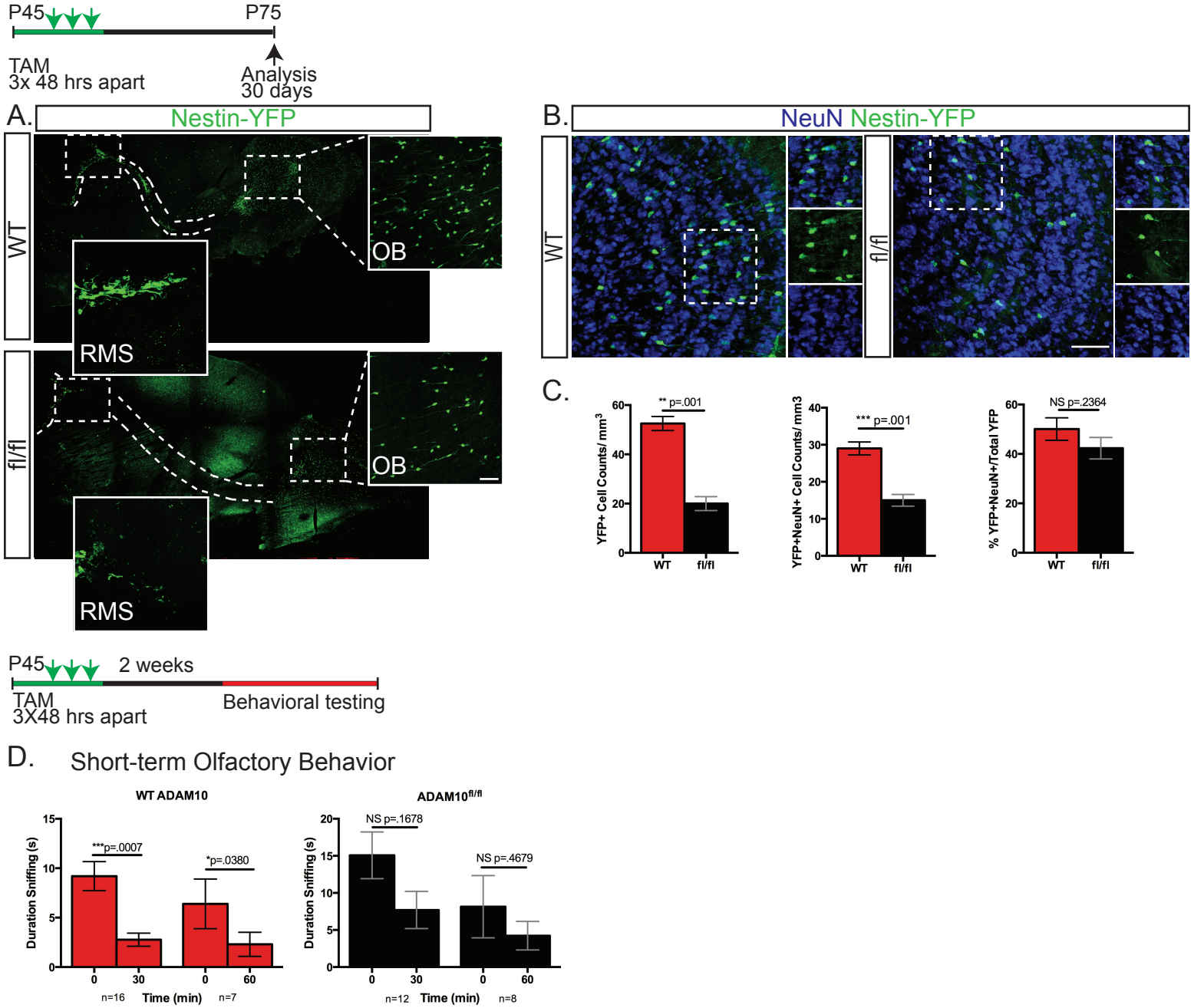

Figure 7. ADAM10 deletion in the adult SVZ decreases olfactory neurogenesis in the GCL of the OB in vivo. A)Top: Experimental scheme. Bottom: Representative sagittal sections of wild type and ADAM10fl/fl Nestin:CreER;Rosa26YFP animals 30 days after tamoxifen injections. Immunostaining for YFP (green) shows the SVZ-RMS-OB route SVZ progenitors take to the OB. Inserts show high magnification view of the RMS and OB in WT and ADAM10fl/fl mice. B) Representative immunostaining for YFP (geen) and NeuN (blue) in the GCL of the OB with the quantification shown in C.) A significant decrease in YFP+ and YFP+NeuN+ double positive cells but not YFP+NeuN+/Total YFP cells in ADAM10fl/fl versus wild type mice. 2196 and 1174 WT and ADAM10fl/fl YFP+ cells were quantified in the OB, respectively. D) Top: Experimental paradigm. Bottom: Behavioral testing for short-term olfactory memory. When presented with the same odor at a short interval, there is a significant reduction in odor investigation at 30 min and 60 min intervals in the WT group but not the ADAM10fl/fl group suggesting impaired short-term olfactory memory. Scale bars: 50μ m. in b) n=4. C) Students unpaired t-test. D) Paired t-test. Error bars represent the mean ± s.e.m.

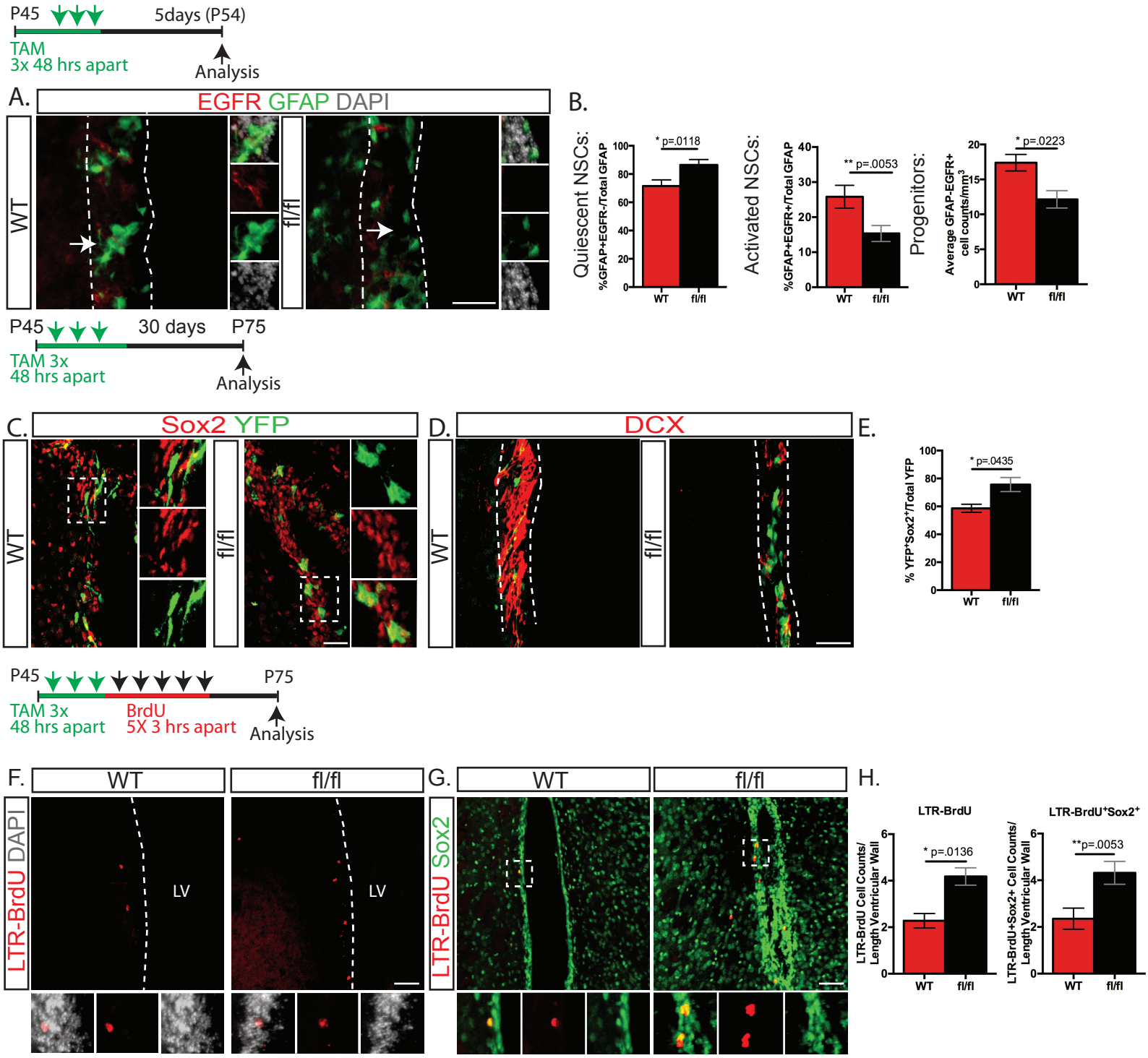

Figure 8. ADAM10 fl/fl mice have an increase in slowly cycling cells. A) Top: Experimental Paradigm. Bottom: Representative coronal SVZ (dashed line) sections from WT and ADAM10fl/fl;GFAP-GFP mice immunostained for EGFR. B.) Quantification of the quiescent: GFAP+EGFR-activated: GFAP+EGFR+, and progenitor: GFAP-EGFR+ populations. 615 and 388 WT and fl/fl GFAP-GFP+ cells, respectively, were analyzed. C) Top: Experimental Paradigm. Bottom: Representative coronal SVZ images of Nestin:CreER;Rosa26YFP mice one monther after TAM immunostained for YFP and Sox2. 362 and 386 YFP+ WT and fl/fl cells were analyzed, respectively D) Coronal ADAM10fl/fl SVZ sections immunostained for DCX and YFP show a decrease in neuroblasts. E) Percentage of YFP+Sox2+ per total YFP. F) Top: Experimental Paradigm. Bottom: Mice were injected intraperitoneally with TAM and BrdU five times every 3 hours followed by a one month chase. Representative immunoflourescence shows more LRC-BrdU in the SVZ of ADAM10 fl/fl mice. In total, 148 and 301 LTR-BrdU+ cells were quantified. G) LTR-BrdU+ cells were co-stained with the NSC marker Sox2 in the SVZ of WT and ADAM10 fl/fl mice. 73 and 164 LTR-BrdU+Sox2+ double positive cells were observed in the WT and ADAM10fl/fl SVZ, respectively. A-E) n=3 F-H)n=4. Scale Bars: 50 μm. A-H) Student's unpaired t-test. Error bars represent the mean ± s.e.m. LRC=label retaining cells

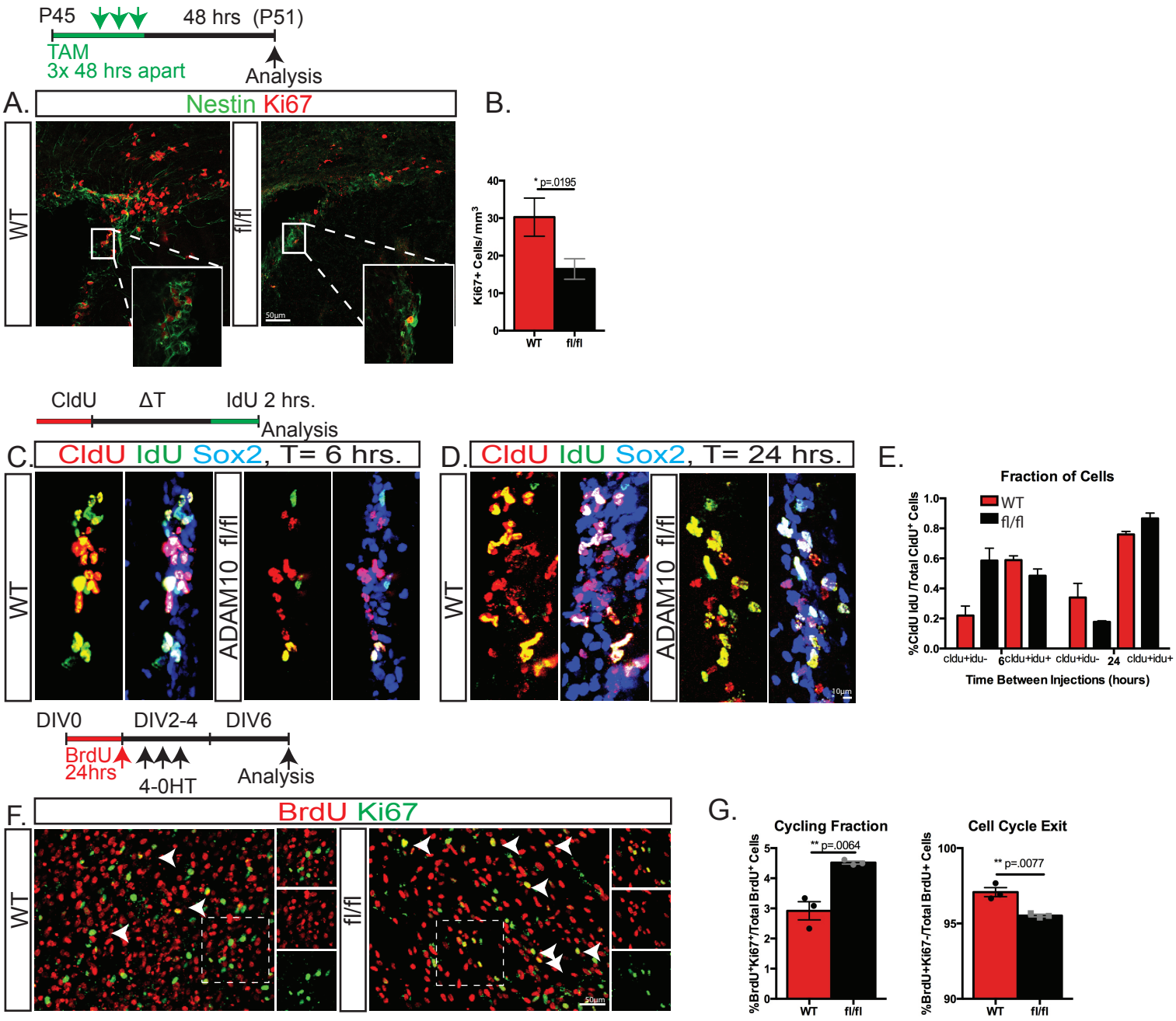

Figure 9. ADAM10 fl/fl NSCs are retained in the cell cycle. A) Representative immunofluorescence of Nestin and Ki67 with the quantification in B) shows decreased Ki67 in the ADAM10 fl/fl SVZ. 1302 and 691 Ki67+ cells were quantified in the WT and ADAM10fl/fl SVZ. C-D) Top: Experimental Paradigm. Bottom: Representative immunoflourescence of the SVZ following CldU and IdU injections separated by a Δt of 6 and 24 hrs. E) Analysis of WT and ADAM10fl/fl SVZ sections revealed trends towards an increase in S phase re-entry at 6 hrs in the WT while at 24 hrs the trend is increased in the ADAM10fl/fl mice. F) Top: Experimental Paradigm. Dissociated secondary neurospheres were plated on PLL treated coverslips. Cells were administered BrdU in vitro for 24 hrs. before addition of hydroxy-tamoxifen (4-OHT) and growth factor removal. Bottom: Co-staining for BrdU and Ki67 reveal the cycling cells (BrdU+Ki67+ cells; arrows) and those that have left the cell cycle (BrdU+Ki67-). Inserts show individual channels of dashed white box. G) (left) Quantification of the percentage of BrdU+Ki67+/Total BrdU+ cells show more cycling cells in the ADAM10 fl/fl cells. (right) Quantification of the percentage of BrdU+Ki67-/Total BrdU shows decreased cell cycle exit in the ADAM10 fl/fl cells. 8662 and 9107 BrdU+ WT and fl/fl cells were analyzed, respectively. For A, F) n=3 mice per group. At least 5 images per biologic replicate were analyzed. For C) n=2. Scale Bars indicated. B,G) Students unpaired t-test. Error bars represent the mean ± s.e.m.

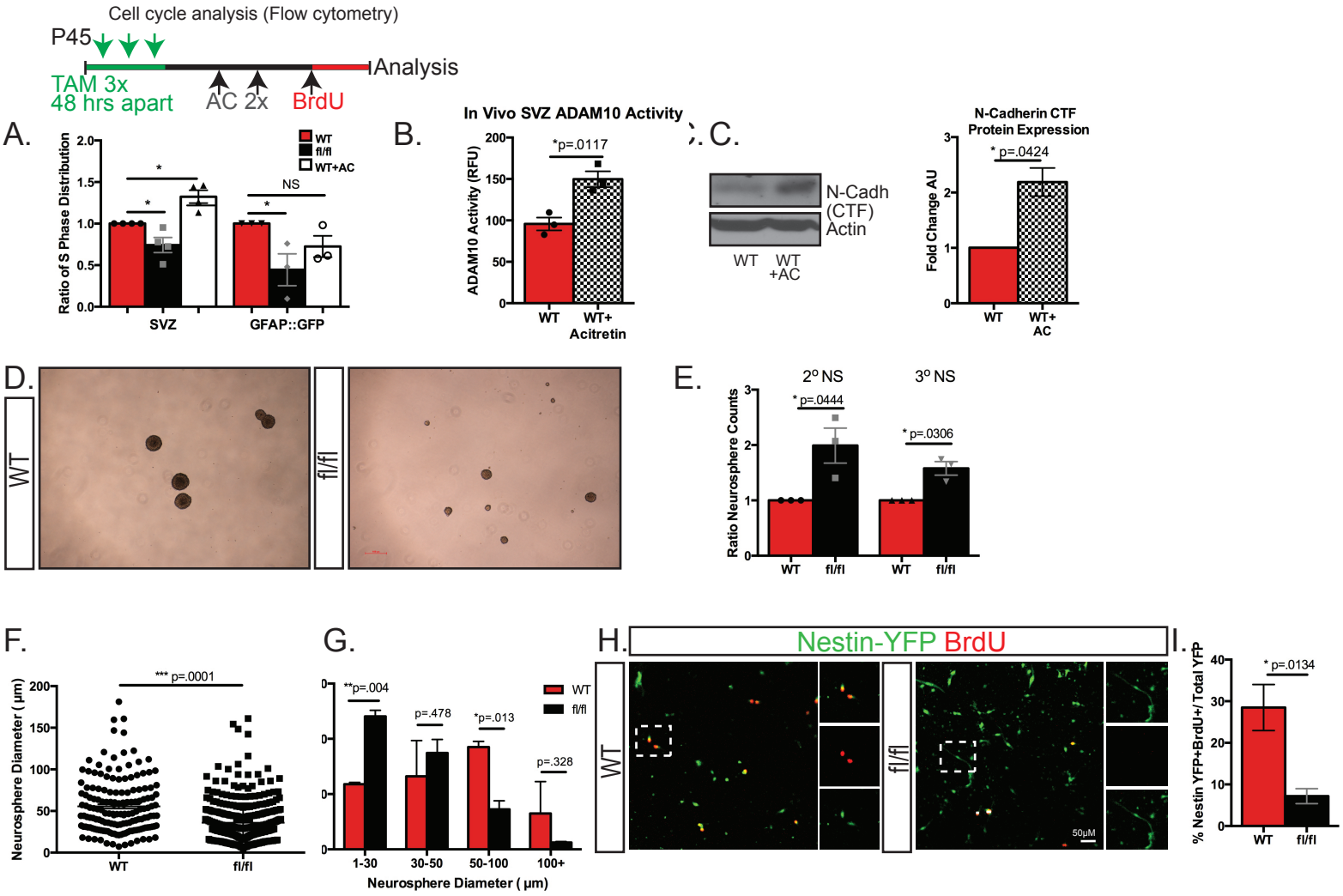

Figure 10. ADAM10 regulates proliferation and self-renewal. A) Top: Experimental Paradigm. Bottom: WT and ADAM10 fl/fl mice were injected with BrdU 2 hours prior to SVZ tissue processing for cell cycle analysis using the entire SVZ or GFAP-GFP sorted cells. Analysis of the relative proportion of cells in S phase of the cell cycle showed a decrease in the S phase fraction in ADAM10 fl/fl. WT mice also received IP injections of acitretin 18 hrs. and 6 hrs. prior to SVZ dissection and subsequent cell cycle analysis. Mice treated with acitretin showed increased proliferation and cell cycle progression B.) ADAM10 activity assay kit (Anaspec) shows an increase in ADAM10 activity in SVZ tissue lysates following IP injections with the ADAM10 transcriptional activator, acitretin (AC). C) SVZ protein lysates from WT and acitretin treated mice were immunoblotted for the C-terminal fragment (CTF) of N-cadherin, demonstrating increased cleavage. D) Representative images of WT and ADAM10 fl/fl secondary neurospheres from YFP sorted cells. E.) Analysis of WT and ADAM10 fl/fl YFP+ sorted cells in vitro demonstrated an increased formation of neurospheres following passaging. F) Analysis of sphere diameter demonstrated YFP+ ADAM10fl/fl sorted cells were smaller compared to WT spheres. G) Bins of neurosphere size showed WT spheres with wider diameter while more of the ADAM10 fl/fl spheres were 1-30um in size. H) Representative images from YFP sorted cells treated with BrdU 2 hours before processing for YFP and BrdU with the quantification in I.) shows a decrease in the percentage of YFP+BrdU+ /Total YFP+ cells. In total, 427 WT and 727 fl/fl YFP cells were quantified. Scale bars=50µM. C) n=2 A-K) n=3. For A) One-way ANOVA (compared to WT controls). C, E) Paired t-test all others unpaired t-test. Error bars represent the mean ± s.e.m.

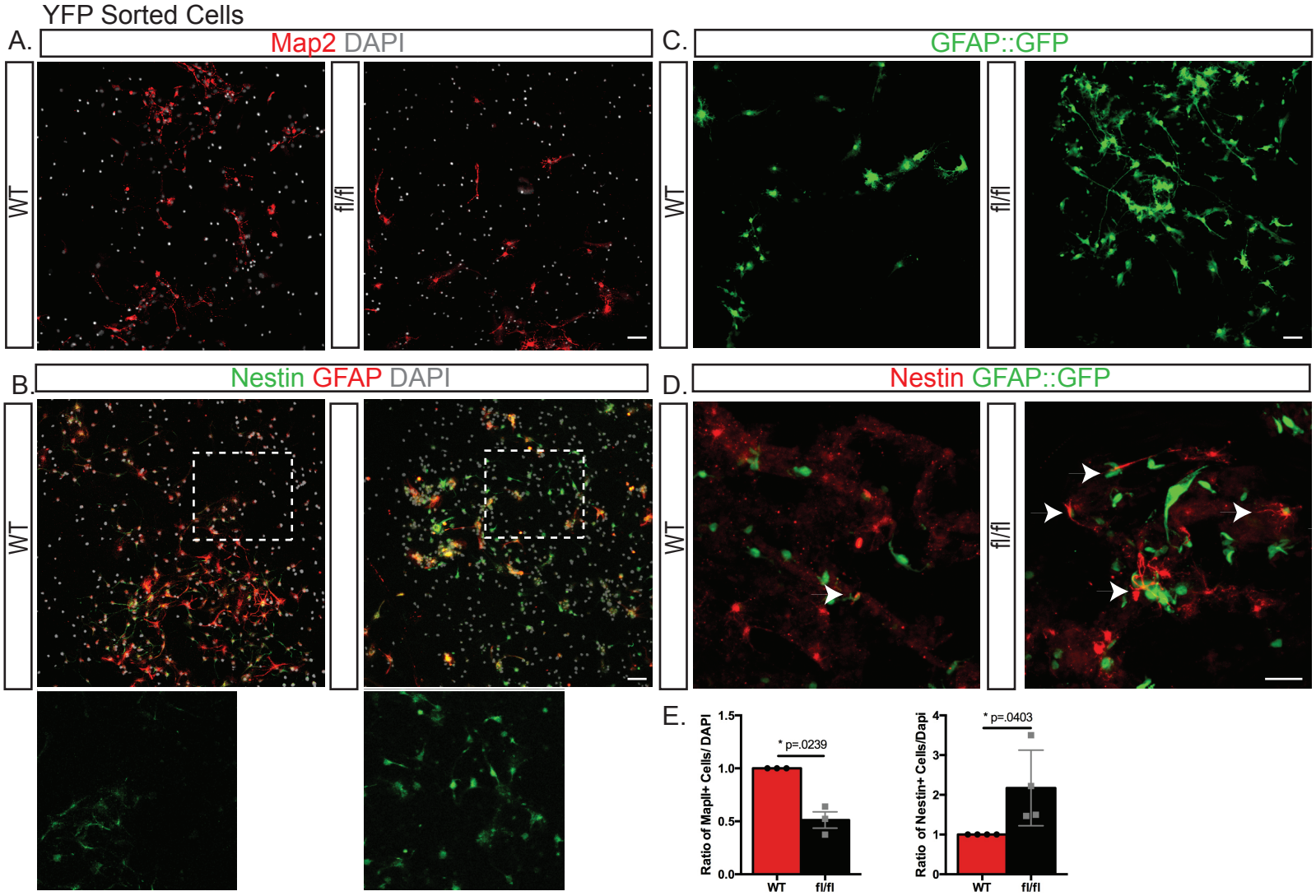

Figure 11. Immunofluorescence analysis of WT and ADAM10 fl/fl YFP sorted cells after differentiation reveals decreased neurogenesis in ADAM10 fl/fl cells. A) Representative images of YFP+ sorted 2° neurosphere derived cells after in vitro differentiation stained for Map2 (red) and B.) Nestin (green) and GFAP (red) C) Representative images of WT and ADAM10 fl/fl NSCs from GFAP::GFP mice differentiated in vitro show increased GFAP::GFP+ cells D) co-expressing with the NSC marker Nestin (arrows). E) Quantification of YFP sorted cell differentiation shows (left) the percentage of Map2+ cells and (right) Nestin+ cells (right) per total dapi expressed as a ratio. 5804 and 5475 WT and fl/fl cells were counted, respectively. E) Statistical analysis used paired t-test. Scale bars: 50μm

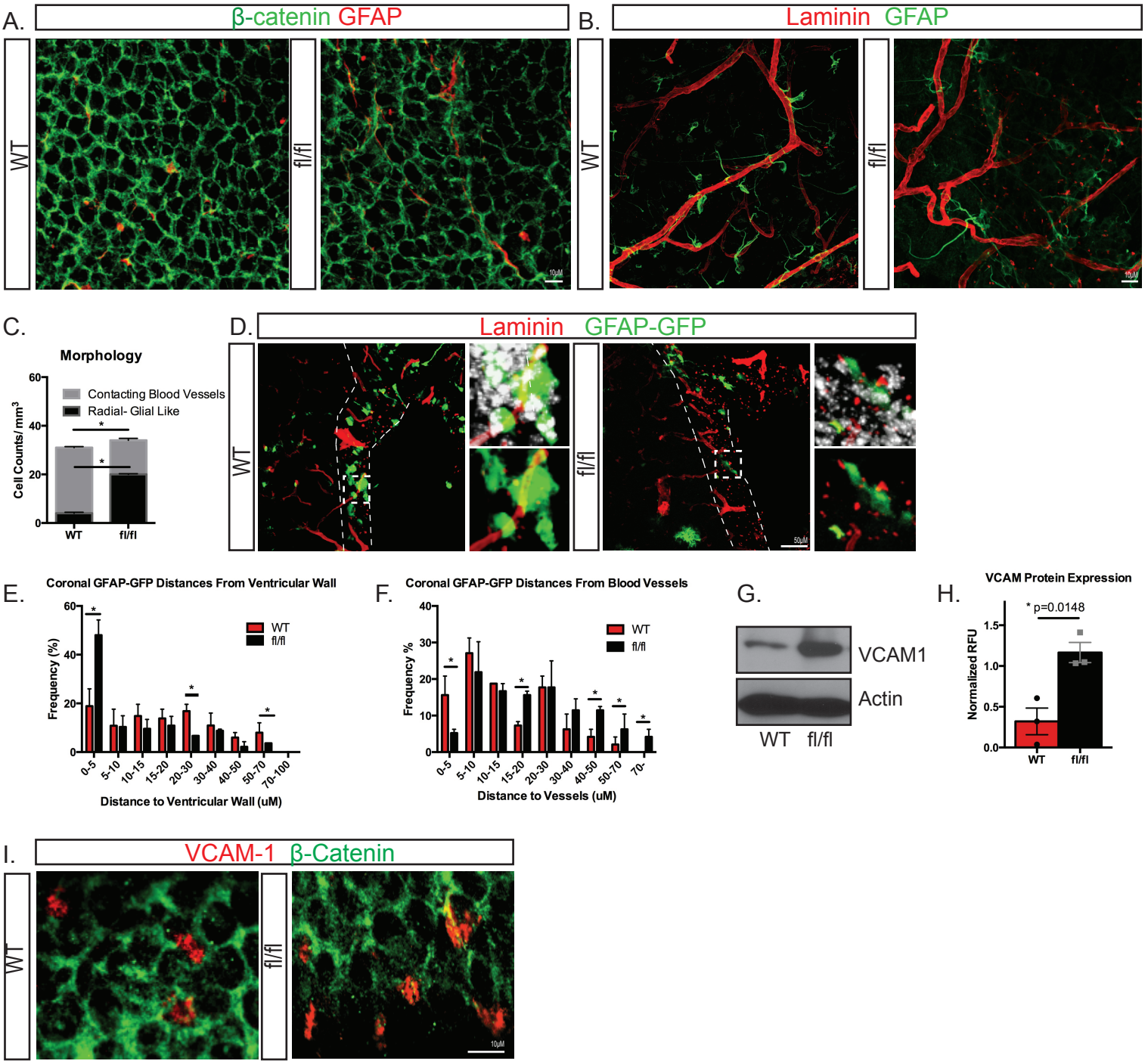

Figure 12. ADAM10 fl/fl GFAP+ cells in the SVZ have altered morphology and increased distribution towards the ventricular wall. A) Representative wholemount staining (5 days after the final TAM injection) for GFAP (red) and β-catenin (green) show normal pinwheel architecture in the apical niche. B) Wholemount SVZ preparations stained for GFAP (green) and Laminin (red) in WT and ADAM10 fl/fl mice depict different GFAP+ NSC morphologies and contacts in the basal SVZ niche. C) Quantification of basal niche characteristics show more radial glia-like cells found away from the blood vessels in the ADAM10fl/fl SVZ compared to WT. D) Coronal and GFAP::GFP SVZ sections immunostained for laminin showed ADAM10 fl/fl GFAP-GFP+ NSCs closer to the ventricular wall and farther from the blood vessels. E) Quantification showing the distribution frequency of cells from the ventricular wall and F) blood vessels. G-H) Immunoblotting for VCAM-1 in WT and ADAM10 fl/fl cell lysates shows increased expression in the ADAM10 fl/fl samples. I) Wholemounts stainined for β-catenin and VCAM-1. n=3. Scale bars indicated. C) Two-way ANOVA all others unpaired t-test. Error bars represent the mean ± s.e.m.

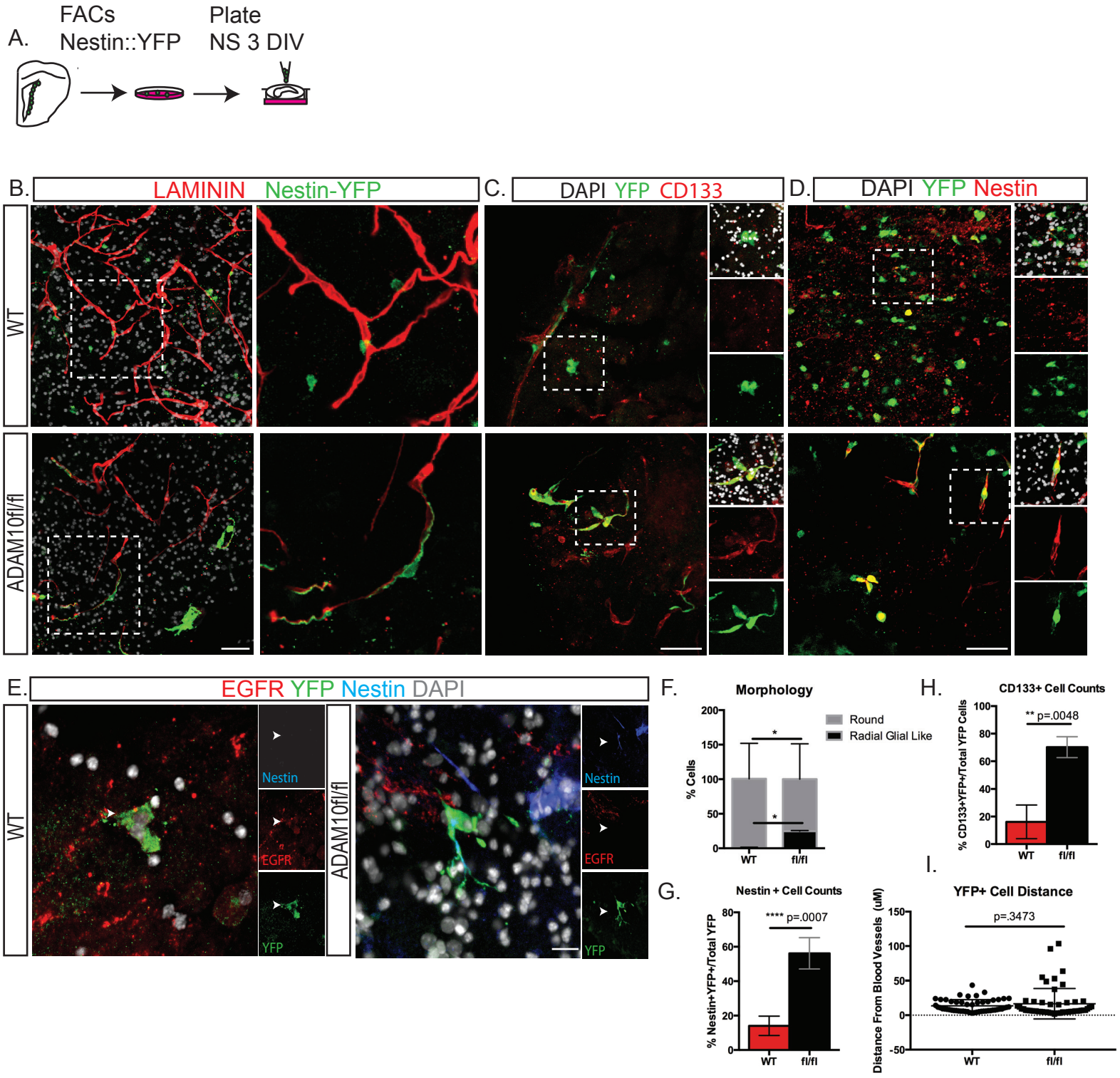

Figure 13. ADAM10 deletion promotes stemness in a cell-autonomous manner. A) Paradigm showing FAC sorted Nestin-YFP+ cells from WT and ADAM10 fl/fl mice grown in vitro before plating on WT SVZ slice cultures for three days followed by IF processing. B) Representative slice cultures immunostained for YFP and laminin. Secondary neurospheres obtained from YFP sorted cells show the same radial glia-like morphology observed in the ADAM10 fl/fl SVZ wholemnounts as revealed with GFAP staining (figure 11). 704 and 274 WT and fl/fl YFP+ cells were analyzed for morphology, respectively. Inserts show high magnification of dotted white box. C) Representative image of an SVZ slice culture immunostained for YFP (green) and the NSC marker CD133 (red) with high magnification insert of dotted white box. In total, 52 and 91 WT and fl/fl YFP cells were analyzed for co-expression with CD133 D.) Representative slice culture shows YFP (green) and Nestin (red) co-expression. High magnification inserts of dotted white box shown to the right. In total, 330 and 128 WT and fl/fl YFP+ cells were analyzed for co-expression with nestin, respectively E.) WT YFP+ cells are actively dividing and co-expess with EGFR and not nestin while ADAM10 fl/fl YFP+ cells co-express with nestin and not EGFR (arrows). F) Quantification of morphology in WT and ADAM10fl/fl YFP+ cells H) Quantification of the percentage of CD133+YFP+/Total YFP cells. G) Quantification of Nestin+YFP+/Total YFP I) YFP+ cell distance from laminin + blood vessels. At least 4 explants were analyzed in two independent experiments. Scale Bars: A-D) 50 µm E)10 µm. F) Two-way ANOVA all others are unpaired t-test. Error bars represent the mean ± s.e.m.

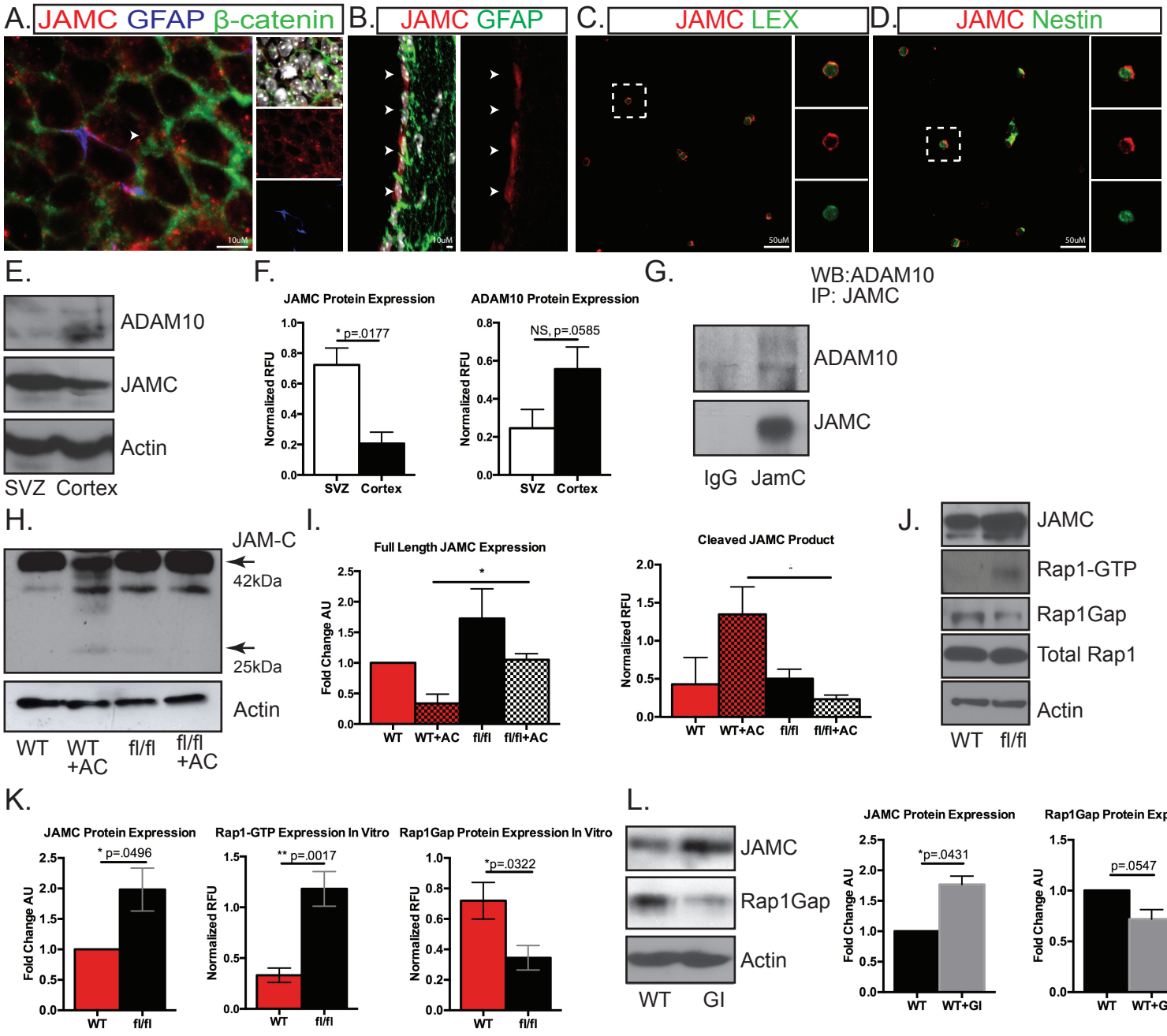

Figure 14. JAMC is a feature of adult NSCs and is cleaved by ADAM10 in the WT SVZ. A.) Wholemount staining shows JAMC (red) co-localizing to GFAP+ (blue) NSC contacts at the center (arrowhead) of pinwheels (green). B) JAMC co-expresses with GFAP+ NSCs along the wall of the lateral ventricle(arrowheads). C) Acutely dissociated WT SVZ tissue shows JAMC co-expresses with Lex+ and D) Nestin+ stem cells. High magnification inserts of dashed white box. E) Immunoblotting for JAMC and ADAM10 protein expression in the SVZ and cortex shows co-expression in the SVZ. F) Quantification shows JAMC enrichment in the SVZ vs. cortex. G) JAMC immunoprecipitates ADAM10 in SVZ tissue lysates, demonstrating interaction. H.) SVZ slice cultures from WT and ADAM10 fl/fl mice treated with hydroxy-tamoxifen in vitro and acitretin (AC) reveal a JAMC fragment (25kDa) only in WT AC treated samples I) Quantification of the full length and cleaved JAMC forms shows a significant difference in WT and ADAM10fl/fl samples treated with AC. J) Rap1Gap protein expression is decreased in ADAM10 fl/fl cells and correlates with an increase in the full length of JAMC. Additionally, Rap1-GTP (active Rap1) is increased. K) Quantification shows Rap1Gap, Rap1-GTP, and JAMC protein expression in WT and ADAM10fl/fl NSCs. L) Represenative western blot of WT NSCs treated with control or the small molecule ADAM10 inhibitor GI254023X (GI;10 uM). Quantification shows a decrease in Rap1Gap expression and an increase in full length JAMC. For E-I and L) n=3 For J-K) n=5. Scale Bars: A-B) 10 µm D-D)50 µm. For K) JAM-C expression and L) paired t-test were performed all others unpaired t-test or Anova (groups). Error bars represent the mean ± s.e.m.

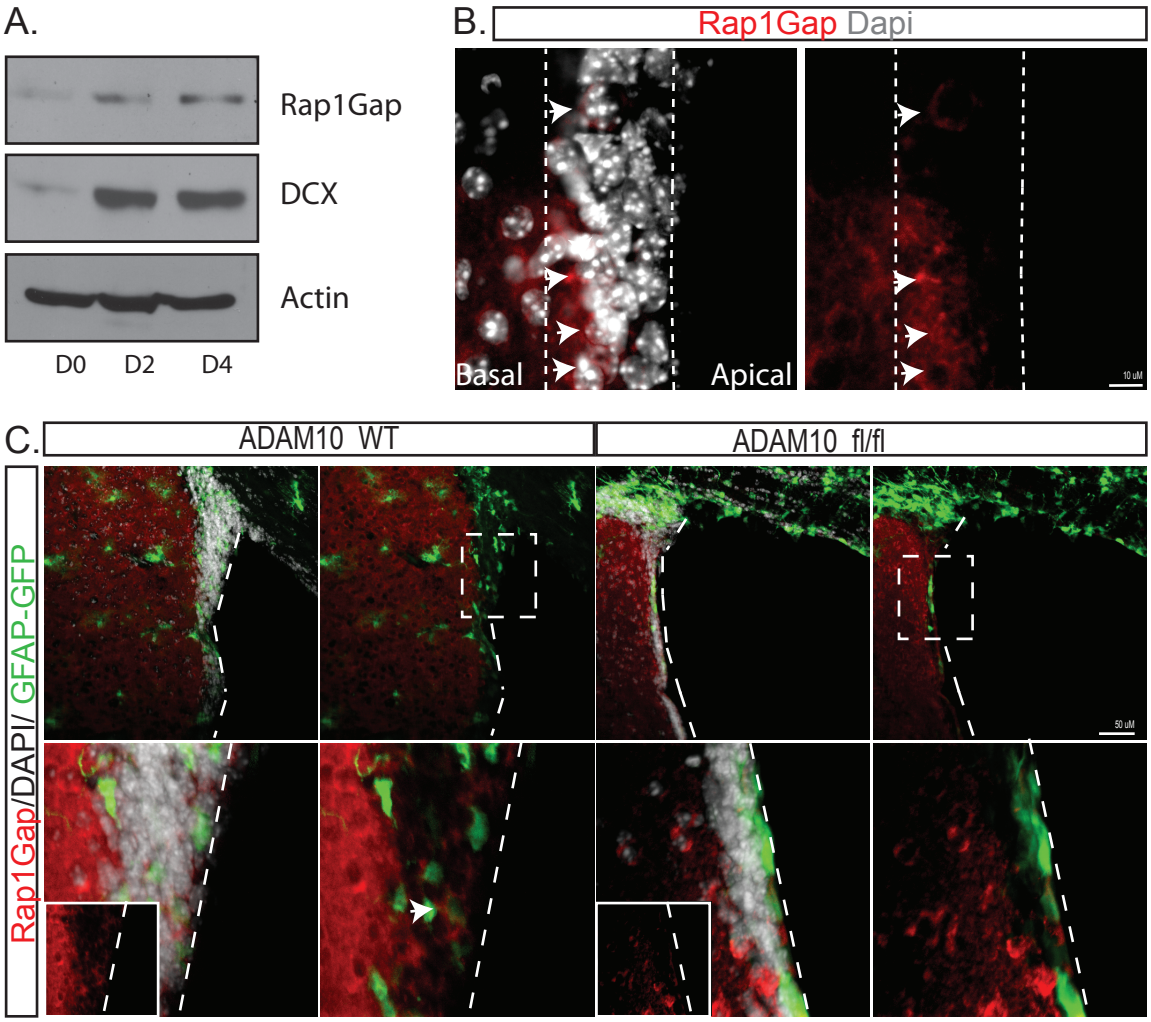

Figure 15. Rap1Gap is expressed in progenitors in the basal adult SVZ niche. A) Representative western blot of WT NSCs in differentiating conditions for the indicated days (D) shows an increase in Rap1Gap expression from D0 to D4. B) Represenative sagittal SVZ section shows Rap1Gap expression is highest in cells away from the ventricular wall. The apical SVZ on the ventricular side does not express Rap1Gap while cells in basal niche on the striatal side of the SVZ expess high Rap1Gap levels (arrowheads). C) Similarly, in coronal SVZ sections Rap1Gap is enriched in the GFAP-GFP+ NSCs leaving the ventricular wall. Rap1Gap does not co-express with GFAP-GFP+ NSCs in the ADAM10fl/fl SVZ (high magnification insert). For A n=3. Scale bars= B) 10uM C) 50uM.

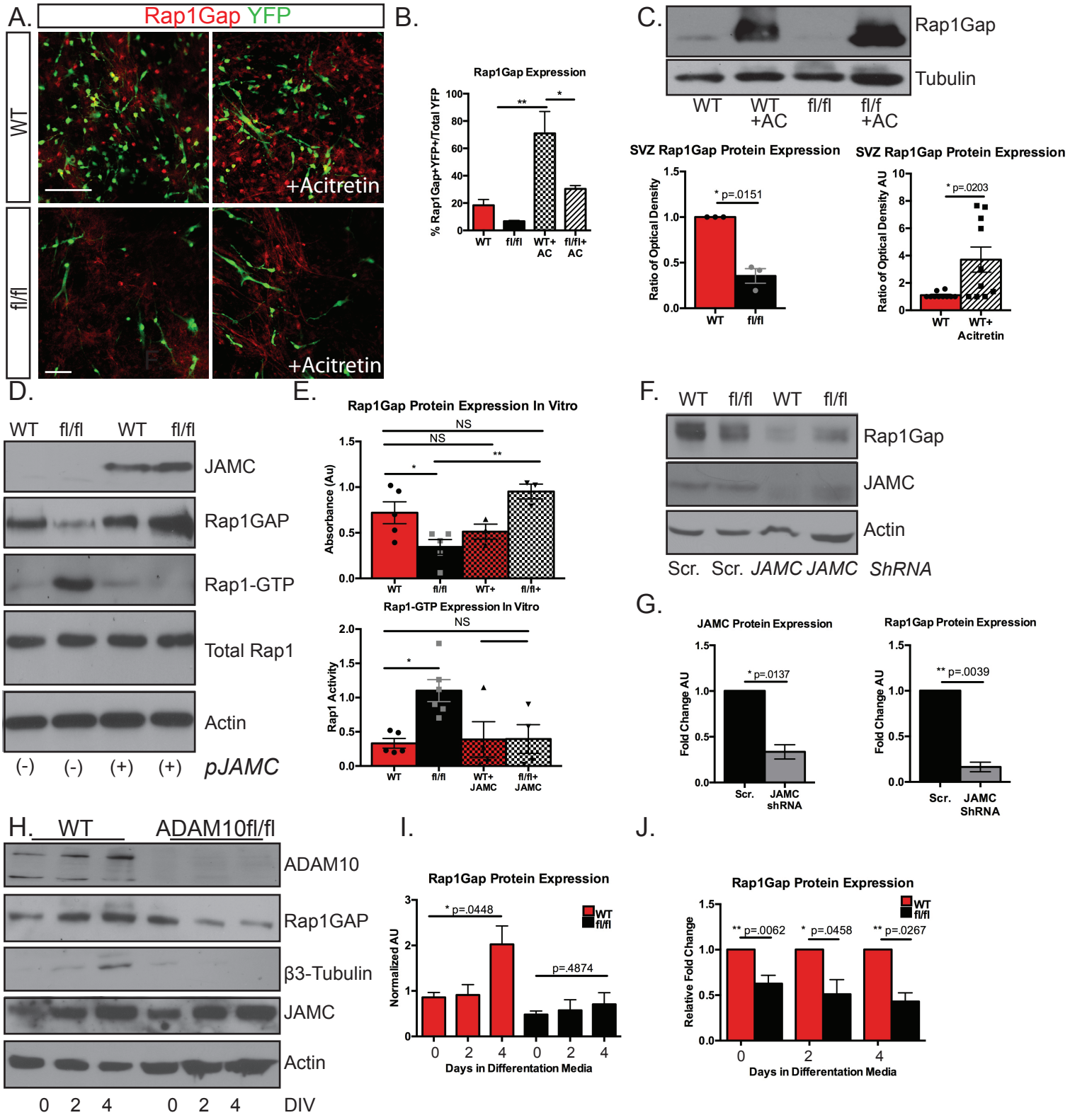
A.
Rap1Gap YFP
WT
fl/fl
+Acitretin
+Acitretin
B.
Rap1Gap Expression
% Rap1Gap+YFP+/Total YFP
WT
fl/fl
WT+ AC
fl/fl+ AC
C.
Rap1Gap
Tubulin
WT
WT +AC
fl/fl
fl/f +AC
SVZ Rap1Gap Protein Expression
Ratio of Optical Density
* p=.0151
WT
fl/fl
SVZ Rap1Gap Protein Expression
Ratio of Optical Density AU
* p=.0203
WT
WT+ Acitretin
D.
WT
fl/fl
WT
fl/fl
JAMC
Rap1GAP
Rap1-GTP
Total Rap1
Actin
(-) (-) (+) (+) pJAMC
E.
Rap1Gap Protein Expression In Vitro
Absorbance (Au)
NS
NS
*
**
WT
fl/fl
WT+
fl/fl+
Rap1-GTP Expression In Vitro
Rap1 Activity
NS
*
WT
fl/fl
WT+ JAMC
fl/fl+ JAMC
F.
WT
fl/fl
WT
fl/fl
Rap1Gap
JAMC
Actin
Scr. Scr. JAMC JAMC ShRNA
G.
JAMC Protein Expression
Fold Change AU
* p=.0137
Scr.
JAMC shRNA
Rap1Gap Protein Expression
Fold Change AU
** p=.0039
Scr.
JAMC ShRNA
H.
WT
ADAM10fl/fl
ADAM10
Rap1GAP
β3-Tubulin
JAMC
Actin
0 2 4 0 2 4 DIV
I.
Rap1Gap Protein Expression
Normalized AU
* p=.0448
p=.4874
WT
fl/fl
0 2 4 0 2 4
Days in Differentation Media
J.
Rap1Gap Protein Expression
Relative Fold Change
** p=.0062
* p=.0458
** p=.0267
WT
fl/fl
0 2 4
Days in Differentation Media
K.
WT
fl/fl
WT
fl/fl
VCAM1
JAMC
Actin
(-) (-) (+) (+) pJAMC
L.
VCAM Protein Expression
Absorbance (Au)
*
NS
NS
WT
fl/fl
WT+JAMCfl/fl+JAMC
M.
VCAM1
Actin
WT 8CPT
N.
VCAM Protein Expression
Normalized RFU
NS, p=.3766
WT
8CPT

Figure 16. Rap1Gap acts downstream of ADAM10 and JAMC. A-B.) Rap1gap IF is decreased in the ADAM10 fl/fl cells and increases in WT cells after acitretin treatment but not YFP+ fl/fl cells. C) Immunoblotting of SVZ tissue in WT , ADAM10 fl/fl and acitretin treated mice demonstrates decreased Rap1Gap in the ADAM10 fl/fl SVZ and increased expression in the acitretin treated mice. D-E.) Active Rap1-GTP pulldown assays in WT, ADAM10fl/fl and JAM-C overexpressing cells inversely correlates with Rap1 Gap expression. Rap1Gap expression in ADAM10 fl/fl cells recovers to WT levels after JAMC overexpression while Rap1-GTP decreases to WT levels. F) Rap1Gap expression decreases after lentivirally delivered shRNA targeted to JAMC in WT cells with the .quantification show in H.) Rap1Gap and JAMC protein expression during in vitro differentation in WT and ADAM10 fl/fl cells with the quantification in I-J.) showing no increase in Rap1Gap expression in ADAM10 fl/fl cells during differentiation. K) Representative western blots of VCAM-1 protein expression in WT, ADAM10 fl/fl, and JAM-C overexpressing cells. I.) The increased VCAM-1 in ADAM10fl/fl cells recovers to WT levels after JAM-C overexpression. For A-L) n=3 unless otherwise indicated. Dots represent biologic replicates. Scale Bars:50 μm. B,E,L) ANOVA with multiple compairson, N) unpaired t-test, all others paired t-test. Error bars represent the mean ± s.e.m.

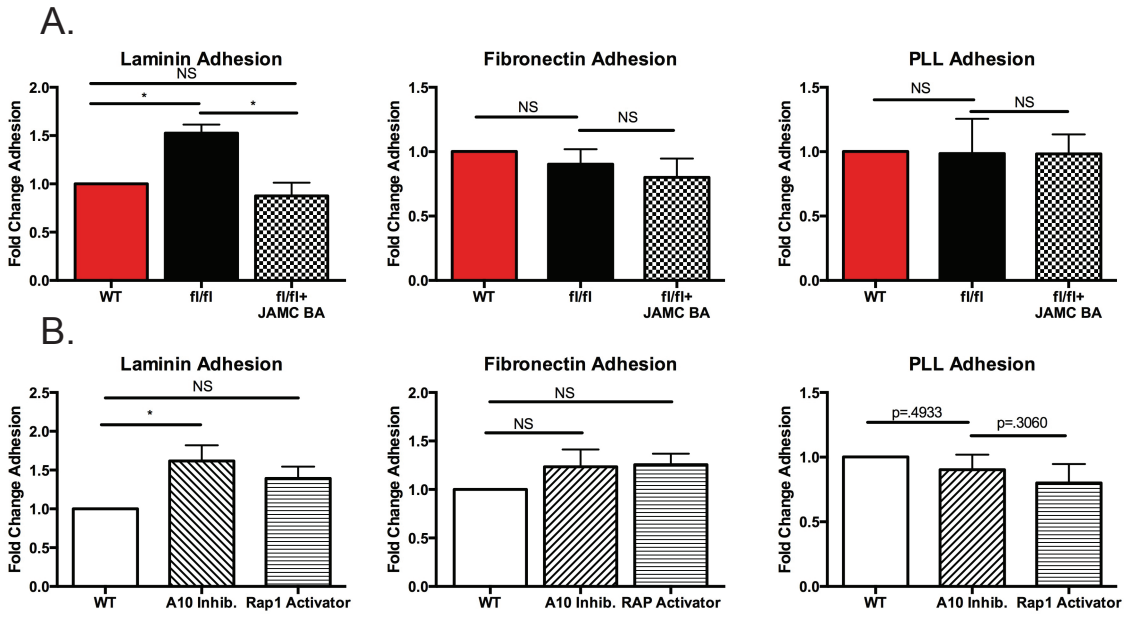

Figure 17. JAMC and Rap1 direct NSC Adhesion. A) Calcein-stained WT and ADAM10 fl/fl NSCs were plated in the presence of JAM-C blocking antibody or isotype control IgG and allowed to adhere to laminin, fibronectin, or PLL substrate. After a 20 minute incubation, non-adherent cells were gently washed away and the remaining fluorescence was calculated as a percentage of total fluorescence before washing. B.) WT NSCs were treated with ADAM10 small molecule inhibitor GI254023X or the small molecule Rap1 activator 8-CPT-2-O- Me-cAMP before adhesion to laminin, fibronectin, and PLL were assesed. n=3 in triplicate. One-way ANOVA with multiple compairsons. Error bars represent the mean ± s.e.m.

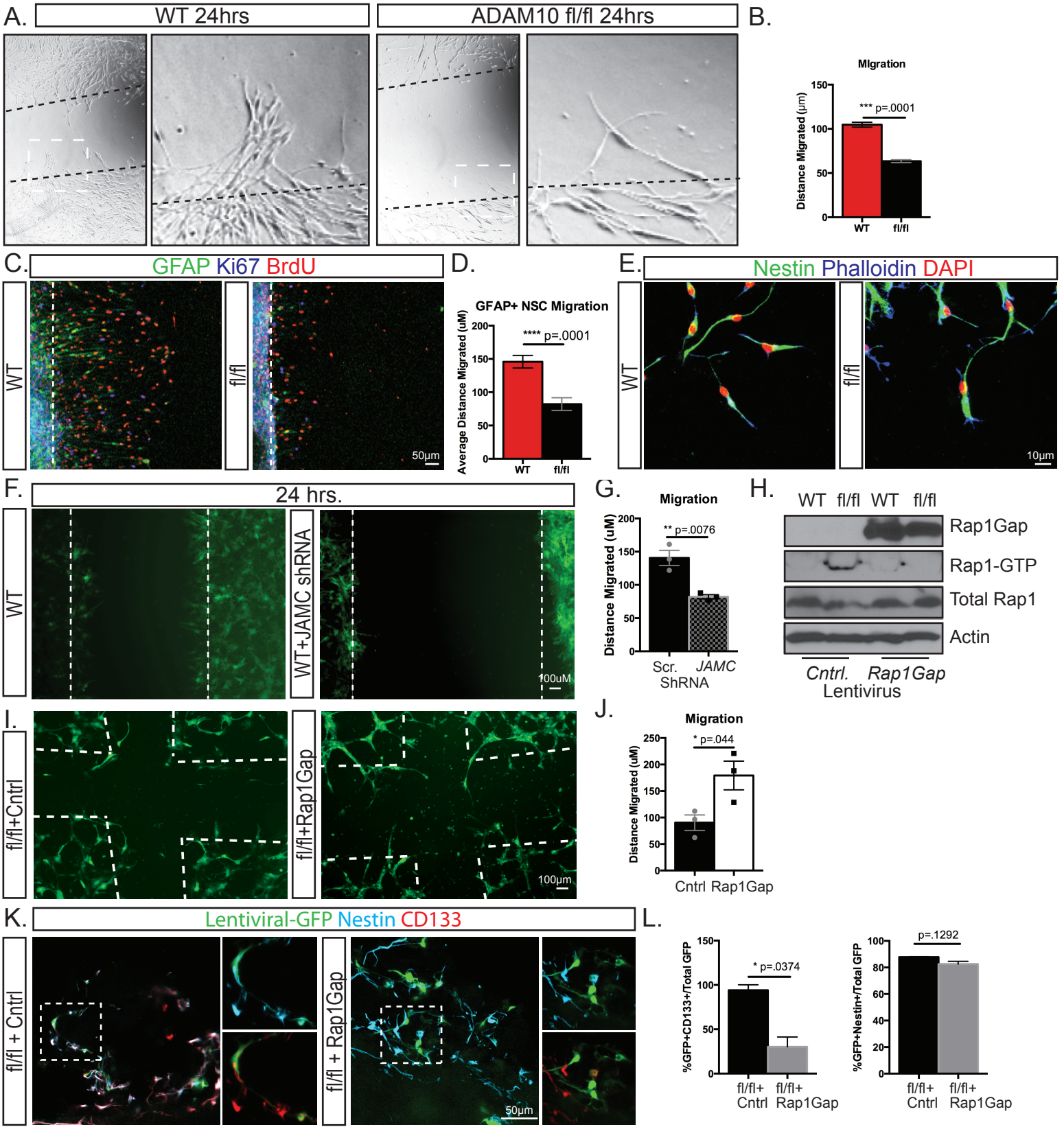
A.
WT 24hrs
ADAM10 fl/fl 24hrs
B.
MIgration
*** p=.0001
Distance Migrated (µm)
150
100
50
0
WT
fl/fl
C.
GFAP Ki67 BrdU
WT
fl/fl
50µm
D.
GFAP+ NSC Migration
**** p=.0001
Average Distance Migrated (uM)
200
150
100
50
0
WT
fl/fl
E.
Nestin Phalloidin DAPI
WT
fl/fl
10µm
F.
24 hrs.
WT
WT+JAMC shRNA
100uM
G.
Migration
** p=.0076
Distance Migrated (uM)
200
150
100
50
0
Scr. ShRNA
JAMC
H.
WT fl/fl WT fl/fl
Rap1Gap
Rap1-GTP
Total Rap1
Actin
Cntrl.
Rap1Gap
Lentivirus
I.
fl/fl+Cntrl
fl/fl+Rap1Gap
100µm
J.
Migration
* p=.044
Distance Migrated (uM)
250
200
150
100
50
0
Cntrl
Rap1Gap
K.
Lentiviral-GFP Nestin CD133
fl/fl + Cntrl
fl/fl + Rap1Gap
50µm
L.
* p=.0374
%GFP+CD133+/Total GFP
150
100
50
0
fl/fl+ Cntrl
fl/fl+ Rap1Gap
p=.1292
%GFP+Nestin+/Total GFP
100
80
60
40
20
0
fl/fl+ Cntrl
fl/fl+ Rap1Gap

Figure 18. ADAM10 fl/fl cells display decreased migration and changes in cell morphology due to decreased JAMC-Rap1Gap signaling A-B) A pipet tip was used to create a scratch in monolayers of WT and ADAM10 fl/fl NSCs. Distance of individual cell migration from the edge was analyzed 24 hours later. Analysis shows a decreased number of fl/fl NSCs were able to migrate from the edge of the scratch in the given time. 551 WT cells and 304 cells from 3 wells performed in triplicate (biologic replicates) were analyzed C-D) 24 hrs after plating on PLL coated coverslips, cultures were processed for cell migration and immunocytochemistry. Representative immunofluorescence of GFAP::GFP cell migration shows a decrease in migration. Migratory cells co-express with proliferation markers Ki67 and BrdU. 100 WT GFAP-GFP+ cells and 50 ADAM10fl/fl GFAP-GFP+ cells were quantified from 3 coverslips repeated in triplicate. E.) Immunofluorescence analysis with anti-F-actin and anti-nestin antibodies were used to detect cell morphology in WT and ADAM10fl/fl cells. Note the blunted leading process in the fl/fl derived cells. F) Scratch test migration assays were performed in monolayer cells treated with scramble or JAMC lentivirus-shRNA with the quantification in G.) showing decreased migration in JAMC-shRNA treated cells H) Representative western blots show lentivirally delivered Rap1Gap rescues the elevated Rap1-GTP in ADAM10fl/fl NSCs. I) Migration assay was performed in monolayers of ADAM10fl/fl NSCs treated with control or Rap1Gap lentivirus. J) Quantification shows an increase in migration following Rap1Gap overexpression. K) Lentiviral transduced cells were plated on WT SVZ explants in vitro before processing for CD133 and Nestin co-expression. L) Analysis shows a decrease in CD133 expression in Rap1Gap overexpressing cells. For H) n=2. A-J) n=3. For slice cultures at least 4 explants were ana-

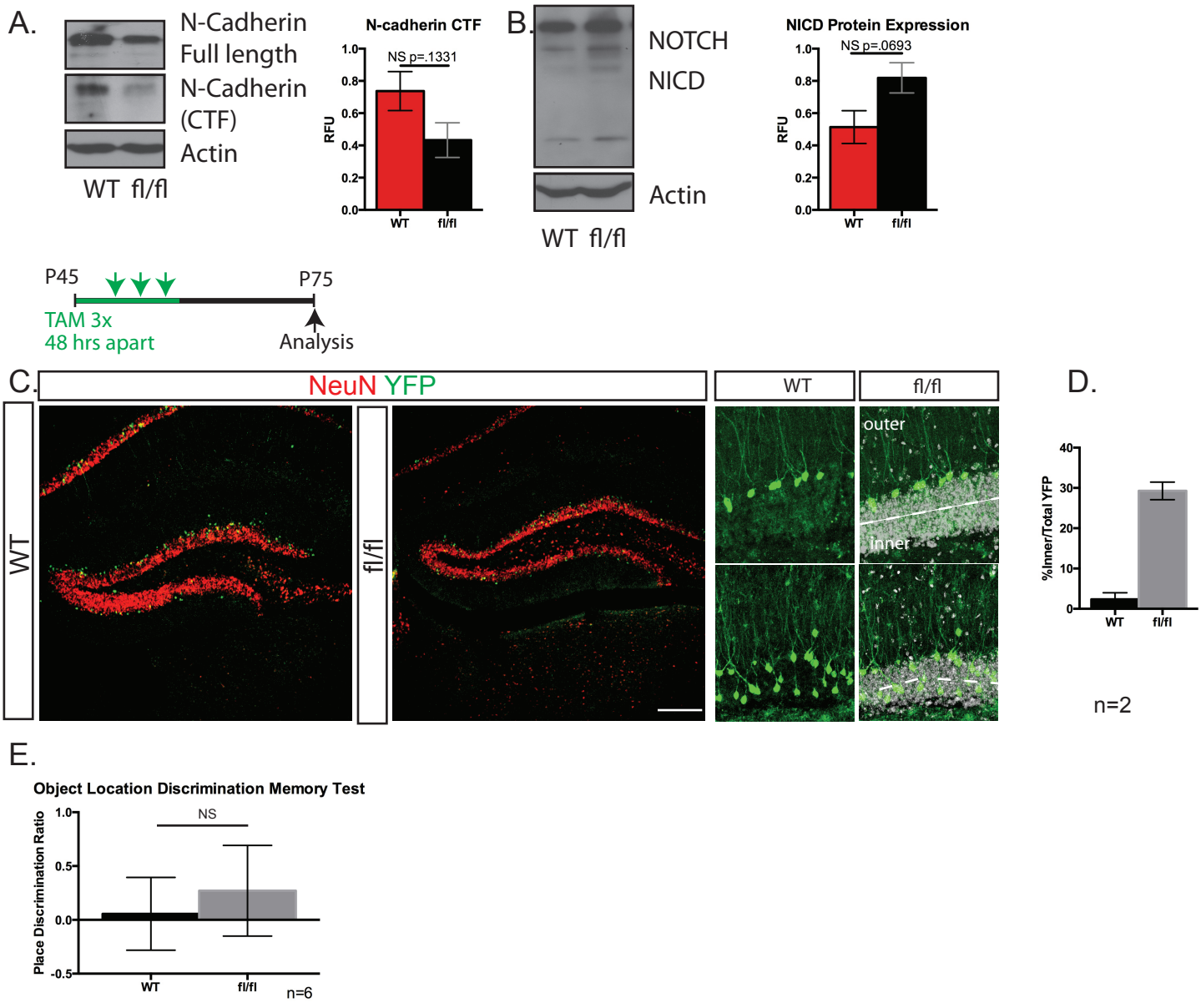

Figure 19. Additional roles for ADAM10 in substrate cleavage and the hippocampus. A) WT and ADAM10fl/fl NSC protein lysates were immunblotted for N-cadherin to detect the full length (135 kDa) and the CTF (35kDa). Quantification shows a trend towards a decrease in release of the CTF in ADAM10fl/fl NSCs compared to WT cells. B) Immunoblotting for Notch to detect the NICD (70kDa) released by ADAM10 following a series of cleavages does not reveal any significant differences. C) Top: Experimental Paradigm. Mice were analyzed 30 days following TAM injection. Quantification of cells in the inner or the outer dentate gyrus show ADAM10fl/fl YFP+ cells found throughout the dentate gyrus while WT YFP+ cells are largely found within the outer layer. E) Object placement memory test does not show any significant differences in WT vs ADAM10fl/fl NSCs. A-B) n=3 C) n=2 E) n=6. Scale bars=50uM. A) Paired t-test. Error bars represent the mean ± s.e.m.

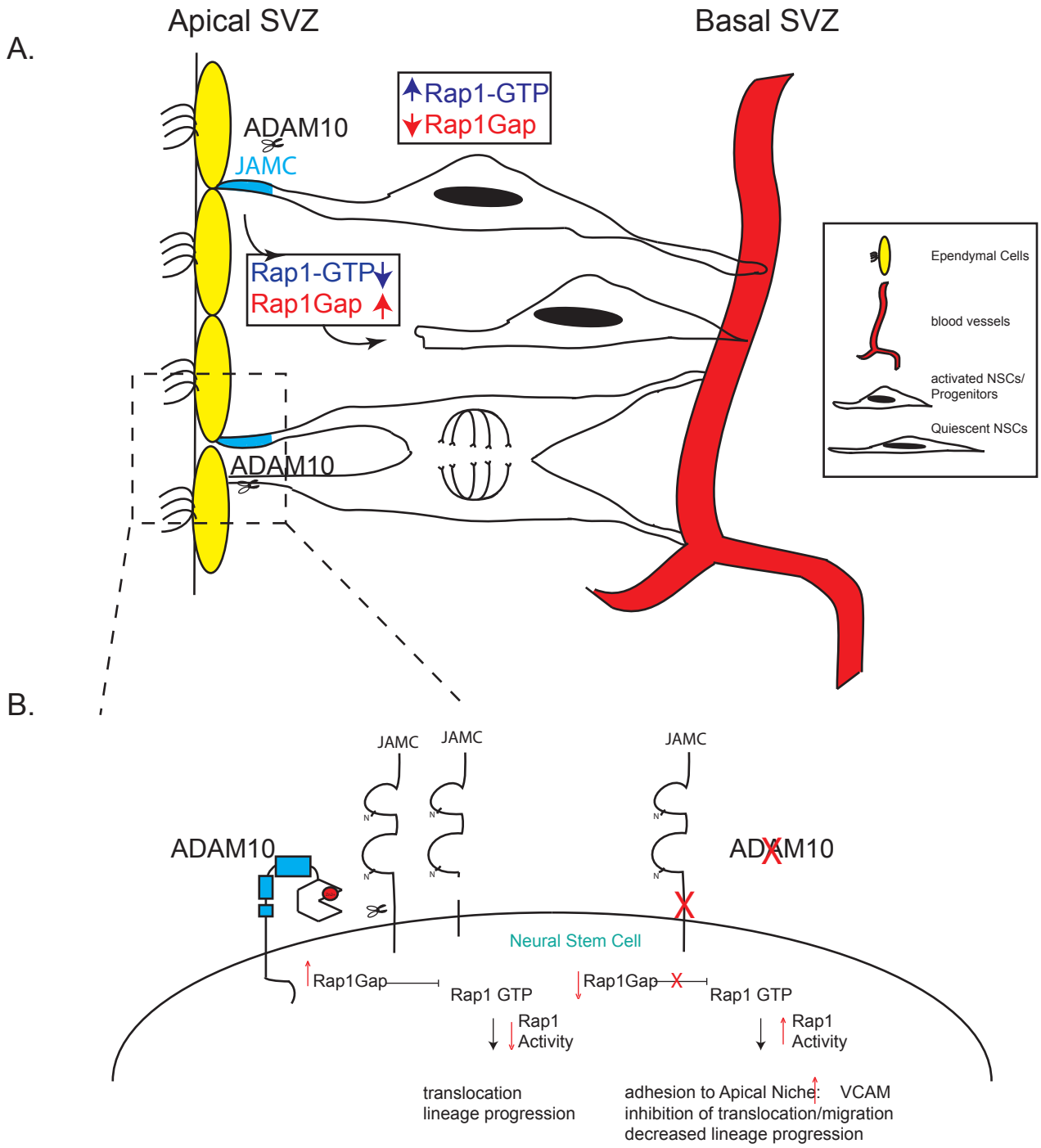

Figure 20. Summary diagram. A) JAM-C located at the apical plasma membrane of NSCs is processed by ADAM10. A) Without ADAM10, Rap1Gap expression is decreased and Rap1-GTP is high, promoting adhesion and retention in the apical SVZ. ADAM10 processing of JAMC or Rap1Gap over-expression promotes translocation to the basal SVZ. B) Magnified schematic of the NSC-Niche interaction.